HEP'99 # 4_520
Submitted to Pa 4, 5
Pl 4, 5

DELPHI 99-109 CONF 296
15 June 1999

Search for $B_s^0 - \overline{B_s^0}$ oscillations, measurement of the B_s lifetime and limit on the lifetime difference.

Preliminary

DELPHI Collaboration

A. Borgland[1], P. Checchia[2], G. Eigen[1], P. Kluit [3], O. Kouznetsov[4], F. Parodi[5], F. Pierre[4], O. Rohne[6], P. Roudeau[7] and A. Stocchi[7]

[1] Bergen, [3] Padova, [3] NIKHEF, [4] Saclay, [5] Genova, [6] Oslo, [7] LAL

Oscillations of B_s^0 mesons have been studied in several analyses which correspond to various B_s decay modes. Some analyses use events containing simply a lepton emitted at large p_t relative to its jet axis. In this case, the proper time is measured using an inclusive vertex algorithm to reconstruct the decay distance and the energy of the B hadron candidate. In other analyses, like $D_s^{\pm}\ell^{\mp}$, the identified lepton is accompanied, in the same hemisphere, by an exclusively reconstructed D_s. In $D_s^{\pm}h^{\mp}$ analyses the lepton is replaced by a charged hadron. Exclusive (completely reconstructed) decays of B_s have been also used. Using all these channels a limit on the mass difference between the physical B_s^0 states has been obtained. Using the $D_s^{\pm}\ell^{\mp}$ and the $D_s^{\pm}h^{\mp}$ samples the B_s lifetime and the lifetime difference between the two physical B_s states have been also measured.

Paper submitted to the HEP'99 Conference
Tampere, Finland, July 15-21

1 Introduction

Oscillations of B_s^0 mesons have been studied from events selected from about 3.5 million hadronic Z^0 decays registered by DELPHI between 1992 and 1995. Three different studies have been done :

- using events containing a lepton emitted with a large transverse momentum relative to its jet axis. This analysis has not been updated with respect to the contribution which has been sent to l998 Summer Conferences [1], and will be not described in this paper.

- using events with a large transverse momentum lepton and a D_s of opposite electric charge emitted in the same hemisphere. Using this sample the B_s^0 lifetime and the lifetime difference between the two physical B_s^0 states have been also measured. This note updates the contribution sent to 1998 Summer Conferences [2]

- using an exclusively reconstructed B_s^0 sample. In addition the oscillations have been studied in events with a D_s exclusively reconstructed accompanied by a large momentum hadron of opposite electric charge emitted in the same hemisphere. Using this sample, the B_s^0 lifetime and the lifetime difference between the two physical B_s^0 states have been also measured. This note updates the contribution sent to 1998 Summer Conferences [3]

For the last two studies, two complete papers are jointed to this short note.

2 Combination of the analyses

DELPHI has performed four analyses on Δm_s using $D_s - \ell$ candidates, events containing a high p_t lepton, $D_s^{\pm}h^{\mp}$ and exclusively reconstructed B_s^0 mesons. These analyses have been combined, taking into account correlations between the events samples and between systematic uncertainties in the different amplitude measurements (Figure 1). This gives the following allowed intervals for Δm_s:

$$\Delta m_s \ > \ 5.0 \ ps^{-1} \text{ at } 95\% \text{ C.L.}$$
$$\text{with a sensitivity equal to } 9.7 \text{ ps}^{-1}$$

(with statistical errors only the limit would be the same and the sensitivity would increase at $\Delta m_s = 10.0$ ps^{-1}.) The variations, with Δm_s, of the exclusion probability and of the error on the amplitude are given in Figure 2.
The B_s lifetime and the lifetime difference between the two physical B_s states, measured in the $D_s^{\pm}\ell^{\mp}$ and $D_s^{\pm}h^{\mp}$ samples, have been also combined. The result is :

$$\tau(B_s^0) = (1.46 \pm 0.11) \text{ ps}$$

$$\Delta\Gamma_{B_s}/\Gamma_{B_s} < 0.42 \text{ at } 95\% \text{ C.L.}$$

The $\Delta\Gamma_{B_s}/\Gamma_{B_s}$ probability distribution is shown in Figure 3. In this last result it has been assumed that $\tau_{B_s^0} = \tau_{B_d}$.

References

[1] (DELPHI Coll.) " Study of $B_s^0 - \overline{B_s^0}$ oscillations using inclusive leptons with large P_t ", ICHEP'98 # 236 and DELPHI 98-132 CONF 193

[2] (DELPHI Coll.) " Study of $B_s^0 - \overline{B_s^0}$ oscillations and B_s^0 lifetime using $D_s - \ell$ events ", ICHEP'98 # 235 and DELPHI 98-131 CONF 192

[3] (DELPHI Coll.) " Study of $B_s^0 - \overline{B_s^0}$ oscillations using exclusively reconstructed B_s^0 and $D_s^{\pm}$ events", ICHEP'98 # 237 and DELPHI 98-133 CONF 194

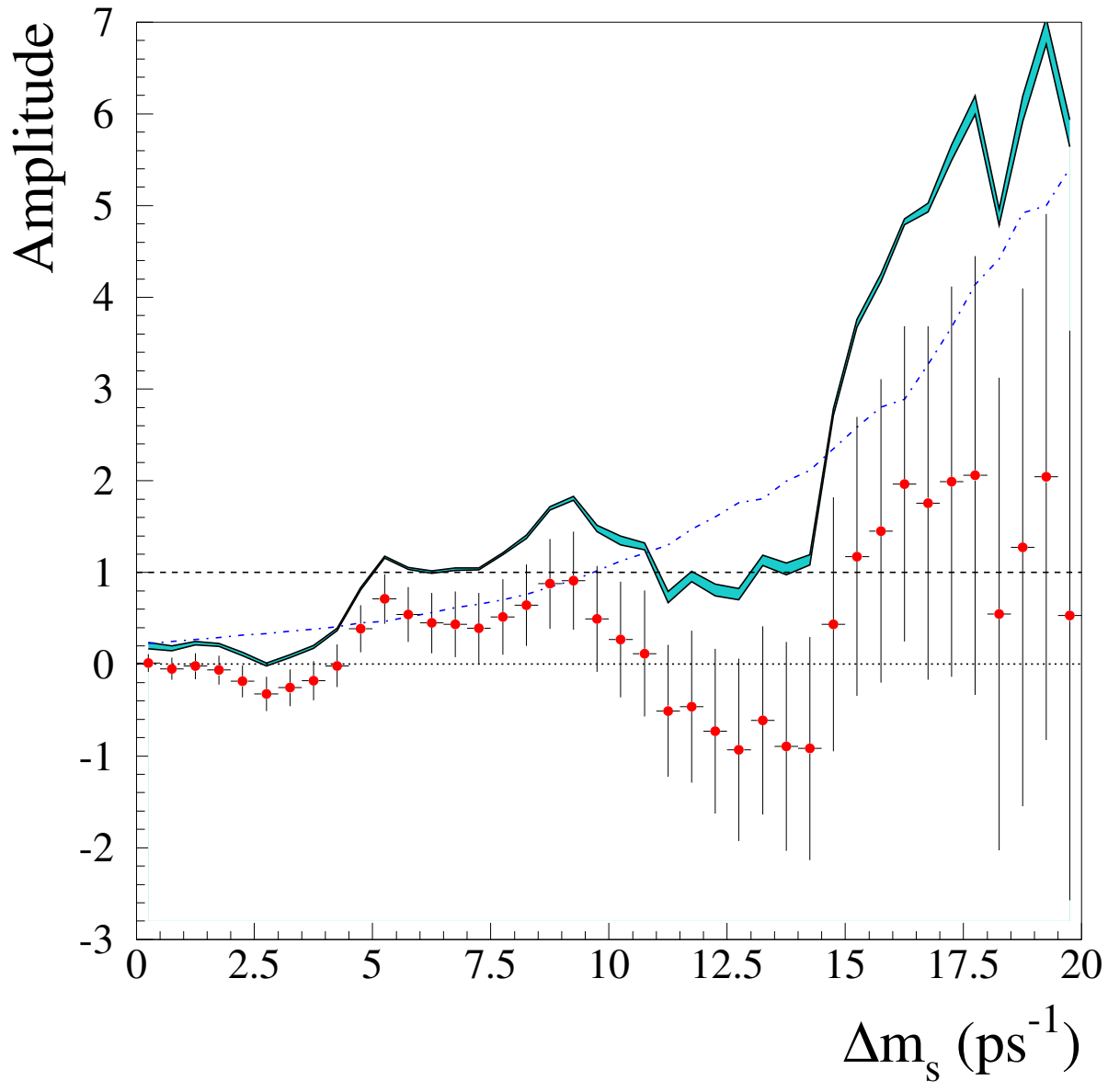

Figure 1: *DELPHI combined Δm_s analyses : variation of the oscillation amplitude A as a function of Δm_s. The lower continuous line corresponds to $A + 1.645\ \sigma_A$ where σ_A includes statistical uncertainties only, while the shaded area shows the contribution from systematics. The dashed-dotted line corresponds to the sensitivity curve. The lines at A=0 and A=1 are also given.*

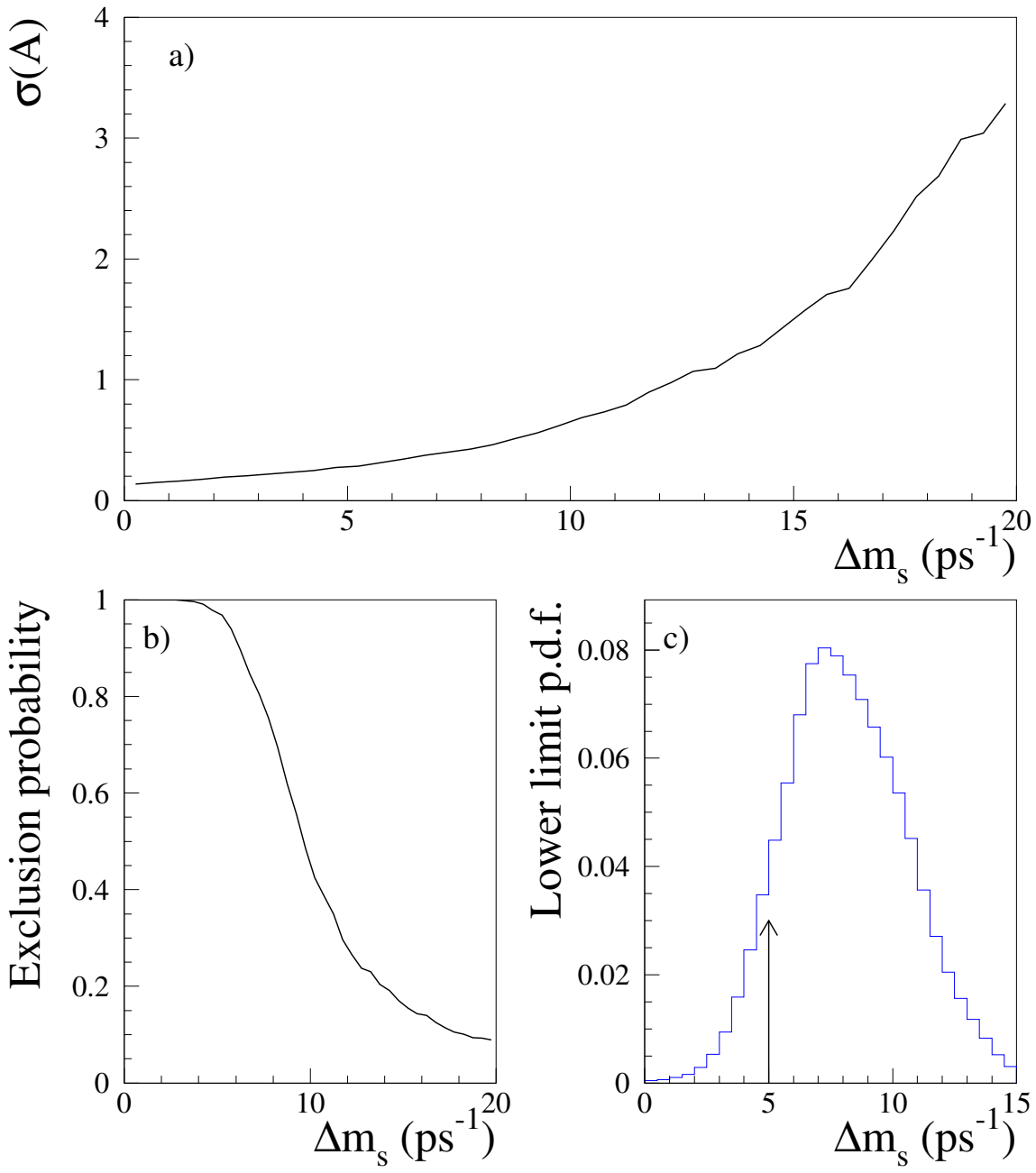

Figure 2: *DELPHI combined Δm_s analyses: a) variation of the error on the amplitude as a function of Δm_s, b) exclusion probability vs. Δm_s, c) lower limit probability density vs. Δm_s.*

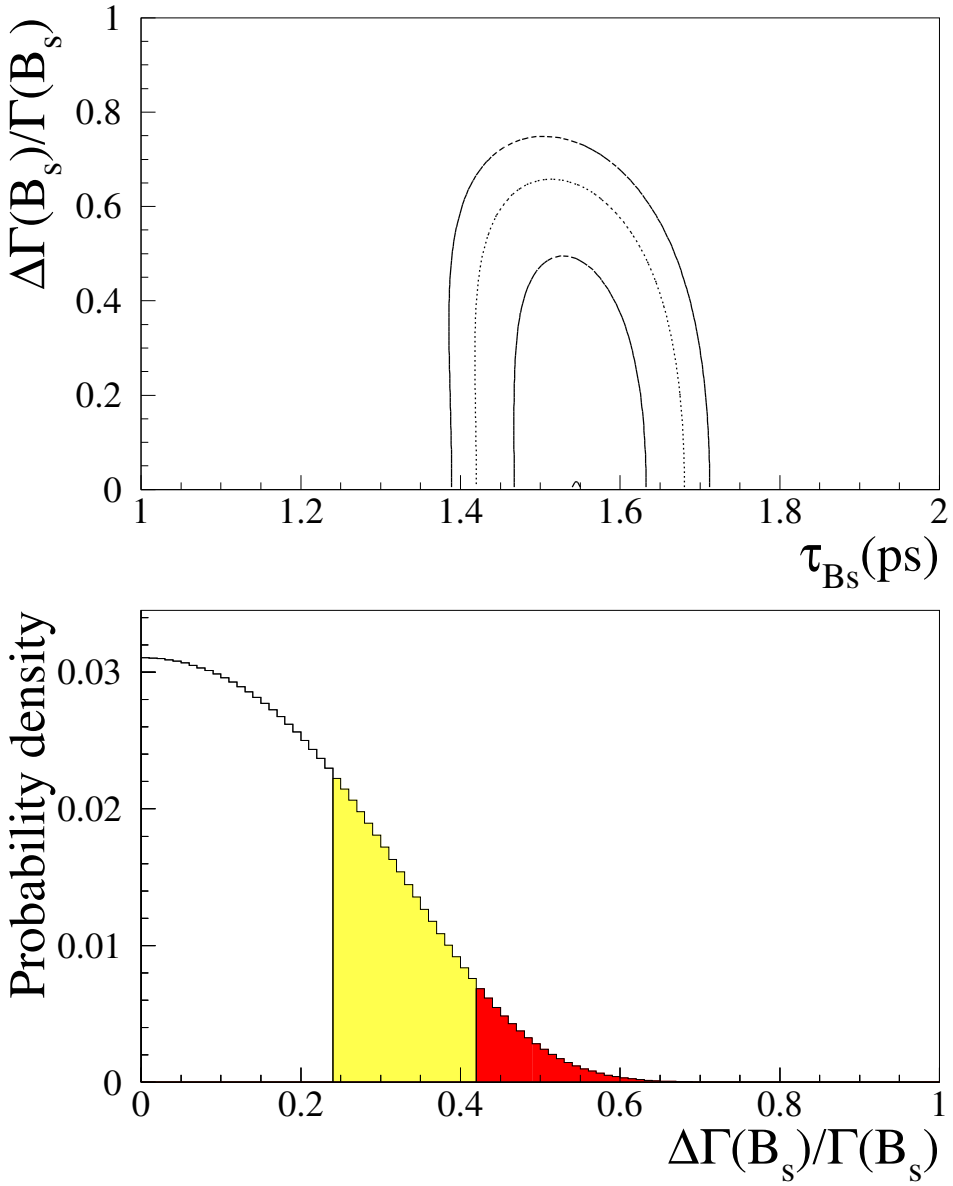

Figure 3: *Upper plot: contours corresponding to 68, 95 and 99 % C.L. of the negative log-likelihood in the plane* $\Delta\Gamma_{B_s}/\Gamma_{B_s}$-$\tau_{B_s^0}$. *Lower plot: probability density distribution for* $\Delta\Gamma_{B_s}/\Gamma_{B_s}$*; the two shaded regions show the limits at 68 % C.L. and 95 % C.L. respectively.*

Study of $B_s^0 - \overline{B_s^0}$ oscillations using exclusively reconstructed B_s^0 and $D_s^{\pm}h^{\mp}$ events

Preliminary

DELPHI Collaboration

Abstract

Oscillations of B_s^0 mesons have been studied using a sample of exclusively reconstructed B_s^0 decays, selected from about 3.5 million hadronic Z^0 decays registered by DELPHI between 1992 and 1995. $B_s^0 \to D_s^- \pi^+ (a_1^+)$ where the D_s is reconstructed in six decay channels and $B_s^0 \to \overline{D}^0 K^- \pi^+ (a_1^+)$ where the $\overline{D}^0$ is reconstructed in two decay channels have been used. In addition $B_s^0 - \overline{B_s^0}$ oscillations have been studied in events with a D_s exclusively reconstructed accompanied, in the same hemisphere, by a large momentum hadron of opposite electric charge. Combining the two analyses, a limit on the mass difference between the physical B_s^0 states has been obtained :

$$\Delta m_s > 4.0 \text{ ps}^{-1} \text{ at } 95\% \text{ C.L.}$$
$$\text{with a sensitivity of } \quad \Delta m_s = 3.2 \text{ ps}^{-1}$$

Using the last sample of events, the B_s^0 lifetime and the lifetime difference between the two physical B_s^0 states have been also measured :

$$\tau(B_s^0) = 1.49^{+0.16}_{-0.15}(\text{stat.})^{+0.07}_{-0.08}(\text{syst.}) \text{ ps}$$

$$\Delta\Gamma_{B_s^0}/\Gamma_{B_s^0} < 0.58 \text{ ps at } 95\% \text{ C.L.}$$

1 Introduction

A measurement or even a limit on the $B_s^0 - \overline{B_s^0}$ oscillation frequency, Δm_s, allows to restrict the accessible domain for the ρ and η parameters of the CKM matrix. At present it can be shown that, in the Standard Model, the 68% confidence limit range for Δm_s is between 10.2 ps^{-1} and 17.6 ps^{-1} [1].
The search for $B_s^0 - \overline{B_s^0}$ oscillations has been the subject of an intense activity during the last years. No signal has been observed so far and the lower limit on the oscillation frequency comes from the combination of the results obtained at LEP and by the CDF and SLD experiments: $\Delta m_s > 12.4\ ps^{-1}$ at $95\% C.L.$ [2]. The sensitivity of present measurements is at 13.8 ps^{-1}. These results have been obtained by combining analyses which select various B_s^0 decay channels. Some analyses use events containing simply a lepton emitted at large p_t relative to its jet axis. In this case, the proper time is measured using an inclusive vertex algorithm to reconstruct the decay distance and the energy of the B hadron candidate. In other analyses, like $D_s^{\pm}\ell^{\mp}$, the identified lepton is accompanied, in the same hemisphere, by an exclusively reconstructed D_s. In $D_s^{\pm}h^{\mp}$ analyses the lepton is replaced by a charged hadron.

Progress, in the near future is expected to come from improved analyses of these channels, but the sensitivity at high frequency is essentially limited by the damping of the reconstructed oscillation amplitude due to the limited resolution on the B_s^0 proper time. In a simplified approximation (convolution of the physics function and of a Gaussian distribution for the time resolution), the damping is given by the following expression:

$$damping = e^{-(\Delta m_s \sigma_t)^2/2} \quad , \quad \sigma_t = \sqrt{a^2 + (\sigma_P/P)^2 \times t^2} \tag{1}$$

where a is related to the decay distance resolution and σ_P/P is the relative error on the momentum reconstruction. Exclusive (completely reconstructed) decays have a better time resolution for two reasons. As there is no missing particle in the decay, the B_s^0 momentum is known with good precision, and therefore the contribution of the momentum uncertainty to the proper time resolution is negligible. In addition the reconstructed channels are 2-body or quasi 2-body decay channels, with an opening angle of their decay products which is on average larger than in multi-body final states; this results in a better accuracy on their decay position determination. The first part of the paper describes an analysis of B_s^0-$\overline{B_s^0}$ oscillations from a sample of 44 B_s^0 candidates: 11 candidates (including 30% background) are completely reconstructed, and 33 candidates (including 55% background) are partially reconstructed with missing low energy π^0 or/and γ. The second part of the paper describes the $D_s^{\pm}h^{\mp}$ analysis which allows, in addition, to measure the the B_s^0 meson lifetime and to set a limit on the difference between the decay widths of the physical B_s^0 states, $\Delta\Gamma_{B_s^0}/\Gamma_{B_s^0}$. These samples have been selected from about 3.5M hadronic Z^0 registered by DELPHI between 1992 and 1995.

2 Evaluation of B_s^0 branching fractions

In this paper B_s^0 mesons have been reconstructed in $D_s^-\ \pi^+(a_1^+)$ and $\overline{D}^0 K^-\pi^+(a_1^+)$ decay channels. Contributions to the mass spectrum can come also from other decay channels as $D_s^{*-}\pi^+$, $D_s^{*-}a_1{}^+$, $\overline{D^*}(2007)^0K^-\pi^+$, $\overline{D^*}(2007)^0K^-a_1{}^+$, $D_s^-\rho^+$ and $D_s^{*-}\rho^+$ where the cascade photon or neutral pion has not been reconstructed. All corresponding branching fractions

are unmeasured. To evaluate the two-body ($D^*\pi(a_1)$) branching fractions for B_s^0 mesons the equivalent decay channels for non-strange mesons have been used. The decay channels : $B_d^0 \to D^-\pi^+$ and $B_d^0 \to D^{*-}\pi^+$ have been measured [3] and found to be $(3.0 \pm 0.4) \times 10^{-3}$ and $(2.8 \pm 0.3) \times 10^{-3}$ respectively which indicates the equivalence of the branching ratios of the two-body decays containing D or D^* mesons. Using this fact and the measured values, the branching ratios of $B_d^0 \to D^- {a_1}^+$ and $B_d^0 \to D^{*-} {a_1}^+$ decays are estimated to be equal and three times larger than the equivalent decay channels with pions.
The branching ratios $Br(B_s^0 \to D_s^- \rho^+)$ are also evaluated using the equivalent channels in the non-strange sector. Analog considerations are applied to the three body decays ($D^{(*)}K\pi(a_1)$) using the measurement of the $Br(B_d^0 \to \overline{D}^0 \pi^- \pi^+ + \overline{D}^0 \pi^- {a_1}^+)$ which is described in this paper. Table 1 gives the evaluations of several branching ratios of interest for this paper.

B_s^0 decay channel	Estimated Br
$Br(B_s^0 \to {D_s}^{(*)-}\pi^+)$	$(3.0 \pm 0.4) \times 10^{-3}$
$Br(B_s^0 \to {D_s}^{(*)-} {a_1}^+)$	$(9.0 \pm 3.3) \times 10^{-3}$
$Br(B_s^0 \to D_s^{(*)-}\rho^+)$	$(7.4 \pm 1.3) \times 10^{-3}$
$Br(B_s^0 \to \overline{D^{(*)}}(2007)^0 K^-\pi^+)$	$(0.9 \pm 0.5) \times 10^{-3}$
$Br(B_s^0 \to \overline{D^*}(2007)^0 K^- {a_1}^+)$	$(2.7 \pm 1.4) \times 10^{-3}$

Table 1: *Values of the* B_s^0 *branching ratios used in the current analysis.*

3 Completely reconstructed B_s^0 decays

3.1 Event Sample

Events have been selected using the following decay channels [1] :

$B_s^0 \to D_s^-\pi^+$ $\quad D_s^- \to \phi\pi^-, \phi\pi^-\pi^+\pi^-, f(980)\pi^-, K_s^0 K^-, K^{\star 0}K^-, K^{\star 0}K^{\star -}$
$B_s^0 \to D_s^- a_1^+$ $\quad D_s^- \to \phi\pi^-, K^{\star 0}K^-$
$B_s^0 \to \overline{D}^0 K^-\pi^+$ $\quad \overline{D}^0 \to K^+\pi^-, K^+\pi^-\pi^+\pi^-$
$B_s^0 \to \overline{D}^0 K^- a_1^+$ $\quad \overline{D}^0 \to K^+\pi^-, K^+\pi^-\pi^+\pi^-$

where the ϕ , K_s^0 , $f(980)$, $K^{\star 0}$, $K^{\star -}$ and a_1 are reconstructed in their charged decay channels : $\phi \to K^+K^-$, $K_s^0 \to \pi^+\pi^-$, $f(980) \to \pi^+\pi^-$, $K^{\star 0} \to K^+\pi^-$, $K^{\star -} \to K_s^0\pi^-$ and ${a_1}^+ \to \rho^0\pi^+$, $\rho^0 \to \pi^+\pi^-$. K mesons have been identified using the RICH and dE/dx informations and have been classified as "super tight", "tight", "standard", "loose" or "very loose" [5]. All particles which have not been explicitly identified as protons, kaons or leptons, have been classified as pions. D_s and D^0 mesons have been reconstructed considering tracks in the same hemisphere with at least 1 VD hit. Charmed D mesons candidates have been accepted if their mass is within the intervals $(1.93 - 2.01)\ GeV/c^2$ for D_s and $(1.83 - 1.90)\ GeV/c^2$ for D^0 candidates. The D's decay length has been imposed

[1] Unless explicitly stated otherwise, charge conjugate states are always implied.

to be positive and the χ^2–probability of the fitted vertex to be larger than 10^{-5} (10^{-3} for the $D^0 \to K\pi\pi\pi$ decay). Detailed selection criteria have been used for different decay channels; they are described in the following.

• $\underline{D_s^- \to \phi\pi^-}$

The ϕ meson has been reconstructed in the decay mode $\phi \to K^+K^-$ by taking all possible pairs of oppositely charged tracks if at least one of them has been identified as at least a "very loose" kaon. The invariant mass of these pairs has to be within $\pm$ 12 MeV/c^2 of the nominal ϕ mass value [3]. The momenta of all three tracks have been requested to be above 1 GeV/c. Since the pseudoscalar D_s meson decays into a vector (ϕ) and a pseudoscalar meson (π), because of helicity conservation, the angle ψ, measured in the vector meson rest frame, between the directions of its decay products and of the pseudoscalar π, has a $cos^2\psi$ distribution. The value of $|\cos(\psi)|$ has to be larger than 0.3.

•$\underline{D_s^- \to \phi\pi^-\pi^+\pi^-}$

The ϕ meson reconstruction is the same as in the previous channel. The momenta of all three π mesons have to be larger than 0.6 GeV/c.

•$\underline{D_s^- \to f(980)\pi^-}$

The $f(980)$ meson has been reconstructed in the decay mode $f(980) \to \pi^+\pi^-$ by taking all possible pairs of oppositely charged tracks classified as pions. This channel suffers from a huge combinatorial background which has been reduced by selecting candidates having an invariant $\pi\pi$ mass within 15 MeV/c^2 of the nominal $f(980)$ mass [3] and a total momentum larger than 8 GeV/c. The momenta of all three π mesons have to be larger than 1 GeV/c.

•$\underline{D_s^- \to K_s^0K^-}$

K_s^0 mesons have been reconstructed in the decay $K_s^0 \to \pi^+\pi^-$ by combining all pairs of tracks of opposite electric charge and applying the "tight" selection criteria described in [5]. The decay length of K_s^0 candidates has to be positive and their momentum to be larger than 2.5 GeV/c. The momentum of the bachelor charged track, identified at least as a "very loose" kaon, has to be larger than 1 GeV/c^2.

•$\underline{D_s^- \longrightarrow K^{\star 0}K^-}$

The $K^{\star 0}$ meson has been reconstructed in the charged decay mode $K^{\star 0} \to K^+\pi^-$ by taking all possible pairs of oppositely charged tracks with at least one identified as a "very loose" kaon. The momenta of both particles have to be larger than 1 GeV/c and the invariant mass of the pair has to be within $\pm$ 40 MeV/c^2 of the nominal $K^{\star 0}$ mass [3]. The value of $|\cos(\psi)|$ (see the $D_s^- \to \phi\pi^-$ reconstruction) has to be larger than 0.3. The momentum of the bachelor track has to exceed 2.5 GeV/c, and, because of the large combinatorial background, this particle has to be identified, at least, as a "loose" kaon.

•$\underline{D_s^- \longrightarrow K^{\star 0}K^{\star -}}$

The $K^{\star 0}$ meson has been reconstructed in the charged decay mode $K^{\star 0} \to K^+\pi^-$ by taking all possible pairs of oppositely charged tracks with at least one identified as a "very loose" kaon. The invariant mass of these pairs has to be within $\pm$ 60 MeV/c^2 of the nominal $K^{\star 0}$ mass [3]. The $K^{\star -}$ meson has been reconstructed in the decay mode $K^{\star -} \to K_s^0\pi^-$.

The K_s^0 meson reconstruction has been discussed previously. The invariant mass of $K^{\star -}$ candidates has to be within $\pm$ 60 MeV/c^2 of the nominal $K^{\star -}$ mass [3]. The decay length of K_s^0 candidates has to be positive and their momenta to be above 2.5 GeV/c. The momentum of charged kaons and pions (including pions from K_s^0) has to be larger than 1 GeV/c.

•$\overline{D}^0 \to K^+\pi^-$, $\overline{D}^0 \to K^+\pi^-\pi^+\pi^-$

The $\overline{D}^0$ meson of the two-prongs decay mode has been reconstructed by combining a kaon candidate identified, at least, with the "loose"criteria with an oppositely charged pion with momentum larger than 1 GeV/c. The $\overline{D}^0$ meson of the four-prong decay mode has been reconstructed by combining a kaon candidate identified, at least, with the "standard"criteria with three pions, each of them having a momentum larger than 0.5 GeV/c. In order to reduce the combinatorial background, the kaon momentum has been requested to be above 2.5 GeV/c and the $\overline{D}^0$ momentum candidate to be above 10 GeV/c.

Selected charmed D mesons have been used to reconstruct B_s^0 candidates by fitting a common vertex for the $D_s\pi$, $D_s a_1$, $D^0K\pi$ or D^0Ka_1 systems. The π momentum has to be larger than 4 GeV/c. a_1 candidates have been reconstructed using the combination of three pions with momenta larger than 0.8 GeV/c and with an invariant mass situated within the interval $(0.95-1.50)$ GeV/c^2. At least one of the two $\pi^+\pi^-$ combinations must have an invariant mass within $\pm$ 150 MeV/c^2 of the nominal ρ mass [3].
The a_1 momentum has to be larger than 5 GeV/c (6 GeV/c for candidates where $D^0 \to K^-\pi^+\pi^-\pi^+$). For all candidates, the D meson decay distance, relative to the B vertex has to be positive. Events with an estimated error on the B_s^0 decay distance larger then 250 μm or those having a χ^2 vertex probability lower than 10^{-3} have been removed. In order to reduce the combinatorial background from charm and light quarks the b-tag probability[2] for the whole event and for the hemisphere opposite to the reconstructed B meson have to be smaller than 0.1 [6]. Additional cuts, which depend on the B_s^0 decay channel have been applied, mainly for $\overline{D^0}$ decays which suffer from a larger combinatorial background than for D_s^- candidates.

•$B_s^0 \to D_s^-\pi^+$, $B_s^0 \to D_s^- a_1^+$

The momentum of the B_s^0 has to be larger than 22 GeV/c. For $B_s^0 \to D_s^- {a_1}^+$ candidates, only the combination with the highest B_s^0 momentum has been kept.

•$B_s^0 \to \overline{D^0}K^-\pi^+$, $B_s^0 \to \overline{D^0}K^- a_1^+$

For $B_s^0 \to \overline{D^0}K^-\pi^+$ decays, the B_s^0 momentum has to be larger than 27 GeV/c, for $B_s^0 \to \overline{D^0}K^- a_1^+$ the B_s^0 momentum has to be larger than 29 GeV/c, for $\overline{D^0} \to K^+\pi^-$, and larger than 33 GeV/c, for $\overline{D^0} \to K^+\pi^-\pi^+\pi^-$ decay channels. In each event, only the candidate with the highest B_s^0 momentum has been kept. The momentum of the bachelor kaon, identified at least as "standard", the momentum has to be larger than 2 GeV/c.

The mass spectrum, obtained by summing up the contributions from the different

[2]This variable is related to the probability that the track originate from the beam interaction point owing to their measured impact parameters. Small values for this variable tag events containing B-hadrons.

channels is shown in Figure 1-a. The data are indicated with points and error bars, and the result of the fit has been superimposed. The mass distribution in the signal region has been fitted using two Gaussian distributions of different widths to account for the exclusive B_s^0 signal (main narrow peak) and for the presence of partially reconstructed B_s^0 decays (satellite wider peak). It has been assumed that the satellite peak is composed of the following decay channels: $D_s^{*-}\pi^+$, $D_s^{*-}{a_1}^+$, $\overline{D^*}(2007)^0K^-\pi^+$, $\overline{D^*}(2007)^0K^-{a_1}^+$, $D_s^-\rho^+$ and $D_s^{*-}\rho^+$ where the cascade photon or neutral pion (or both) have not been reconstructed. In the simulation it has been verified that the mass distribution of the satellite peak can be described by a Gaussian distribution as shown in Figure 2. The central values and the widths of the Gaussian distributions (main and satellite peaks) in Figure 1-a have been left free to vary in the fit. The combinatorial background has been fitted using an exponential function with a slope fixed according to the simulation. This slope has been verified in several ways. Using 2.9 million $b\overline{b}$ and 5.3 million $q\overline{q}$ simulated events, the expected mass spectrum has been obtained after having removed the B_s^0 contribution in the signal mass region. The sum of the contribution from b events, charm events and light quark events is shown in Figure 1-a and is in agreement with the one obtained in data. Two further checks have been performed, using events selected in the side-bands of the D_s^- and $\overline{D^0}$ candidates (Figure 1-b) and from wrong sign combinations (Figure 1-c). Both these distributions are in agreement with the evaluation of the background obtained by fitting the data.

Main peak					
Data set	Mass GeV/c^2	Width GeV/c^2	N_{events}	Comb. bkg %	Reflection %
Real Data	5.373 ± 0.016	0.029 ± 0.012	8 ± 4	27 ± 16	-
simulation	5.370	0.037 ± 0.002	5 ± 1	-	6 ± 3
Satellite peak					
Real Data	5.050 ± 0.054	0.111 ± 0.054	15 ± 8	55 ± 13	-
simulation	5.099 ± 0.007	0.148 ± 0.007	10 ± 2	-	12 ± 6

Table 2: *Characteristics of the B_s^0 signals and comparison with the simulation. The expected numbers of events have been calculated taking into account the different branching fractions as given in Section 2 and the corresponding reconstruction efficiencies. These efficiencies vary from $(0.2 \pm 0.1)\%$ for the $B_s^0 \to \overline{D^0}K^-{a_1}^+$, with $\overline{D}^0 \to K^+\pi^-\pi^+\pi^-$ decay channel, up to $(10.2 \pm 0.8)\%$ for the $B_s^0 \to D_s^-\pi^+$, with $D_s^- \to \phi\pi^-$ decay channel. The fitted or expected number of signal events and the fraction of combinatorial background are given inside a mass window corresponding, respectively, to $\pm 3\sigma$ and $\pm 2\sigma$ for the main and satellite peaks.*

The fit to the mass distribution yielded a signal of (8 ± 4) B_s^0 decays in the main peak and 15 ± 8 events in the satellite peak. Table 2 gives the characteristics of the observed signals and the comparison with simulation.

3.2 Reflections from B_d^0 and $\overline{\Lambda}_b^0$ decays

For several B_s decay channels a possible physical background originates in non strange B decays when one of the pions or proton has been misidentified as a kaon (kinematical reflections). The main decay channels are $B_d^0 \to D^-\pi^+(a_1)$, $D^- \to \overline{K}^{\star 0}\pi^-$ (which can contribute to $B_s^0 \to D_s^-\pi^+(a_1)$, $D_s^- \to \overline{K}^{\star 0}K^-$ candidates) and from $B_d^0 \to \overline{D}^0\pi^-\pi^+$, $\overline{D}^0 \to K^+\pi^-$ (which can contribute to $B_s^0 \to \overline{D}^0K^-\pi^+$, $\overline{D}^0 \to K^+\pi^-$ and $\overline{D}^0 \to K^+\pi^-\pi^+\pi^-$ candidates). In the mass region of the main peak, 0.32 ± 0.13 events are expected to originate from B_d^0 kinematical reflections, with an additional 20% contribution from $\overline{\Lambda_b^0}$ decays. These estimates have been obtained using dedicated Monte-Carlo samples of B_d^0 and $\overline{\Lambda_b^0}$ events passed through the full reconstruction algorithms and satisfying the selection criteria. The corresponding uncertainties come from the limited knowledge of the considered branching fractions and from simulated events statistics.
To study the contribution, in the satellite peak, of events from kinematical reflections, the same decay processes have been considered with, in addition, channels in which the D meson is accompanied by a ρ. This gives 1.2 ± 0.7 events.
In order to look for possible signal coming from kinematical reflections, in real data, B_s^0 candidates have been considered in turn as B_d^0 or $\overline{\Lambda}_b^0$ hadrons by changing the kaon into a pion or a proton respectively. The obtained mass distributions are similar with those expected from genuine simulated B_s^0 mesons and do not show any accumulation of events in the B_d^0 or $\overline{\Lambda}_b^0$ mass regions.

3.3 Reconstruction of non strange B meson decays

Non strange B mesons, decaying into a $\overline{D}^0$ and a small number of pions, have been reconstructed in order to verify the B_s^0 reconstruction algorithms. The $B^+ \to \overline{D}^0\pi^+$ and $B_d^0 \to D^*(2010)^-\pi^+$ decay channels have a similar topology as the $B_s^0 \to D_s^-\pi^+$ channel. The obtained mass distributions are shown in Figures 3-a and 3-b. They have been fitted using a Gaussian function for the signal, of $\sim 50\ MeV/c^2$ width as determined from the simulation, and using an exponential function for the combinatorial background. An additional Gaussian function has been used to account for the signal from the $B^+ \to \overline{D^*}(2007)^0\pi^+$ decay where the photon (π^0) from the $\overline{D^{*0}}$ decay has not been reconstructed. B_d^0 decay channels including an a_1 meson have also been reconstructed. The $B_d^0 \to D^*(2010)^-{a_1}^+$ decay channel should be kinematically similar to $B_s^0 \to D_s^-{a_1}^+$. The corresponding mass spectrum is shown in Figure 3-c. The main selection criteria which have been imposed are rather similar to those used in the B_s^0 analysis. The informations relevant to these reconstructed channels are given in Table 3. The numbers of observed events are in agreement with expectations.

Finally two B_d^0 decay channels, which are not yet well established, have been considered: $B_d^0 \to \overline{D^0}\pi^-\pi^+$, $B_d^0 \to \overline{D^0}\pi^-{a_1}^+$.
They are analogous to the $B_s^0 \to \overline{D}^0K^-\pi^+$ and $B_s^0 \to \overline{D}^0K^-{a_1}^+$ decays, in the strange B sector. B_d^0 mesons have been reconstructed using the same selection criteria as for the corresponding B_s^0 decay channel but replacing a K meson by π. All particles, not explicitly identified as protons or kaons have been accepted as pions. Finally in order to remove the $B_d^0 \to D^*(2010)^-\pi^+$ and $B_d^0 \to D^*(2010)^-{a_1}^+$ contamination, candidates satisfying $M(\overline{D}^0\pi) - M(\overline{D}^0) > 0.16$ GeV/c^2 have been required.

Channel	B meson mass (GeV/c^2)	N_{obs}	N_{exp}
$B^+ \to \overline{\mathrm{D}}^0\pi^+$	5.283 ± 0.015	29 ± 8	~ 28
$\mathrm{B_d^0} \to \mathrm{D^*(2010)^-}\pi^+$	5.266 ± 0.024	9 ± 4	~ 5
$\mathrm{B_d^0} \to \mathrm{D^*(2010)^-a_1}^+$	5.300 ± 0.019	5 ± 3	~ 5
$\mathrm{B_d^0} \to \overline{\mathrm{D}}^0\pi^-\pi^+(\mathrm{a_1}^+)$	5.287 ± 0.024	8 ± 4	–

Table 3: *Characteristics of the B non-strange signals and comparison with expected rates from simulation.*

Figure 4-a shows the mass distribution for these two decay channels. It has been fitted using an exponential function for the background and two Gaussian distributions for the signals corresponding to the main and satellite peaks, with respective widths equal to ~ 34 MeV/c^2 and ~ 60 MeV/c^2, as obtained from the simulation. The position of the wider Gaussian, corresponding to $\mathrm{B_d^0} \to \overline{\mathrm{D^*}}(2007)^0\pi^-\pi^+$ and $\mathrm{B_d^0} \to \overline{\mathrm{D^*}}(2007)^0\pi^-\mathrm{a_1}^+$ signals with not reconstructed π^0 or γ, and the slope of the background exponential function have been also taken from the simulation. The number of observed events can be translated into a branching ratio : $Br(\mathrm{B_d^0} \to \overline{\mathrm{D^{(*)}}}^0\pi^+\pi^-(\mathrm{a_1}^-)) = (3.6 \pm 1.8) \times 10^{-3}$. For this evaluation it has been assumed (see Section 2) that the decay channel with an a_1 is produced with a rate which is three times larger than the channel with a π.

4 The algorithm for tagging at production time.

The signature of the initial production of a $b(\overline{b})$ quark in the jet containing the $\mathrm{B_s^0}$ or $\overline{\mathrm{B_s^0}}$ candidate has been determined using a combination of different variables sensitive to the initial quark state. For each individual variable X_i, the probability density functions $f_b(X_i)$ ($f_{\overline{b}}(X_i)$) for b ($\overline{b}$) quarks have been built and the ratio $R_i = f_{\overline{b}}(X_i)/f_b(X_i)$ has been computed. The combined tagging variable is defined as:

$$x_{tag} = \frac{1-R}{1+R} \quad , \text{ where } \quad R = \prod R_i. \tag{2}$$

The variable x_{tag} varies between -1 and 1. High values of x_{tag} correspond to a high probability that a given hemisphere contains a b quark in the initial state.

A set of nine discriminant variables has been selected for this analysis. One set (three variables) is determined in the hemisphere which contains the $\mathrm{B_s^0}$ meson, the other set (five variables) in the hemisphere opposite to the $\mathrm{B_s^0}$ meson, and one variable is common to both hemispheres. Details concerning the definition of these variables and the method are given in [4].

4.1 Tagging procedure

An event has been classified as a mixed or as an unmixed candidate according to the sign, Q_D, of the $\mathrm{D_s}$ electric charge for decay channels containing a $\mathrm{D_s}$ meson or according to the sign of the kaon for $\overline{\mathrm{D}}^0\mathrm{K}^-\pi^+$ decay channels, relative to the sign of x_{tag} variable. Mixed

candidates are defined by requiring $x_{tag} \times \mathrm{Q}_D < 0$, and unmixed candidates correspond to $x_{tag} \times \mathrm{Q}_D > 0$. The probability, ϵ_b^{tag}, for tagging correctly the b or $\bar{b}$ quark, from the measurement of x_{tag}, is evaluated using a dedicated simulated event sample and is found to be (74.5±0.5)%.
The corresponding probability for events in the combinatorial background is obtained using real data candidates selected in the wings of the D signal: the probabilities to classify these events as mixed or unmixed candidates are called ϵ_{bkg}^{mix} and ϵ_{bkg}^{unmix}, respectively.

5 Proper time resolution

For each event, the $\mathrm{B_s^0}$ proper decay time is obtained from the measured decay length ($L_{\mathrm{B_s^0}}$) and the estimate of the $\mathrm{B_s^0}$ momentum ($p_{\mathrm{B_s^0}}$). The measured position of the $\mathrm{D_s^+}$ or $\mathrm{D^0}$ decay vertex, the momentum, and the corresponding measurement errors, have been used to reconstruct a $\mathrm{D_s^+}$ or a $\mathrm{D^0}$ particle. A candidate $\mathrm{B_s^0}$ decay vertex is obtained by intercepting the trajectory of this particle with the other charged tracks which are supposed to come from the $\mathrm{B_s^0}$ decay vertex.
For the main peak, the $\mathrm{B_s^0}$ momentum, $\mathrm{p_{B_s^0}}$, is precisely known since all decay products are reconstructed.
For the satellite peak, this is no longer true, because there are one or two undetected neutral(s)(π^0 and/or γ) in the $\mathrm{B_s^0}$ decay. As discussed previously in Section 3.1, the satellite peak is assumed to be composed by $\mathrm{D_s^{*-}}\pi^+$, $\mathrm{D_s^{*-}a_1}^+$, $\mathrm{D_s^-}\rho^+$, $\mathrm{D_s^{*-}}\rho^+$ and $\overline{\mathrm{D^*}}(2007)^0\mathrm{K^-a_1}^+$ decays. The first four decay channels give $\mathrm{D_s^-}\pi^+(\mathrm{a_1}^+)$ and the last two channels give $\overline{\mathrm{D^0}}\mathrm{K^-}\pi^+(\mathrm{a_1}^+)$ final states. The kinematic fits have been performed assuming that the missing γ is coming from the $\mathrm{D_s^{*-}}$ or $\overline{\mathrm{D^{*0}}}$ mesons. This is a good approximation also for decay channels containing a ρ^+ meson. Mass constrained fits have been performed on events situated in the mass region corresponding to $\pm$ 2 σ of the fitted mass of the satellite peak.
As shown in Table 4, the time resolution for events in the satellite peak is only slightly worse than for those belonging to the main peak.

Except for the combinatorial background contribution, the predicted proper time distributions have been obtained by convoluting the theoretical functions with resolution functions evaluated from simulated events. Due to the different decay length resolutions (for the two Vertex Detector configurations), proper time resolutions have been used for data samples registred in 92-93 and 94-95, respectively. The proper time resolution is defined as the difference between the generated time (t) and the reconstructed time (t_i). The following parametrization has been used:

$$R(t - t_i) = (1 - f_2)G(t - t_i, \sigma_1) + f_2 G(t - t_i, \sigma_2)$$

where $\sigma_1 = \sqrt{\sigma_{L1}^2 + \sigma_{P1}^2 t^2}$ and $\sigma_2 = \sqrt{\sigma_{L2}^2 + \sigma_{P2}^2 t^2}$.
The values of the corresponding parameters, obtained from simulated events, are given in Table 4.

The time distribution $\mathcal{P}_{bkg}(t_i)$ for the combinatorial background, under the main peak, is obtained from real data, by fitting the time distribution of wrong-sign and right-sign events situated in the side-bands of the $\mathrm{B_s^0}$ mass distribution. It has been verified in the simulation that the time distribution for these classes of events is very similar to the

Main peak				
Decay channels	Year	$\sigma_1(ps)$	$\sigma_2(ps)$	f_2
all B_s^0 channels	(92-93)	0.068	0.18	0.27
all B_s^0 channels	(94-95)	0.065	0.12	0.42
Satellite peak				
$D_s^{*-}\pi^+(a_1^+)$, $D^{*0}K\pi^+(a_1^+)$	(92-93)	0.066	0.15	0.48
$D_s^{*-}\pi^+(a_1^+)$, $D^{*0}K\pi^+(a_1^+)$	(94-95)	0.081	0.17	0.30
$D_s^-\rho^+$, $D_s^{*-}\rho^+$	(92-93)	0.085	0.21	0.65
$D_s^-\rho^+$, $D_s^{*-}\rho^+$	(94-95)	0.092	0.20	0.57

Table 4: *Proper time resolution for the two different configurations of the Vertex Detector. and for the different analysed decay channels. It has been parametrized by the sum of two Gaussian distributions.*

one obtained for events situated under the B_s^0 mass peak. The time distribution $\mathcal{P}_{bkg}(t_i)$ for the combinatorial background under the satellite peak has been taken directly from the simulation since it has a strong dependence versus the measured B_s^0 mass due to the procedure used to reconstruct the B momentum in these events.

6 Oscillation analysis

The oscillation analysis is usually performed in the framework of the amplitude method [8] which consists in measuring, for each value of the frequency Δm_s, an amplitude A and its error $\sigma(A)$. The parameter A is introduced in the time evolution of pure B_s^0 or $\overline{B_s^0}$ states so that the value $A = 1$ corresponds to a genuine signal for oscillation:

$$\mathcal{P}(B_s^0 \to (B_s^0,\ \overline{B_s^0})) \ = \ \frac{1}{2\tau_s} e^{-\frac{t}{\tau_s}} \times (1 \pm A\ cos(\Delta m_s t))$$

The 95% C.L. excluded region for Δm_s is obtained by evaluating the probability that, in at most 5% of the cases, a real signal having an amplitude equal to unity would give an observed amplitude smaller than the one measured. This corresponds to the condition:

$$A(\Delta m_s) + 1.645\ \sigma(A(\Delta m_s)) \ < \ 1.$$

In the amplitude approach, the error $\sigma(A(\Delta m_s))$ is related to the probability to exclude a given value of Δm_s. The sensitivity is defined as the value of Δm_s which would just be excluded if the value of A, as measured in the experiment, has been zero for all values of Δm_s i.e. it is the expected 95% confidence limit that an experiment of the same statistics and resolution would be expected to achieve. (An actual experiment would set a higher or lower limit, because of fluctuations in the values of A as a function of Δm_s.)

The probability distributions for mixed and unmixed events have been computed [3]:

$$P^{mix}(t_i) = f_{B_s} P^{mix}_{B_s}(t_i) + f_{ref} P^{mix}_{ref}(t_i) + f_{bkg} P^{mix}_{bkg}(t_i) \qquad (3)$$

[3]In the following, only the probability distribution for mixed events is written explicitly; the corresponding probability for unmixed events can be obtained by changing ϵ into $(1-\epsilon)$.

The expressions for the different probability densities are :

- B_s mixing probability.

$$P_{B_s}{}^{mix}(t_i) \;\; = \{ \;\; \epsilon_b^{tag} \mathcal{P}_{B_s}^{mix}(t) + (1 - \epsilon_b^{tag}) \mathcal{P}_{B_s}^{unmix}(t) \;\; \} \otimes \mathcal{R}_{B_s}(t - t_i) \tag{4}$$

- Reflection mixing probability.

$$\mathrm{P}_{ref}^{mix}(t_i) = \epsilon_{ref}^{mix} \mathcal{P}_{ref}(t_i) \tag{5}$$

- Combinatorial background mixing probability:

$$\mathrm{P}_{bkg}^{mix}(t_i) = \epsilon_{bkg}^{mix} \mathcal{P}_{bkg}(t_i) \tag{6}$$

The amplitude analysis is then performed using all events selected in a region between 4.85 and 5.45 GeV/c^2. The variation of the background level, as a function of the recontructed mass, has been included in this analysis on an event by event basis. Figure 5 shows the variation of the measured amplitude as a function of Δm_s. As expected this analysis does not provide a limit. On the other hand its most important feature is the relatively low amplitude error at high values of Δm_s. Figure 6 shows the variation of the measured error on the amplitude as a function of Δm_s and Table 5 gives the values of $\sigma(A)$ in the high Δm_s region. Due to the limited statistics the error on A can be asymmetric. The error has been symmetrized and the largest value has been quoted.

Δm_s	$\sigma(A)$(stat.)	$\sigma(A)$(stat. + syst.)
2.5 ps^{-1}	1.03	1.17
5.0 ps^{-1}	0.97	1.12
7.5 ps^{-1}	1.37	1.43
10.0 ps^{-1}	1.71	2.41
12.5 ps^{-1}	3.05	4.04
15.0 ps^{-1}	4.01	4.72

Table 5: *$\sigma(A)$ for different values of Δm_s*

The behaviour of $\sigma(A)$ has been investigated using a "toy" MC generated with the same characteristics as those measured in real data. The individual toy experiments show a similar "bumpy" behaviour of $\sigma(A)$ as a function of Δm_s. For each value of Δm_s, the distribution of $\sigma(A)$ and its variance have been obtained. The central value and the region corresponding to a $\pm 2\sigma$ variation are also shown in Figure 6.

6.1 Study of systematic uncertainties

Systematic uncertainties have been evaluated by varying the parameters which have been kept constant in the fit according to their measured or expected errors.

- Systematics from the tagging purity.
  A variation of $\pm$ 3 % on the expected tagging purity for the signal has been considered, following results given in [4].

- Systematics from the background level and from the contribution of kinematical reflections. The levels of background and of kinematical reflections have been varied separately for the main and the satellite peaks according to the statistical uncertainties given in Table 2. Since the level of the combinatorial background has been used as a function of the reconstructed mass, on an event by event basis, the measured central mass position and the corresponding width have been also varied by $\pm 1\sigma$ around their fitted values.

- Systematics from the expected resolution on the B decay proper time.
  The widths $\sigma_1(ps)$ and $\sigma_2(ps)$ described in Section 5 and given in Table 4 have been varied by $\pm 10\%$.

Finally uncertainties in the values of the B_s^0 meson lifetime and in the parametrization of the proper time of the combinatorial background have been taken into account. The error on A, $\sigma(A)$, evaluated for different values of Δm_s and including the contributions of systematic uncertainties is given in Table 5.

7 Completely reconstructed D_s decays

7.1 Event Selection

Events with an exclusively reconstructed D_s accompanied by a large momentum hadron have been used to perform a second oscillation analysis. This channel is similar to the $D_s^{\pm}\ell^{\mp}$ final states [4] but, instead of a lepton, it uses a charged hadron. It provides larger statistics but suffers from an ambiguity in the choice of the hadron and from a reduced B_s^0 purity of the selected sample. This approach has been already used in DELPHI to measure the B_s^0 lifetime [9] and to study $B_s^0 - \overline{B_s^0}$ oscillations [10]. In the present measurement about 3.5 million hadronic Z^0 decays, registred by the DELPHI experiments between 1992 and 1995, have been analysed. The D_s meson is selected in two decay channels:

$$\begin{aligned} &D_s^+ \to \phi\pi^+, \qquad \phi \to K^+K^-; \\ &D_s^+ \to \overline{K}^{\star 0}K^+, \quad \overline{K}^{\star 0} \to K^-\pi^+; \end{aligned}$$

D_s candidates have been reconstructed by making combinations of three charged particles situated in the same event hemisphere, with a momentum larger than 1 GeV/c and with reconstructed tracks associated to at least 1 VD hit. The invariant mass of ϕ candidates has to be within ± 12 MeV/c^2 of the nominal ϕ mass and the ϕ momentum has to be larger than 5 GeV/c. Using the standard DELPHI algorithm [11, 5] for particle identification, at least one charged particle has to be a "loose" kaon if the K^+K^- invariant mass is within ± 4 MeV/c^2 of the nominal ϕ mass, otherwise at least one "standard" kaon is requested. Since, in the considered decay channels, the pseudoscalar D_s meson decays into a vector $\phi(\bar{K}^{\star 0})$ and a pseudoscalar meson $\pi^+(K^+)$, because of helicity conservation, the distribution of the ψ angle in the vector meson rest frame, between the directions of its decay products and of the pseudoscalar π^+ (K^+), has a $cos^2\psi$ distribution. The value of $|\cos(\psi)|$ has to be above 0.4 and 0.6 for $D_s^+ \to \phi\pi^+$ and $D_s^+ \to \overline{K}^{\star 0}K^+$ decay channels respectively. The invariant mass of the $\overline{K}^{\star 0}$ candidates has to be within ± 60 MeV/c^2 of the nominal $\overline{K}^{\star 0}$ mass value and the $\overline{K}^{\star 0}$ momentum has to exceed 6 GeV/c. The

momentum of the bachelor kaon (K^+) has to exceed 3 GeV/c . To suppress the physical background from the $D^+ \to K^-\pi^+\pi^+$ kinematical reflection, the bachelor kaon (K^+) has to be identified at least as a "standard" one. For $\overline{K}^{\star 0} \to K^-\pi^+$ decays, "loose" identified K^- are also accepted. In the D_s decay channels, all particles which are not explicitly identified as protons, kaons or leptons, are assumed to be pions. The D_s decay length has to be positive and the χ^2–probability of the fitted D_s vertex to be larger than 10^{-3}.
The selection of the hadron, accompanying the D_s candidate, is based on an impact parameter technique. A sample of tracks coming predominantly from B hadron decays is preselected using both the impact parameter with respect to the primary vertex and to the D_s decay vertex. The hadron is then searched for, amongst the preselected tracks in the event, by requiring that its charge is opposite to that of the D_s and has the highest momentum. Details on the track preselection as well as on the hadron selection are given in [9].
The B decay vertex is reconstructed by constraining the selected hadron and the D_s candidate to a common vertex. In order to increase the resolution on the measured decay length, only reconstructed events with a decay length error smaller than 0.07 *cm* have been kept. If the previous procedure fails a new attempt, using a more inclusive algorithm which allows several hadrons to be attached to the D_s candidate, has been used. Only events with a decay length error smaller than 0.07 *cm* have been kept also in this case. The selected sample, specified as $D_s^{\pm}h^{\mp}$ in the following, contains about 30% of such multi-hadron events. The multi and single hadron events will be treated in a similar way. Figure 7 shows the D_s^+ signals after selection of the accompanying hadron. The mass distributions have been fitted using two Gaussian distributions of equal widths to account for the D_s and D^+ signals and using an exponential for the combinatorial background. Table 6 gives the number of observed events, after background subtraction, in the D_s^+ signal and the fraction of combinatorial background events. The D_s signal region corresponds to a mass interval of $\pm\ 2\sigma$ centred on the fitted D_s mass.

D_s decay channels	Estimated signal in 92-93 data	Estimated signal in 94-95 data
$D_s \to \phi\pi^+$	322 ± 30 (0.60 ± 0.04)	468 ± 42 (0.53 ± 0.04)
$D_s \to \overline{K}^{\star 0}K^+$	152 ± 28 (0.70 ± 0.06)	324 ± 35 (0.58 ± 0.05)

Table 6: *Number of D_s mesons reconstructed in the $\phi\pi^+$ and $\overline{K}^{\star 0}K^+$ decay channels. The fraction of combinatorial background, given in parentheses, has been evaluated using a mass interval of $\pm 2\sigma$ centred on the D_s fitted mass.*

7.2 Sample composition

The $D_s^{\pm}h^{\mp}$ sample contains a large physics background due to D_s from non-strange B hadron decays and from $c\overline{c}$ fragmentation. To estimate the relative fractions of these different sources, the production rate of D_s mesons from all B species, $B_L = \mathrm{Br}(b \to D_s^{\pm}X) \times \mathrm{Br}(D_s^{\pm} \to \phi\pi^{\pm})$, measured by the ALEPH, DELPHI and OPAL Collaborations[14], and the equivalent quantity $B_2 = \mathrm{Br}(B_{u,d} \to D_s^{\pm}X) \times \mathrm{Br}(D_s^{\pm} \to \phi\pi^{\pm})$, measured at the $\Upsilon(4S)$ by the CLEO and ARGUS Collaborations [13], are also used. The

following relative fractions for the different processes contributing to the $D_s^{\pm}h^{\mp}$ signal have been evaluated:

- Fraction of B_s^0 decaying to a D_s and no other charmed meson : $f_{1D}^{B_s} = (39 \pm 7)$ %
- Fraction of B_s^0 decaying to a D_s and another charmed meson : $f_{2D}^{B_s} = (11 \pm 3)$ %
- Fraction of non-B_s^0 decaying to a D_s and no other charmed meson : $f_{2D}^{B} = (9 \pm 5)$ %
- Fraction of non-B_s^0 decaying to a D_s and another charmed meson : $f_{1D}^{B} = (41 \pm 7)$ %

The relative contribution from direct charm is estimated from the measurement of D_s production in charm events from CLEO and ARGUS [15], taking into account the Z^0 partial widths into b and c quarks.

7.3 Discriminant variables to increase the B_s^0 purity

To increase the effective purity in B_s^0 of the selected sample, five variables have been used which allow to distinguish between signal and background components. These variables are: the D_s mass, the D_s momentum, the value of $|\cos(\psi)|$, the χ^2–probability of the fitted D_s vertex and the value of the b-tag variable measured in the opposite hemisphere with respect to the one containing the D_s meson. The distributions for these variables are shown in Figure 8 for events selected in the signal region after having subtracted the corresponding distributions of background events, which have been obtained using events situated in the side bands of the D_s signal. The corresponding distributions for background events are also shown in Figure 8.

8 Measurement of the B_s^0 lifetime

8.1 Proper time resolution

For each event, the B_s^0 decay time is obtained from the measured decay length ($L_{B_s^0}$) and the estimate of the B_s^0 momentum ($p_{B_s^0}$). The technique used is described in [9]. The predicted decay time distributions have been obtained by convoluting the theoretical distributions with resolution functions evaluated from simulated events. Different parametrizations have been used for the two Vertex Detector configurations installed in 91-93 and 94-95. The proper time resolution is obtained from the distribution of the difference between the generated (t) and the reconstructed (t_i) times. The following distributions have been considered:

- $\mathcal{R}_{1D}^{B}(t-t_i)$ is the resolution function for B decays with only one charmed meson (D_s) in the final state. It is parametrized as the sum of three Gaussian distributions. The width of the second Gaussian is taken to be proportional to the width of the first one. The third Gaussian describes the component with a selected hadron coming from the primary vertex; the fraction of these events decreases exponentially as a function of the proper time.

  $$\mathcal{R}_{1D}^{B}(t-t_i) = (1-f_2-f_3)G(t-t_i,\sigma_1) + f_2 G(t-t_i,\sigma_2) + f_3 G(t-t_i,\sigma_3)$$

  $$\text{with } \sigma_1 = \sqrt{\sigma_{L1}^2 + \sigma_{P1}^2 t^2}, \qquad \sigma_2 = s_1\sigma_1, \qquad \sigma_3 = \sqrt{\sigma_{L3}^2 + \sigma_{P3}^2 t^2}, \qquad f_3 = exp(s_2 + s_3 t)$$

The values for the decay length resolutions, σ_{L_i}, the momentum resolutions, σ_{P_i}, the relative fractions, f_i, and the coefficents, s_1, s_2 and s_3, are given in Table 7.

- $\mathcal{R}^{\rm B}_{2D}(t-t_i)$ is the resolution function for B decays with two D mesons in the final state. It is parametrized in a similar way as $\mathcal{R}^{\rm B}_{1D}(t-t_i)$ and the values of the corresponding parameters are given in Table 7.

D_sh sample								
Resolution function (years)	$\sigma_{L1}(ps)$	σ_{P1}	$\sigma_{L3}(ps)$	σ_{P3}	f_2	s_1	s_2	s_3
$\mathcal{R}^{\rm B}_{1D}(t-t_i)$ (92-93)	0.149	0.140	0.144	0.386	0.15	3.5	2.71	0.14
$\mathcal{R}^{\rm B}_{1D}(t-t_i)$ (94-95)	0.145	0.104	0.169	0.256	0.10	2.5	2.13	0.17
$\mathcal{R}^{\rm B}_{2D}(t-t_i)$ (92-93)	0.236	0.095	0.144	0.386	0.30	3.5	3.04	0.14
$\mathcal{R}^{\rm B}_{2D}(t-t_i)$ (94-95)	0.214	0.094	0.169	0.256	0.25	3.5	2.95	0.17

Table 7: *Fitted values of the parameters used in the resolution functions* $\mathcal{R}^{\rm B}_{1D}(t-t_i)$ *and* $\mathcal{R}^{\rm B}_{2D}(t-t_i)$.

8.2 Likelihood fit

The B^0_s lifetime and the time distribution of the combinatorial background have been fitted simultaneously, using selected events situated within a mass interval of $\pm 2\sigma$ centred on the measured D_s mass (2953 events) and using events lying in the D_s mass side–band (3373 events) between 2.1 and 2.3 GeV/c^2. The probability density function for the measured proper time, t_i, can be written:

$$P(t_i) = f^{\rm B_s}_{1D} P^{\rm B_s}_{1D}(t_i) + f^{\rm B_s}_{2D} P^{\rm B_s}_{2D}(t_i) + f^{\rm B}_{1D} P^{\rm B}_{1D}(t_i) + f^{\rm B}_{2D} P^{\rm B}_{2D}(t_i) + f_{cc} P_{cc}(t_i) + f_{bkg} P_{bkg}(t_i).$$

The different probability densities are expressed as convolutions of the physical probability densities with the appropriate resolution functions:

- For the signal:

$$P^{\rm B_s}_{1D}(t_i) = exp(-t/\tau_{\rm B_s}) \otimes \mathcal{R}^{\rm B}_{1D}(t-t_i)$$

  where t is the true proper time.

- For the physical background coming from all B meson decays:

$$P^{\rm B_s}_{2D}(t_i) = exp(-t/\tau_{\rm B_s}) \otimes \mathcal{R}^{\rm B}_{2D}(t-t_i)$$

$$P^{\rm B}_{1D}(t_i) = exp(-t/\tau_{\rm B}) \otimes \mathcal{R}^{\rm B}_{1D}(t-t_i)$$

$$P^{\rm B}_{2D}(t_i) = exp(-t/\tau_{\rm B}) \otimes \mathcal{R}^{\rm B}_{2D}(t-t_i)$$

Source of systematic error	$\tau_{B_s^0}$ variation (ps)
Sample composition	$^{+0.013}_{-0.016}$
f_{bkg}	$^{+0.046}_{-0.050}$
backg. parametrization	$^{+0.017}_{-0.012}$
B_s purity	$^{+0.005}_{-0.015}$
t resolution	± 0.019
$\tau_{B^+}(1.65 \pm 0.04\ ps)$	± 0.021
$\tau_{B_d^0}(1.56 \pm 0.04\ ps)$	± 0.019
Analysis bias correction	± 0.040
Total	$^{+0.07}_{-0.08}$

Table 8: *Sources of systematic errors on the* B_s^0 *lifetime measurement (*$D_s^{\pm}h^{\mp}$ *analysis).*

- For "charm" candidates the function $P_{cc}(t_i)$ has been parametrized using simulated events; has been used:

$$P_{bkg}(t_i) = f^- exp(-t/\tau^-) \otimes G(t-t_i,\sigma_j) + f^+ exp(-t/\tau^+) \otimes G(t-t_i,\sigma_j) + (1-f^- - f^+) G(t-t_i,\sigma_j)$$

  Three distributions have been considered: a negative exponential for poorly measured events (with lifetime τ^-), an exponential distribution for the flying background (with lifetime τ^+) and a central Gaussian for the non-flying component. The seven parameters (f^-, f^+, τ^+, τ^- and $\sigma_{j(j=1,3)}$) have been left free to vary in the fit.

The result of the fit, shown in Figure 9, is:

$$\tau_{B_s^0} = 1.53\ ^{+0.16}_{-0.15}\ \text{ps}.$$

8.3 Systematic errors on the B_s^0 lifetime

The contributions to systematic uncertainties on the B_s^0 lifetime measurement are summarized in Table 8.

The systematic error due to the uncertainties in the relative fractions of the different D_s sources corresponds to a $\pm 1\sigma$ variation of the fractions f used in the likelihood fit, excluding f_{bkg} which is studied separately.

The estimate of systematics related to the evaluation of the B_s^0 purity, on an event by event basis, has been obtained in the following way. The distributions of the different quantities contributing to the discriminant variable (Figure 8) for signal and background events have been re-weighted with a linear function in order to maximize the agreement beetween data and the simulation. The fit of the B_s lifetime distribution has been redone with new probability distributions and the difference between the corresponding values of the fitted lifetime has been taken as systematic error.

Uncertainties on the determination of the resolution on the proper time receive two contributions: one from errors on the decay distance evaluation and the other from errors on the measurement of the B_s^0 momentum. The systematic error coming from uncertainties on the time resolution has been evaluated by varying by $\pm 10\%$ the widths σ_L and σ_P of the resolution function (see Table 7). Finally simulated B_s^0 events, generated with a lifetime of 1.6 ps and satisfying the same selection criteria as the real data, have a fitted lifetime of 1.64 ± 0.04 ps.

The statistical error of this comparison ($\pm$ 0.04) has been included in the systematic error, the shift (+ 0.04) has been used to correct the measured lifetime in real data. After correcting for this possible analysis bias, the measured B_s^0 lifetime has been found to be

$$\tau_{B_s^0} = 1.49\ ^{+0.16}_{-0.15}\ (stat.)^{+0.07}_{-0.08}\ (syst.)\ \text{ps}.$$

9 Lifetime difference between B_s^0 mass eigenstates

As strange B mesons are selected using their semileptonic decays, the measured decay time distribution is relative to $\overline{B_s^0}$ (or B_s^0) mesons which are well defined superpositions of the two mass eigenstates:

$$|^{(}\overline{B}^{)^0}\rangle = \frac{1}{\sqrt{2}}(|B_H^0\rangle \pm |B_L^0\rangle).$$

The time probability density is then given by:

$$\mathcal{P}(t) = C_{norm}(e^{-\Gamma_H t} + e^{-\Gamma_L t}) \tag{7}$$

where

$$\begin{array}{ll} \Gamma_{L(H)} & = \Gamma \pm \Delta\Gamma/2 \\ C_{norm} & = \Gamma_H\Gamma_L/(\Gamma_H + \Gamma_L) \\ \tau & = 1/\Gamma \end{array}$$

Two independent variables are then considered:

$$\tau_{B_s^0} \quad \text{and} \quad \Delta\Gamma_{B_s^0}/\Gamma_{B_s^0}$$

The method used to extract information on $\Delta\Gamma_{B_s^0}/\Gamma_{B_s^0}$ consists in calculating the log-likelihood for the time distributions measured on the $D_s h$ sample and constraining the B_s^0 lifetime to be equal to the B_d^0 lifetime (1.56 ± 0.04) *ps* (the theory predicts $\tau_{B_s^0}/\tau_{B_d} = 1 \pm \mathcal{O}(0.01)$) :

$$\begin{array}{rl} log\mathcal{L}_{tot}(\tau_{B_s^0}, \Delta\Gamma_{B_s^0}/\Gamma_{B_s^0}) = & log\mathcal{L}_{D_s\ell}(\tau_{B_s^0}, \Delta\Gamma_{B_s^0}/\Gamma_{B_s^0}) + log\mathcal{L}_{\phi\ell h}(\tau_{B_s^0}, \Delta\Gamma_{B_s^0}/\Gamma_{B_s^0}) + \\ & log\mathcal{L}_{(}\tau_{B_s^0} = \tau_{B_d^0})(\tau_{B_s^0}) \end{array} \tag{8}$$

This log-likelihood is minimized in the ($\tau_{B_s^0}$,$\Delta\Gamma_{B_s^0}/\Gamma_{B_s^0}$) plane and the likelihood difference with respect to the minimum $\Delta\mathcal{L}$ (Figure 10-a) is computed:

$$\Delta\mathcal{L} = -log\mathcal{L}_{tot}(\tau_{B_s^0}, \Delta\Gamma_{B_s^0}/\Gamma_{B_s^0}) + log\mathcal{L}_{tot}((\tau_{B_s^0})^{min}, (\Delta\Gamma_{B_s^0}/\Gamma_{B_s^0})^{min})$$

The probability density for the variables $\tau_{B_s^0}$ and $\Delta\Gamma_{B_s^0}/\Gamma_{B_s^0}$ is given by:

$$\mathcal{P}(\tau_{B_s^0}, \Delta\Gamma_{B_s^0}/\Gamma_{B_s^0}) = F_{norm}e^{-\Delta\mathcal{L}}$$

where F_{norm} is a normalization factor defined by:

$$\int \mathcal{P}(\tau_{\mathrm{B_s^0}}, \Delta\Gamma_{\mathrm{B_s^0}}/\Gamma_{\mathrm{B_s^0}}) d\tau_{\mathrm{B_s^0}} d\Delta\Gamma_{\mathrm{B_s^0}}/\Gamma_{\mathrm{B_s^0}} \;=\; 1.$$

The $\Delta\Gamma_{\mathrm{B_s^0}}/\Gamma_{\mathrm{B_s^0}}$ probability distribution is then obtained by integrating over $\tau_{\mathrm{B_s^0}}$. The upper limit on $\Delta\Gamma_{\mathrm{B_s^0}}/\Gamma_{\mathrm{B_s^0}}$ is:

$$\Delta\Gamma_{\mathrm{B_s^0}}/\Gamma_{\mathrm{B_s^0}} < 0.55 \text{ at the } 95\% \text{ C.L.}$$

This limit takes into account statistical uncertainties and the systematic coming from the uncertainty on the $\mathrm{B_d^0}$ lifetime.
The systematic uncertainty originating from other sources has been evaluated by convoluting the probability function $\mathcal{P}(\tau_{\mathrm{B_s^0}}, \Delta\Gamma_{\mathrm{B_s^0}}/\Gamma_{\mathrm{B_s^0}})$ with the probability function of the corresponding parameters:

$$\mathcal{P}(\Delta\Gamma_{\mathrm{B_s^0}}/\Gamma_{\mathrm{B_s^0}}) = \int \mathcal{P}(\tau_{\mathrm{B_s^0}}, \Delta\Gamma_{\mathrm{B_s^0}}/\Gamma_{\mathrm{B_s^0}}, x^1_{sys}, ..., x^n_{sys}) d\tau_{\mathrm{B_s^0}} dx^1_{sys} ... dx^n_{sys}$$

where x^i_{sys} are the n parameters considered in the systematic uncertainty.
Since the method implies heavy numerical integrations over a n-dimensional grid only two systematics have been considered here: the purity in $\mathrm{B_s^0}$ meson of the selected sample and the parametrization of proper time distribution of the combinatorial backgroud. This approximation is justified since systematic uncertainties are expected to be dominated by these two parameters (as they are in the $\mathrm{B_s^0}$ lifetime measurement).
The $\Delta\Gamma_{\mathrm{B_s^0}}/\Gamma_{\mathrm{B_s^0}}$ probability distribution is shown in Figure 10-b, the most probable value for $\Delta\Gamma_{\mathrm{B_s^0}}/\Gamma_{\mathrm{B_s^0}}$ is 0.22 and the upper limit at 95 % confidence level is:

$$\Delta\Gamma_{\mathrm{B_s^0}}/\Gamma_{\mathrm{B_s^0}} < 0.58 \text{ at the } 95\% \text{ C.L.}$$

10 Study of $\mathrm{B_s^0}$-$\overline{\mathrm{B_s^0}}$ oscillations

The study of $\mathrm{B_s^0}$-$\overline{\mathrm{B_s^0}}$ oscillations requires the tagging of the sign of the b quark in the $\mathrm{B_s^0}$ meson at the decay and production times. The algorithm used for $b(\overline{b})$ tagging at production time has been tuned in order to have the best performances on the $\mathrm{D_s}\ell$ sample, where all charged particles yielded in a $\mathrm{B_s^0}$ decay, have been reconstructed. This algorithm has been already described in [4].

10.1 Tagging procedure

An event is classified as a mixed or an unmixed candidate according to the relative signs of the $\mathrm{D_s}$ electric charge, Q_D, and of the x_{tag} tagging purity variable.

Mixed candidates have $x_{tag} \times \mathrm{Q}_D < 0$, and unmixed ones $x_{tag} \times \mathrm{Q}_D > 0$. The probability, ϵ_b^{tag}, of tagging the b or the $\overline{b}$ quark correctly from the measurement of x_{tag} has been evaluated using a dedicated simulated event sample. The average tagging purity of the x_{tag} variable, given by the simulation for true $\overline{\mathrm{B_s}}^0 \to \mathrm{D_s^+ h^- X}$ decays, is $(71.4 \pm 0.4)\%$. The purity is lower than the one obtained in the $\mathrm{D_s}\ell$ sample because not all $\mathrm{B_s}$ charged decay products are reconstructed in the present analysis. It has been verified that the tagging purity is the same for different B hadron species and varies only slightly when

the B^0 has or not oscillated ($< \pm 0.02$). The corresponding probability distribution for events in the combinatorial background has been obtained using data candidates selected in the wings of the signal: the probabilities of classifying these events as mixed or as unmixed candidates are called ϵ_{bkg}^{mix} and ϵ_{bkg}^{unmix} respectively.

10.2 Fitting procedure

From the expected proper time distributions and the tagging probabilities, the probability functions for mixed and unmixed events candidates have been computed [4]:

$$P^{mix}(t_i) = f_{1D}^{\mathrm{B_s}} P_{1D}^{\mathrm{B_s,mix}}(t_i) + f_{2D}^{\mathrm{B_s}} P_{2D}^{\mathrm{B_s,mix}}(t_i) + f_{1D}^{\mathrm{B}} P_{1D}^{\mathrm{B,mix}}(t_i) + f_{2D}^{\mathrm{B}} P_{2D}^{\mathrm{B,mix}}(t_i) \quad (9)$$

$$+ f_{cc} P_{cc}^{mix}(t_i) + f_{bkg} P_{bkg}^{mix}(t_i) \quad (10)$$

where t_i is the reconstructed proper time. The analytical expressions for the different probability densities are given in the following, with t being the true proper time:

- B_s signal mixing probability.

$$P_{1D}^{\mathrm{B_s,mix}}(t_i) = \{ \ \epsilon_b^{tag} \mathcal{P}_{1D}^{\mathrm{B_s,mix}}(t) + (1-\epsilon_b^{tag}) \mathcal{P}_{1D}^{\mathrm{B_s,unmix}}(t) \ \} \otimes \mathcal{R}_{1D}^{\mathrm{B}}(t-t_i) \quad (11)$$

- Physical background mixing probability.

$$\begin{aligned} P_{2D}^{B,mix}(t_i) = \{ \quad & f_{2D}^{\mathrm{B_d}} (\ \epsilon_b^{tag} \mathcal{P}_{2D}^{\mathrm{B_d,unmix}}(t) + (1-\epsilon_b^{tag}) \mathcal{P}_{2D}^{rmB_d,mix}(t) \ ) + \\ & f_{2D}^{\mathrm{B^+}} \epsilon_b^{tag} / \tau_{\mathrm{B^+}} \exp(-t/\tau_{\mathrm{B^+}}) + \\ & f_{2D}^{\Lambda_b} \epsilon_b^{tag} / \tau_{\Lambda_b} \exp(-t/\tau_{\Lambda_b}) \qquad \} \otimes \mathcal{R}_{2D}^{\mathrm{B}}(t-t_i) \end{aligned} \quad (12)$$

$$P_{2D}^{\mathrm{B_s,mix}}(t_i) = \{ f_{2D}^{\mathrm{B_s}} \epsilon_b^{tag} / \tau_{\mathrm{B_s}} \exp(-t/\tau_{\mathrm{B_s}}) \} \otimes \mathcal{R}_{2D}^{\mathrm{B}}(t-t_i) \quad (13)$$

$$\begin{aligned} P_{1D}^{B,mix}(t_i) = \{ \quad & f_{1D}^{\mathrm{B_d}} (\ \epsilon_b^{tag} \mathcal{P}_{1D}^{\mathrm{B_d,mix}}(t) + (1-\epsilon_b^{tag}) \mathcal{P}_{1D}^{\mathrm{B_d unmix}}(t) \ ) + \\ & f_{1D}^{\mathrm{B^+}} (1-\epsilon_b^{tag}) / \tau_{\mathrm{B^+}} \exp(-t/\tau_{\mathrm{B^+}}) + \\ & f_{1D}^{\Lambda_b} (1-\epsilon_b^{tag}) / \tau_{\Lambda_b} \exp(-t/\tau_{\Lambda_b}) \qquad \} \otimes \mathcal{R}_{1D}^{\mathrm{B}}(t-t_i) \end{aligned} \quad (14)$$

- Mixing probability for the charm component:

$$\mathrm{P}_{cc}^{mix}(t_i) = \epsilon_{cc}^{mix} \mathcal{P}_{cc}(t_i) \quad (15)$$

[4] In the following, only the probability function for mixed events is written explicitly; the corresponding probability for unmixed events can be obtained by changing ϵ into $(1-\epsilon)$.

- Combinatorial background mixing probability:

$$\mathrm{P}_{bkg}^{mix}(t_i) = \epsilon_{bkg}^{mix}\mathcal{P}_{bkg}(t_i) \tag{16}$$

  The proper time distribution for this background has been determined in the lifetime fit.

The oscillation analysis has been performed in the framework of the amplitude method [8] which consists in measuring, for each value of the frequency Δm_s, an amplitude A and its error $\sigma(A)$. The parameter A is introduced in the time evolution of pure B_s^0 or $\overline{\mathrm{B}_s^0}$ states so that the value $A = 1$ corresponds to a genuine signal for oscillation:

$$\mathcal{P}(\mathrm{B}_s^0 \rightarrow (\mathrm{B}_s^0,\ \overline{\mathrm{B}_s^0})) \ = \ \frac{1}{2\tau_s} e^{-\frac{t}{\tau_s}} \times (1 \pm A\ cos(\Delta m_s t))$$

The 95% C.L. excluded region for Δm_s is obtained by evaluating the probability that, in at most 5% of the cases, a real signal having an amplitude equal to unity would give an observed amplitude smaller than the one measured. This corresponds to the condition:

$$A(\Delta m_s) + 1.645\ \sigma(A(\Delta m_s)) \ < \ 1.$$

In the amplitude approach it is possible to define the exclusion probability, that is the probability that a certain Δm_s value lies in an excluded region if the generated Δm_s was very large ($\Delta m_s \rightarrow \infty$). The sensitivity is the value of Δm_s corresponding to 50 % of exclusion probability.

Considering only statistical uncertainties, a limit has been obtained:

$$\Delta m_s > 4.2 \text{ ps}^{-1} \text{ at } 95\% \text{ C.L.} \tag{17}$$

with a corresponding sensitivity equal to 3.1 ps^{-1} (Figure 11). At $\Delta m_s = 10\ ps^{-1}$, the error on the amplitude is 2.3 (Figure 12).

10.3 Study of systematic uncertainties

Systematic uncertainties have been evaluated by varying the parameters which have been kept constant in the fit, according to their measured or expected errors.

- Systematics from the tagging purity.
  A conservative variation of ± 3 % on the expected tagging purity for the signal and for the other three processes contributing to the $\mathrm{D_s h}$ peak has been used. The same variation is assumed for the tagging purity for the charm and combinatorial background events. The central values of these purities have been fixed to the simulated ones.

- Systematics from the $\mathrm{B_s^0}$ purity.
  The same procedure already applied for the lifetime measurement has been used.

- Systematics from the resolution on the B decay proper time.
  The same procedure already applied for the lifetime measurement has been used. In addition, the systematic error due to the variation of the proper time distribution of the combinatorial background, has been considered: the parameters used to define the background shape, in the lifetime fit, have been varied according to their fitted errors.

The inclusion of systematic uncertainties lowers the sensitivity to 2.7 ps^{-1} and the 95% C.L limit becomes $\Delta m_s > 4.1\ ps^{-1}$.

11 Combined limit on Δm_s.

This paper presents two analyses on Δm_s using exclusively reconstructed B_s^0 mesons and $D_s^{\pm}h^{\mp}$ events. These analyses on Δm_s have been combined (Figure 13), taking into account correlations between systematic uncertainties in the two amplitude measurements. A limit at 95% confidence level has been obtained:

$$\Delta m_s > 4.0\ \mathrm{ps}^{-1} \text{ at } 95\% \text{ C.L.} \tag{18}$$

with a corresponding sensitivity equal to 3.2 ps^{-1} (with statistical errors only the limit would be $\Delta m_s > 4.0\ \mathrm{ps}^{-1}$ at 95% C.L. and the sensitivity 4.4 ps^{-1}).
Table 9 gives the error on the amplitude for different values of Δm_s and Figure 14 shows its corresponding variation.

Δm_s	$\sigma(A)$(stat.)	$\sigma(A)$(stat. + syst.)
2.5 ps^{-1}	0.48	0.53
5.0 ps^{-1}	0.63	0.69
7.5 ps^{-1}	0.95	0.98
10.0 ps^{-1}	1.36	1.76
12.5 ps^{-1}	2.49	3.03
15.0 ps^{-1}	3.57	4.06

Table 9: *The error on the amplitude for different values of* Δm_s.

12 Conclusion

Using about 3.5 million hadronic Z^0 decays registered by DELPHI between 1992 and 1995 two samples of events have been selected. The first one consists of 44 reconstructed B_s^0 events: 11 candidates (including 30% background) are completely reconstructed and 33 candidates (including 55% background) are partially reconstructed (π^0 or/and γ are not detected). This analysis used 12 different decay channels of the B_s^0 meson and is a first attempt to use such events for oscillation studies. Due to the excellent proper time resolution this sample gives some contribution essentially in the high Δm_s region.
The second sample contains 2953 $D_s^{\pm}h^{\mp}$ candidates (including 60% background) with

completely reconstructed D_s^+ mesons in the $\phi\pi^+$ and $\overline{K}^{*0}K^+$ decay channels. Using the $D_s^{\pm}h^{\mp}$ sample, three studies have been performed. The B_s^0 lifetime has been measured and a limit on the fractional width difference between the two physical B_s^0 states has been set:

$$\tau(B_s^0) = (1.49^{+0.16}_{-0.15}(\text{stat.})^{+0.07}_{-0.08}(\text{syst.}))\ \text{ps}$$

$$\Delta\Gamma_{B_s^0}/\Gamma_{B_s^0} < 0.58 \text{ at the } 95\% \text{ C.L.}$$

This last result has been obtained under the hypothesis that $\tau_{B_s^0} = \tau_{B_d}$.
Combining the two studies on $B_s^0 - \overline{B_s^0}$ oscillations, a limit at 95% C.L. on the mass difference between the physical B_s^0 states has been set:

$$\Delta m_s > 4.0 \text{ ps}^{-1} \text{ at } 95\% \text{ C.L.} \tag{19}$$

with a corresponding sensitivity equal to $3.2\ \text{ps}^{-1}$.
Previous DELPHI results on B_s^0 lifetime obtained with the $D_s h$ sample [10] are superseeded by the analysis presented in this paper.

References

[1] P. Paganini, F. Parodi, P. Roudeau and A. Stocchi, " Measurement of the ρ and η Parameters of the V_{CKM} Matrix and Perspectives" Physica Scripta Vol. 58, 556-569, 1998.
F. Parodi, P. Roudeau and A. Stocchi " Constraints on the parameters of the V_{CKM} Matrix by the end 1997 " hep-ph/9802289.
F. Parodi, P. Roudeau and A. Stocchi " Constraints on the parameters of the V_{CKM} Matrix by the end 1998 " submitted to Nuovo Cimento Vol. xx, xxx-yyy, 1999 ,hep-ex/9903063

[2] The LEP B Oscillation Working Group " Combined Results on B^0 Oscillations: Update for the Summer 1997 Conferences ", LEPBOSC 97/2, DELPHI 97-35 PHYS 722

[3] Particle Data Group, R. M. Barnett et al., Phys. Rev. **D54** (1996) 1.

[4] (DELPHI Coll.) " Study of $B_s^0 - \overline{B_s^0}$ oscillations and B_s^0 lifetime using $D_s - \ell$ events ", ICHEP'98 # 235 and DELPHI 98-131 CONF 192 , the updated anlaysis is given in this contributed paper.

[5] P. Abreu. et al., DELPHI Coll.,"Performance of the DELPHI Detector", CERN-PPE/95-159, Nucl. Instr. and Methods A378 (1996) 57.

[6] G.V. Borisov and C. Mariotti, Nucl. Instr. and Meth. **A372** (1996) 181.

[7] Deandrea, Di Bartolomeo and Gatto, Preprint University of Geneva, UGVA-DPT 93-07-824.

[8] H.G. Moser and A. Roussarie, *Nucl. Instr. and Meth.* **A384** (1997) 491.

[9] P. Abreu et al. DELPHI Coll. Z. Phys. **C71** (1996) 11.

[10] P. Adam et al. DELPHI Coll. Phys. Lett. **B416** (1998) 233.

[11] E.G. Anassontzis et al., Nucl. Instr. and Meth. **A323** (1992) 351.

[12] P. Abreu et al. DELPHI Coll., Phys. Lett. **B289** (1992) 199.
P. D. Acton et al., OPAL Coll., Phys. Lett. **B295** (1992) 357.
D. Buskulic et al., ALEPH Coll., Phys. Lett. **B361** (1995) 221.

[13] CLEO Coll., "Measurements of the B $\rightarrow$ D_s + X Decays", CLEO-CONF 94-9 contribution to the XXVIIth ICHEP, Glasgow, U.K., (July 1994).
H. Albrecht et al., ARGUS Coll., Z. Phys. **C54** (1992) 1.

[14] P. D. Acton et al., OPAL Coll., Phys. Lett. **B295** (1992) 357.
P. Abreu et al., DELPHI Coll., Z. Phys. **C61** (1994) 407.
D. Buskulic et al., ALEPH Coll., "Measurement of D_s meson production in Z^0 decays and of the B_s^0 lifetime" CERN PPE/95-092 subm. to Z. Phys. C.

[15] H. Albrecht et al., ARGUS Coll., Z. Phys. **C54** (1992) 1.

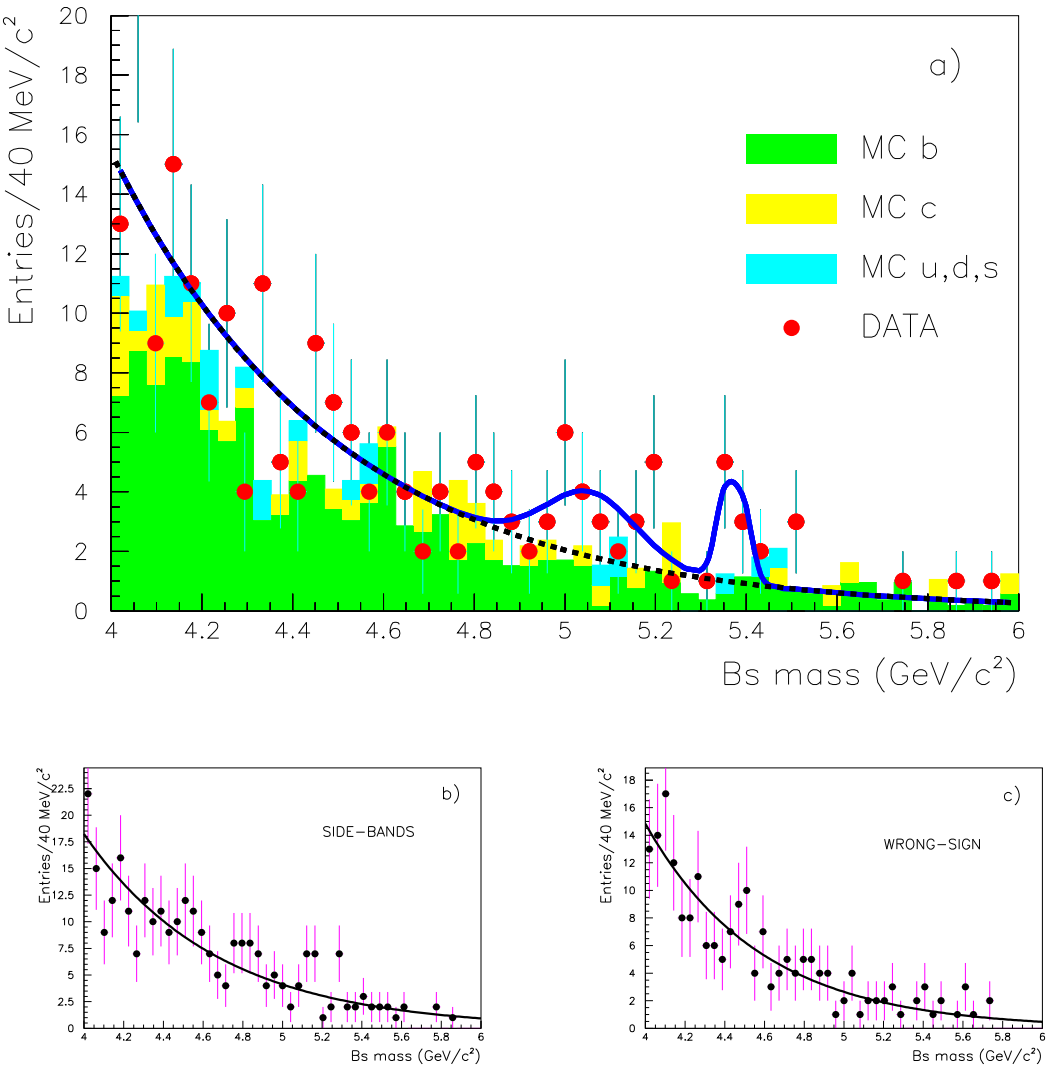

Figure 1: *a)* B_s^0 *mass spectrum for the candidates selected in the twelve decay channels described in Section 3.1. The data are indicated by the points with error bars and the result of the fit has been superimposed. Details on this fit are given in the text. The histograms represent the expected contribution from* B *events after having removed events from the* B_s^0 *signal (black histogram), from charm events (dark grey histogram) and from light quark events (light grey histogram). b) Mass spectrum using events in the side bands of the* D_s *and* D^0 *signals. c) Mass spectrum using wrong sign combinations in the different decay channels.*

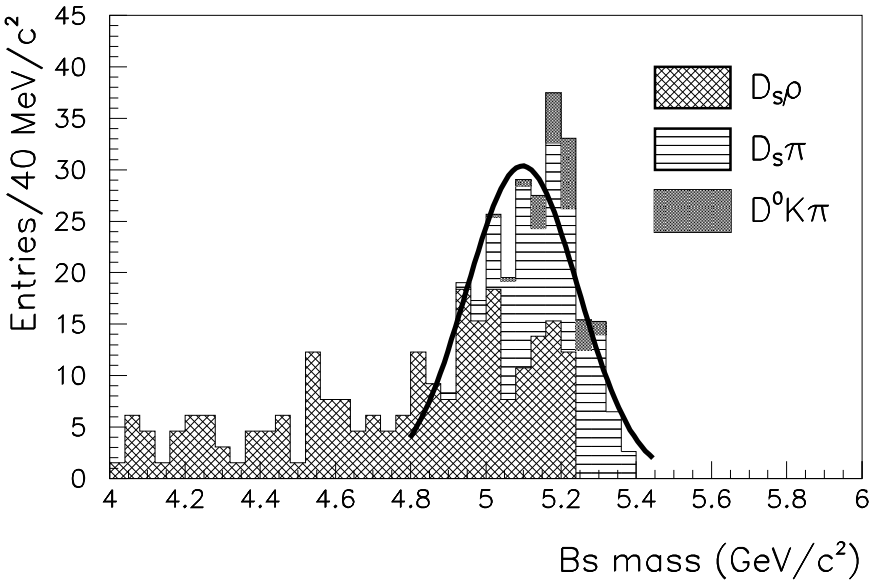

Figure 2: *The Monte Carlo composition of the satellite peak. The notations in the plot are the following:* $D_s\rho$ *corresponds to* $D_s^-\rho^+$ *and* $D_s^{*-}\rho^+$ *decay channels of the* B_s^0*;* $D_s\pi$ *corresponds* $D_s^{*-}\pi^+$ *and* $D_s^{*-}{a_1}^+$*;* $D^0K\pi$ *shows the contribution from* $\overline{D^*}(2007)^0K^-\pi^+$ *and* $\overline{D^*}(2007)^0K^-{a_1}^+$ *decay channels. All contributions have been normalized according to the evaluation of the branching fractions discussed in Section 2 and including reconstruction efficiencies evaluated using simulated events.*

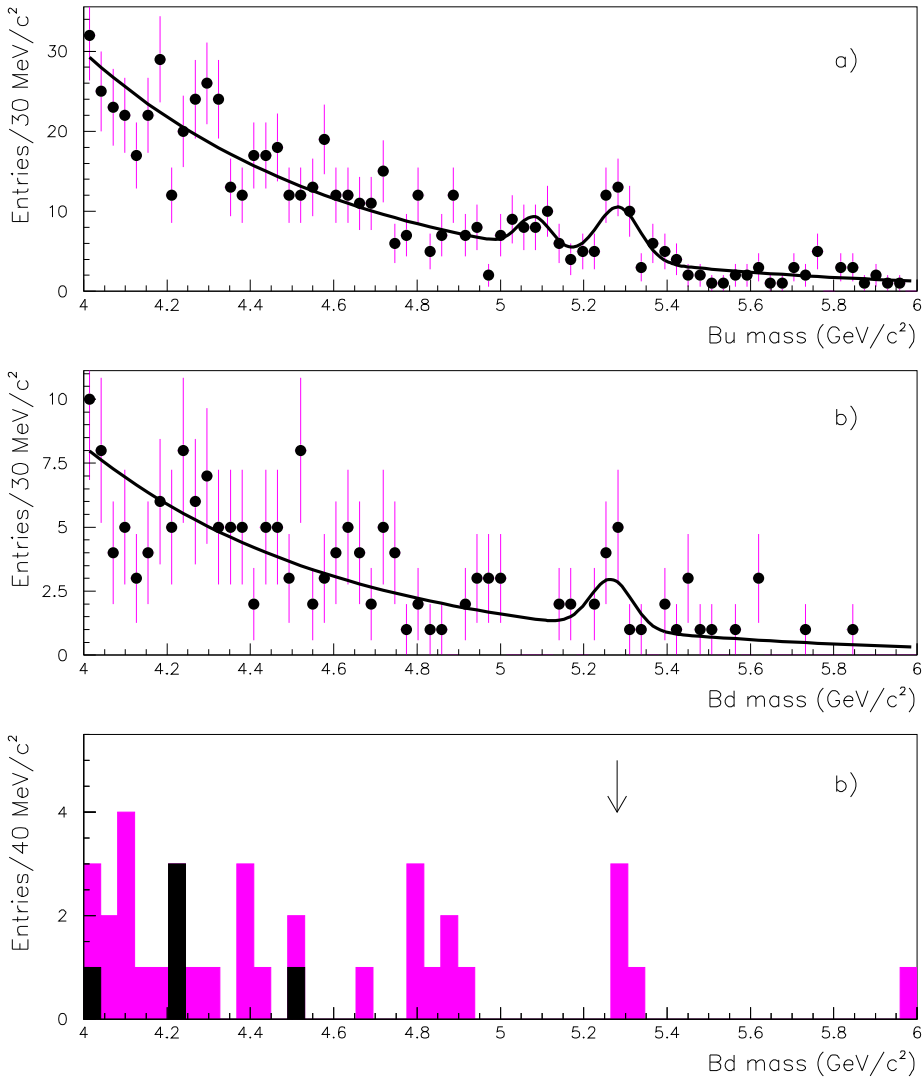

Figure 3: *Mass spectra for a)* $B^+ \to \overline{\mathrm{D}}^0\pi^+$, *b)* $\mathrm{B_d^0} \to \mathrm{D^*(2010)^-}\pi^+$ *and c)* $\mathrm{B_d^0} \to \mathrm{D^*(2010)^-a_1{}^+}$ *decays. In the first plot a signal from* $B^+ \to D^*(2007)^0\pi^+$ *decay is also visible. The widths of the mass peaks have been fixed according to the value found in the simulation. Details on the fit are given in the text. In the third plot the dark grey histogram represents right-sign combinations and the black one the wrong-sign combinations. The arrow indicates the nominal* $\mathrm{B_d^0}$ *meson mass.*

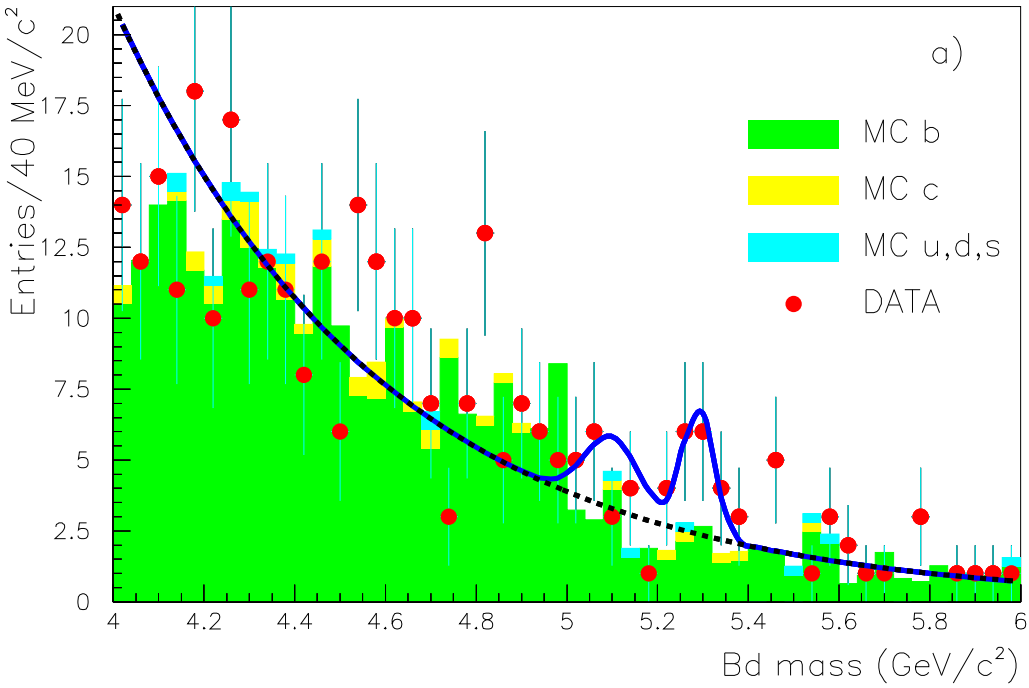

Figure 4: *a)* B_d^0 *mass spectrum for the sum of* $B_d^0 \to \overline{D}^0\pi^-\pi^+$ *and* $B_d^0 \to \overline{D}^0\pi^- a_1{}^+$ *decays selected in the four decay channels described in Section 3.3. The data are indicated by the points with error bars and the result of the fit has been superimposed. The histograms represent the expected contribution from* B *events after having removed signals from* B_d^0 *events (black histogram), from charm events (dark grey histogram) and from light quark events (light grey histogram). The widths of the signals have been fixed according to the values found in the simulation. Details on the fit have been given in the text.*

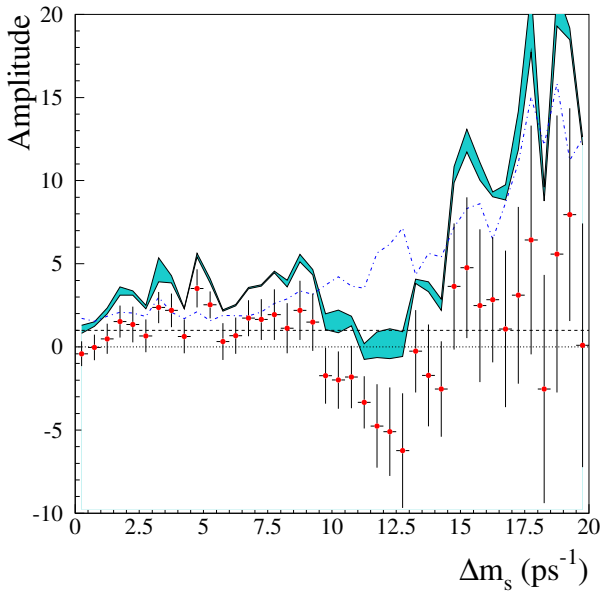

Figure 5: *Exclusive* B_s^0 *analysis: variation of the oscillation amplitude* A *as a function of* Δm_s*. The lower continuous line corresponds to* $A+1.645\ \sigma_A$ *where* σ_A *includes statistical uncertainties only, while the shaded area shows the contribution from systematics. The dashed-dotted line corresponds to the sensitivity curve. The lines at* $A=0$ *and* $A=1$ *are also given.*

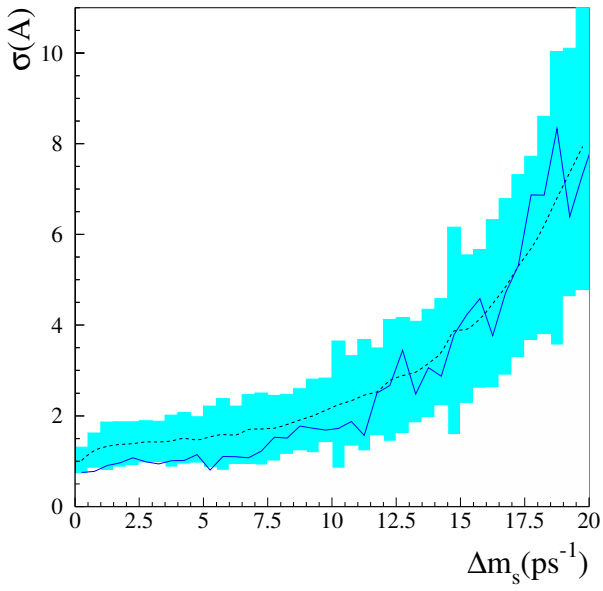

Figure 6: σ_A *as a function of* Δm_s*. The histogram shows the result from the data. The full curve shows the average result from 100 toy experiments with the same statistics as in data and the shaded area gives the* $\pm 2\sigma$ *region around this average.*

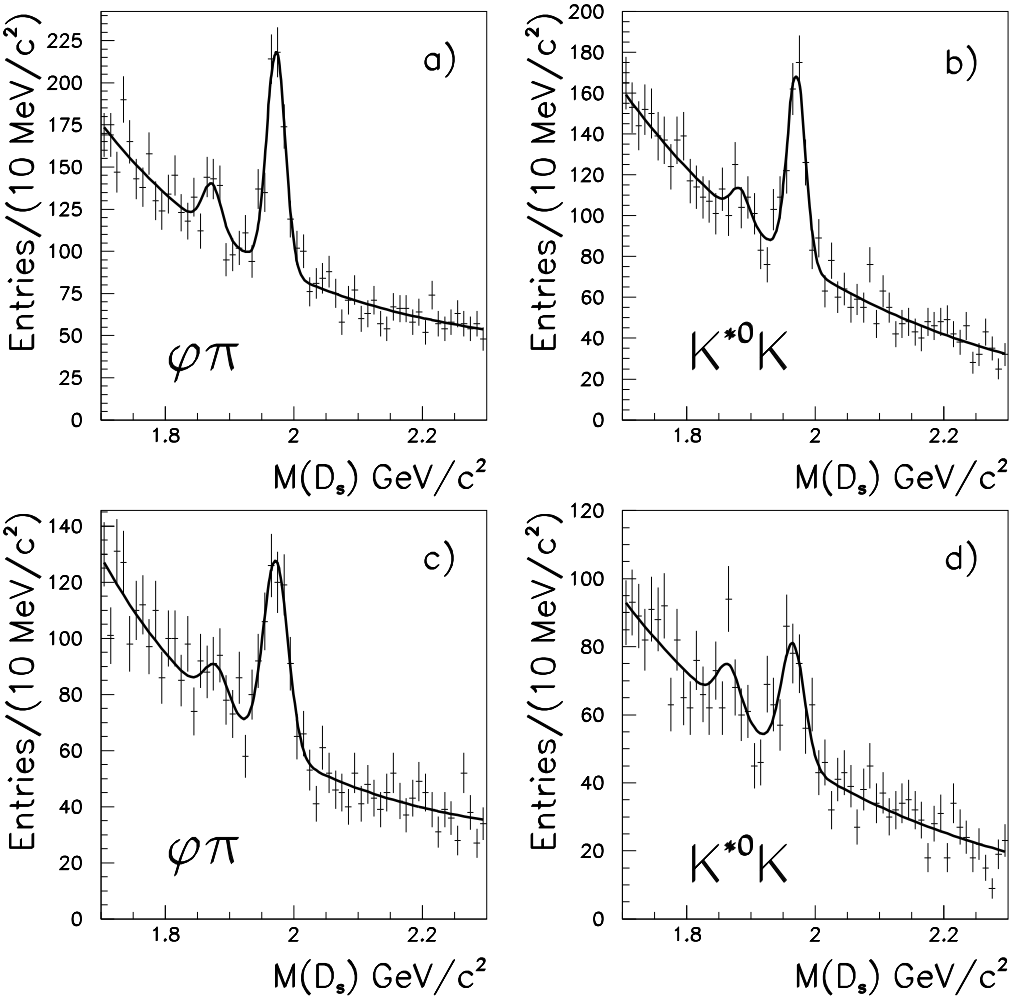

Figure 7: *Invariant mass distributions for D_s candidates selected in $\phi\pi^+$ and $\overline{K}^{*0}K^+$ decay channels. The selected D_s candidates are accompanied by a hadron of opposite electric charge, measured in the same event hemisphere. The curves show the fits described in the text.*

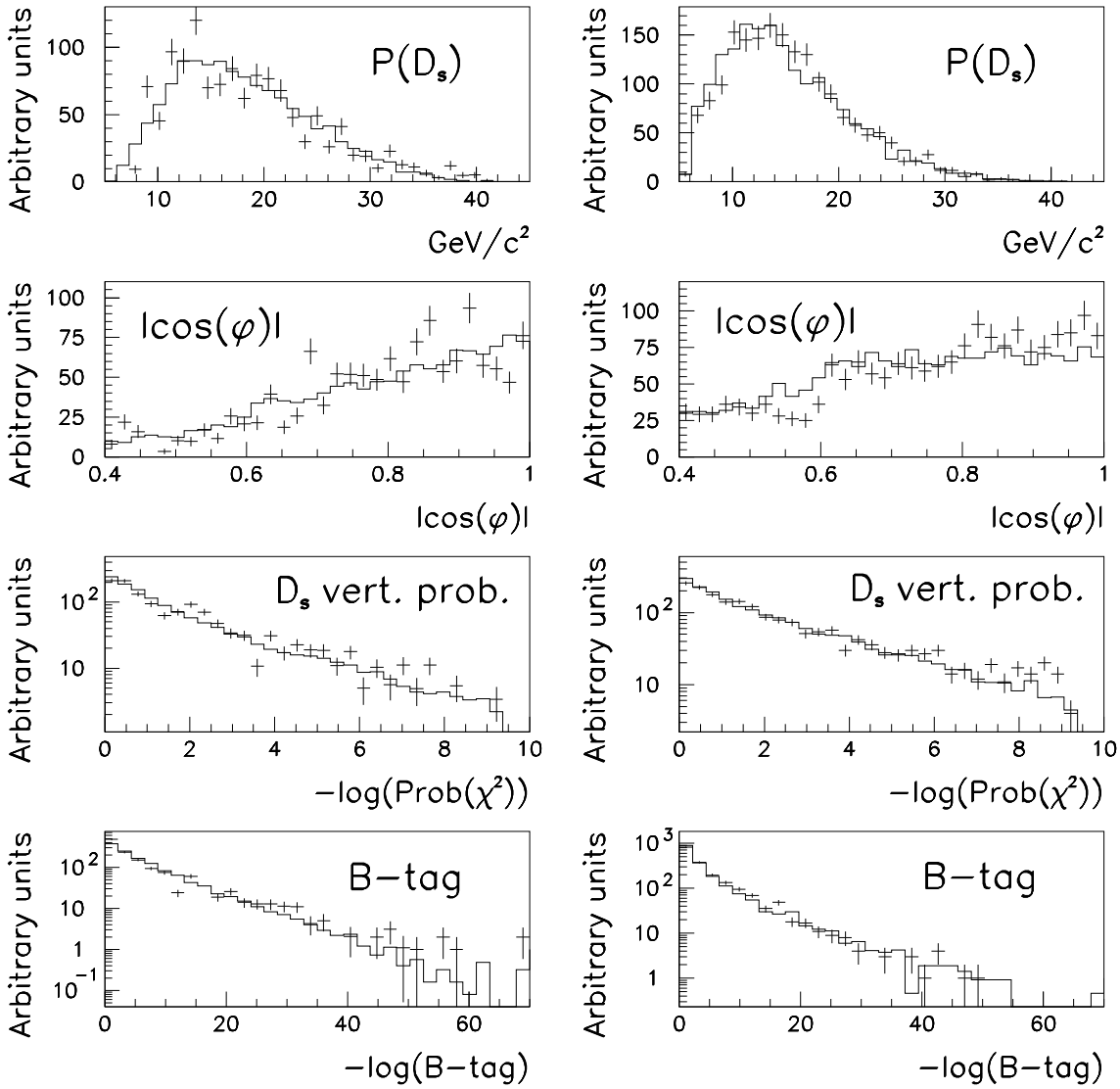

Figure 8: *Distributions of the variables used to increase the effective* B_s *purity. The distributions on the left are relative to events selected in the signal region after having subtracted the corresponding distributions of background events, which have been obtained using events situated the side bands of the* D_s *signal. The corresponding distributions for background events are shown in the right. The points with error bars correspond to the data and the histograms are for simulated events.*

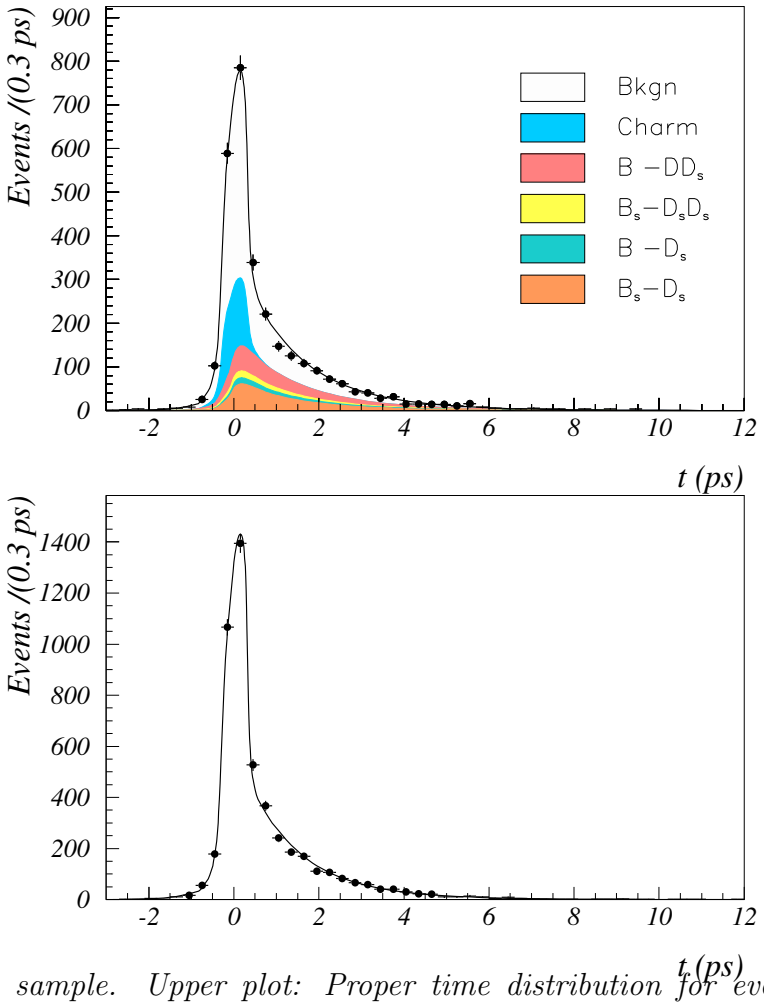

Figure 9: $D_s h$ *sample. Upper plot: Proper time distribution for events in the signal mass region. The points show the data and the histograms correspond to the different contributions to the selected events. The curve shows the result of the fit described in the text.*
Lower plot : same as the upper plot but for for events situated in D_s *mass side band.*

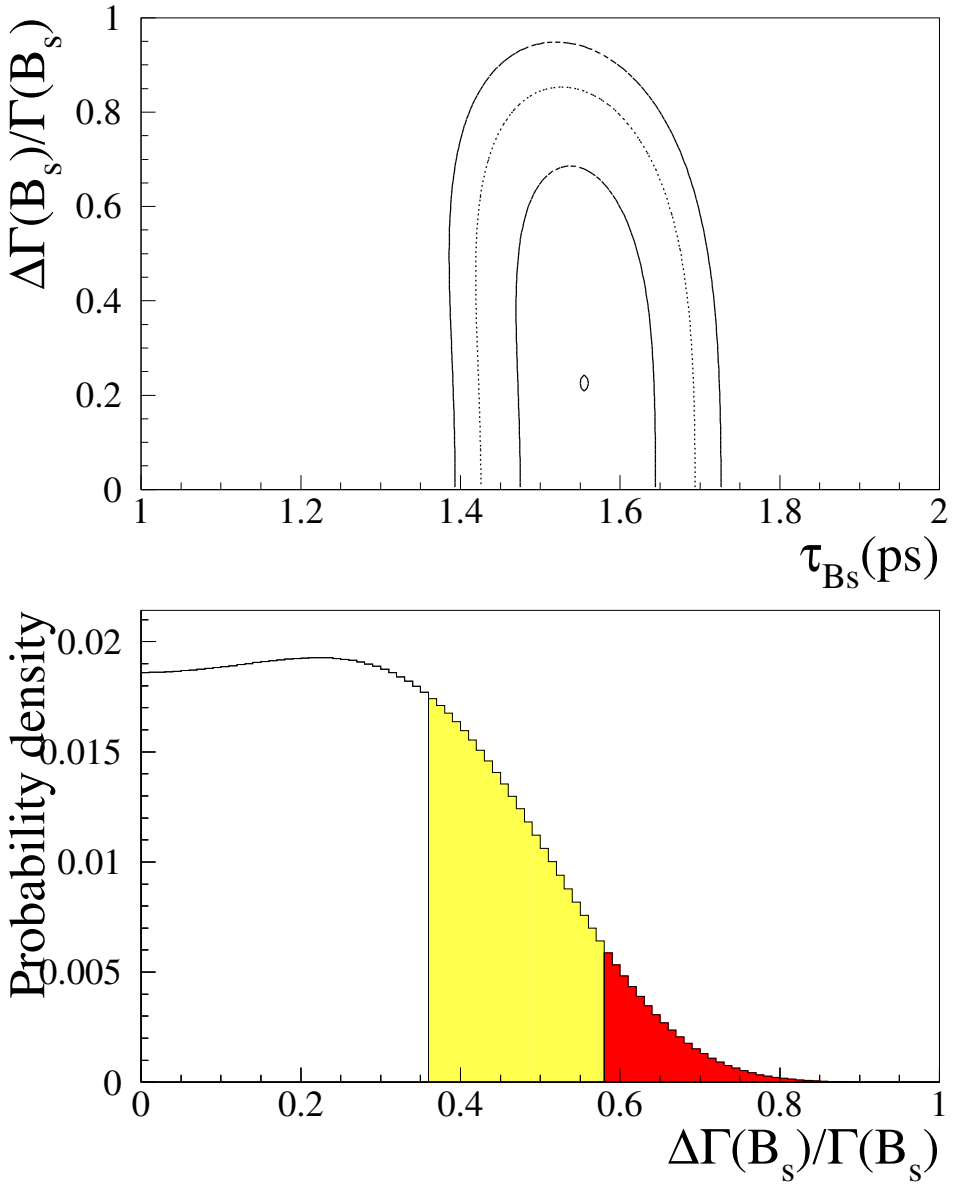

Figure 10: *Upper plot: contours corresponding to 68, 95 and 99 % C.L. of the negative log-likelihood in the plane* $\Delta\Gamma_{B_s^0}/\Gamma_{B_s^0}$-$\tau_{B_s^0}$. *Lower plot: probability density distribution for* $\Delta\Gamma_{B_s}/\Gamma_{B_s}$*; the two shaded regions show the limits at 68 % C.L. and 95 % C.L. respectively.*

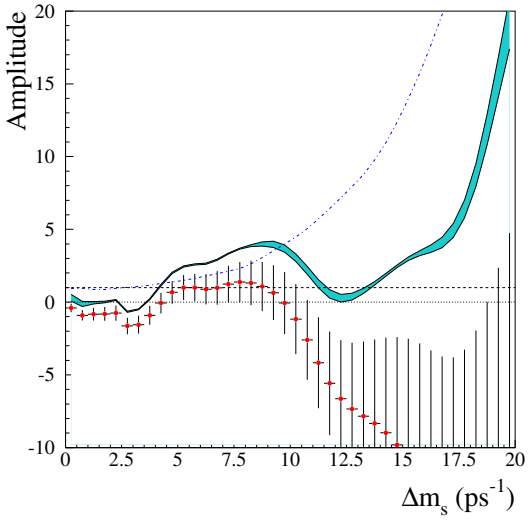

Figure 11: $D_s^{\pm}h^{\mp}$ *analysis: variation of the oscillation amplitude* A *as a function of* Δm_s*. The lower continuous line corresponds to* $A+1.645\ \sigma_A$ *where* σ_A *includes statistical uncertainties only, while the shaded area shows the contribution from systematics. The dashed-dotted line corresponds to the sensitivity curve. The lines at* A*=0 and* A*=1 are also given.*

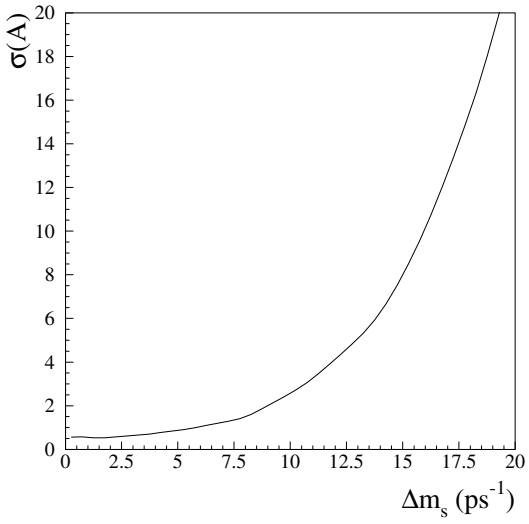

Figure 12: $D_s^{\pm}h^{\mp}$ *analysis: variation of the error on the amplitude as a function of* Δm_s*.*

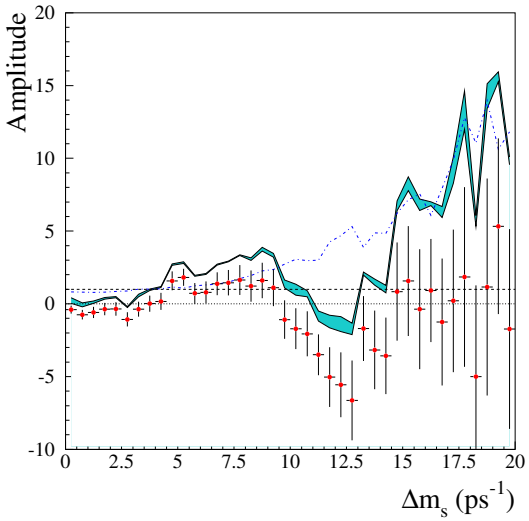

Figure 13: *Combination of the* $D_s^{\pm}h^{\mp}$ *and exclusive* B_s^0 *analyses: variation of the oscillation amplitude* A *as a function of* Δm_s*. The lower continuous line corresponds to* $A + 1.645\ \sigma_A$ *where* σ_A *includes statistical uncertainties only, while the shaded area shows the contribution from systematics. The dashed-dotted line corresponds to the sensitivity curve. The lines at A=0 and A=1 are also given.*

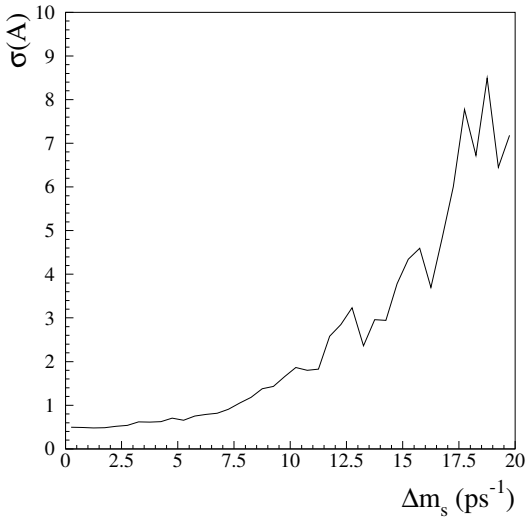

Figure 14: *Combination of the* $D_s^{\pm}h^{\mp}$ *and exclusive* B_s^0 *analyses: variation of the error on the amplitude as a function of* Δm_s*.*

EUROPEAN ORGANIZATION FOR NUCLEAR RESEARCH

Measurement of the B_s^0 Lifetime and Study of B_s^0-$\overline{B_s^0}$ Oscillations using $D_s\ell$ Events

DELPHI Collaboration

Preliminary

Abstract

Lifetime and oscillations of B_s^0 mesons have been studied in events with a large transverse momentum lepton and a D_s of opposite electric charge in the same hemisphere, selected from about 3.6 million hadronic Z^0 decays accumulated by DELPHI between 1992 and 1995.
The B_s^0 lifetime and the fractional width difference between the two physical B_s^0 states have been found to be:

$$\tau_{B_s^0} = (1.42^{+0.14}_{-0.13}(stat.) \pm 0.03(syst.))\ ps$$

$$\Delta\Gamma_{B_s^0}/\Gamma_{B_s^0} < 0.46 \text{ at the } 95\% \text{ C.L.}$$

In the latter result it has been assumed that $\tau_{B_s^0} = \tau_{B_d^0}$.
Using the same sample, a limit on the mass difference between the physical B_s^0 states has been set:

$$\Delta m_{B_s^0} > 7.5 \text{ ps}^{-1} \text{ at the } 95\% \text{ C.L.}$$

with a corresponding sensitivity equal to 8.2 ps^{-1}.

P.Abreu[21], W.Adam[49], T.Adye[36], P.Adzic[11], Z.Albrecht[17], T.Alderweireld[2], G.D.Alekseev[16], R.Alemany[48], T.Allmendinger[17], P.P.Allport[22], S.Almehed[24], U.Amaldi[9], N.Amapane[44], S.Amato[46], E.G.Anassontzis[3], P.Andersson[43], A.Andreazza[9], S.Andringa[21], P.Antilogus[25], W-D.Apel[17], Y.Arnoud[9], B.Åsman[43], J-E.Augustin[25], A.Augustinus[9], P.Baillon[9], P.Bambade[19], F.Barao[21], G.Barbiellini[45], R.Barbier[25], D.Y.Bardin[16], G.Barker[17], A.Baroncelli[38], M.Battaglia[15], M.Baubillier[23], K-H.Becks[51], M.Begalli[6], A.Behrmann[51], P.Beilliere[8], Yu.Belokopytov[9,52], N.C.Benekos[31], A.C.Benvenuti[5], C.Berat[14], M.Berggren[25], D.Bertini[25], D.Bertrand[2], M.Besancon[39], F.Bianchi[44], M.Bigi[44], M.S.Bilenky[16], M-A.Bizouard[19], D.Bloch[10], H.M.Blom[30], M.Bonesini[27], W.Bonivento[27], M.Boonekamp[39], P.S.L.Booth[22], A.W.Borgland[4], G.Borisov[19], C.Bosio[41], O.Botner[47], E.Boudinov[30], B.Bouquet[19], C.Bourdarios[19], T.J.V.Bowcock[22], I.Boyko[16], I.Bozovic[11], M.Bozzo[13], P.Branchini[38], T.Brenke[51], R.A.Brenner[47], P.Bruckman[18], J-M.Brunet[8], L.Bugge[32], T.Buran[32], T.Burgsmueller[51], P.Buschmann[51], S.Cabrera[48], M.Caccia[27], M.Calvi[27], T.Camporesi[9], V.Canale[37], F.Carena[9], L.Carroll[22], C.Caso[13], M.V.Castillo Gimenez[48], A.Cattai[9], F.R.Cavallo[5], V.Chabaud[9], Ph.Charpentier[9], L.Chaussard[25], P.Checchia[35], G.A.Chelkov[16], R.Chierici[44], P.Chochula[7], V.Chorowicz[25], J.Chudoba[29], K.Cieslik[18], P.Collins[9], R.Contri[13], E.Cortina[48], G.Cosme[19], F.Cossutti[9], J-H.Cowell[22], H.B.Crawley[1], D.Crennell[36], S.Crepe[14], G.Crosetti[13], J.Cuevas Maestro[33], S.Czellar[15], M.Davenport[9], W.Da Silva[23], A.Deghorain[2], G.Della Ricca[45], P.Delpierre[26], N.Demaria[9], A.De Angelis[9], W.De Boer[17], C.De Clercq[2], B.De Lotto[45], A.De Min[35], L.De Paula[46], H.Dijkstra[9], L.Di Ciaccio[37,9], J.Dolbeau[8], K.Doroba[50], M.Dracos[10], J.Drees[51], M.Dris[31], A.Duperrin[25], J-D.Durand[9], G.Eigen[4], T.Ekelof[47], G.Ekspong[43], M.Ellert[47], M.Elsing[9], J-P.Engel[10], B.Erzen[42], M.Espirito Santo[21], E.Falk[24], G.Fanourakis[11], D.Fassouliotis[11], J.Fayot[23], M.Feindt[17], P.Ferrari[27], A.Ferrer[48], E.Ferrer-Ribas[19], S.Fichet[23], A.Firestone[1], U.Flagmeyer[51], H.Foeth[9], E.Fokitis[31], F.Fontanelli[13], B.Franek[36], A.G.Frodesen[4], R.Fruhwirth[49], F.Fulda-Quenzer[19], J.Fuster[48], A.Galloni[22], D.Gamba[44], S.Gamblin[19], M.Gandelman[46], C.Garcia[48], C.Gaspar[9], M.Gaspar[46], U.Gasparini[35], Ph.Gavillet[9], E.N.Gazis[31], D.Gele[10], N.Ghodbane[25], I.Gil[48], F.Glege[51], R.Gokieli[9,50], B.Golob[42], G.Gomez-Ceballos[40], P.Goncalves[21], I.Gonzalez Caballero[40], G.Gopal[36], L.Gorn[1,53], M.Gorski[50], V.Gracco[13], J.Grahl[1], E.Graziani[38], C.Green[22], H-J.Grimm[17], P.Gris[39], G.Grosdidier[19], K.Grzelak[50], M.Gunther[47], J.Guy[36], F.Hahn[9], S.Hahn[51], S.Haider[9], A.Hallgren[47], K.Hamacher[51], J.Hansen[32], F.J.Harris[34], V.Hedberg[24], S.Heising[17], J.J.Hernandez[48], P.Herquet[2], H.Herr[9], T.L.Hessing[34], J.-M.Heuser[51], E.Higon[48], S-O.Holmgren[43], P.J.Holt[34], S.Hoorelbeke[2], M.Houlden[22], J.Hrubec[49], K.Huet[2], G.J.Hughes[22], K.Hultqvist[43], J.N.Jackson[22], R.Jacobsson[9], P.Jalocha[9], R.Janik[7], Ch.Jarlskog[24], G.Jarlskog[24], P.Jarry[39], B.Jean-Marie[19], E.K.Johansson[43], P.Jonsson[25], C.Joram[9], P.Juillot[10], F.Kapusta[23], K.Karafasoulis[11], S.Katsanevas[25], E.C.Katsoufis[31], R.Keranen[17], B.P.Kersevan[42], B.A.Khomenko[16], N.N.Khovanski[16], A.Kiiskinen[15], B.King[22], A.Kinvig[22], N.J.Kjaer[30], O.Klapp[51], H.Klein[9], P.Kluit[30], P.Kokkinias[11], M.Koratzinos[9], C.Kourkoumelis[3], O.Kouznetsov[39], M.Krammer[49], E.Kriznic[42], J.Krstic[11], Z.Krumstein[16], P.Kubinec[7], J.Kurowska[50], K.Kurvinen[15], J.W.Lamsa[1], D.W.Lane[1], P.Langefeld[51], J-P.Laugier[39], R.Lauhakangas[15], G.Leder[49], F.Ledroit[14], V.Lefebure[2], L.Leinonen[43], A.Leisos[11], R.Leitner[29], J.Lemonne[2], G.Lenzen[51], V.Lepeltier[19], T.Lesiak[18], M.Lethuillier[39], J.Libby[34], D.Liko[9], A.Lipniacka[43], I.Lippi[35], B.Loerstad[24], J.G.Loken[34], J.H.Lopes[46], J.M.Lopez[40], R.Lopez-Fernandez[14], D.Loukas[11], P.Lutz[39], L.Lyons[34], J.MacNaughton[49], J.R.Mahon[6], A.Maio[21], A.Malek[51], T.G.M.Malmgren[43], S.Maltezos[31], V.Malychev[16], F.Mandl[49], J.Marco[40], R.Marco[40], B.Marechal[46], M.Margoni[35], J-C.Marin[9], C.Mariotti[9], A.Markou[11], C.Martinez-Rivero[19], F.Martinez-Vidal[48], S.Marti i Garcia[9], J.Masik[12], N.Mastroyiannopoulos[11], F.Matorras[40], C.Matteuzzi[27], G.Matthiae[37], F.Mazzucato[35], M.Mazzucato[35], M.Mc Cubbin[22], R.Mc Kay[1], R.Mc Nulty[22], G.Mc Pherson[22], C.Meroni[27], W.T.Meyer[1], E.Migliore[44], L.Mirabito[25], W.A.Mitaroff[49], U.Mjoernmark[24], T.Moa[43], M.Moch[17], R.Moeller[28], K.Moenig[9], M.R.Monge[13], X.Moreau[23], P.Morettini[13], G.Morton[34], U.Mueller[51], K.Muenich[51], M.Mulders[30], C.Mulet-Marquis[14], R.Muresan[24], W.J.Murray[36], B.Muryn[14,18], G.Myatt[34], T.Myklebust[32], F.Naraghi[14], F.L.Navarria[5], S.Navas[48], K.Nawrocki[50], P.Negri[27], S.Nemecek[12], N.Neufeld[9], N.Neumeister[49], R.Nicolaidou[39], B.S.Nielsen[28], M.Nikolenko[10,16], V.Nomokonov[15], A.Normand[22], A.Nygren[24], A.G.Olshevski[16], A.Onofre[21], R.Orava[15], G.Orazi[10], K.Osterberg[15], A.Ouraou[39], M.Paganoni[27], S.Paiano[5], R.Pain[23], R.Paiva[21], J.Palacios[34], H.Palka[18], Th.D.Papadopoulou[31], K.Papageorgiou[11], L.Pape[9], C.Parkes[9], F.Parodi[13], U.Parzefall[22], A.Passeri[38], O.Passon[51], M.Pegoraro[35], L.Peralta[21], M.Pernicka[49], A.Perrotta[5], C.Petridou[45], A.Petrolini[13], H.T.Phillips[36], F.Pierre[39], M.Pimenta[21], E.Piotto[27], T.Podobnik[42], M.E.Pol[6], G.Polok[18], P.Poropat[45], V.Pozdniakov[16], P.Privitera[37], N.Pukhaeva[16], A.Pullia[27], D.Radojicic[34], S.Ragazzi[27], H.Rahmani[31], D.Rakoczy[49], P.N.Ratoff[20], A.L.Read[32], P.Rebecchi[9], N.G.Redaelli[27], M.Regler[49], D.Reid[30], R.Reinhardt[51], P.B.Renton[34], L.K.Resvanis[3], F.Richard[19], J.Ridky[12], G.Rinaudo[44], O.Rohne[32], A.Romero[44], P.Ronchese[35], E.I.Rosenberg[1], P.Rosinsky[7], P.Roudeau[19], T.Rovelli[5], Ch.Royon[39], V.Ruhlmann-Kleider[39], A.Ruiz[40], H.Saarikko[15], Y.Sacquin[39], A.Sadovsky[16], G.Sajot[14], J.Salt[48], D.Sampsonidis[11], M.Sannino[13], H.Schneider[17], Ph.Schwemling[23], B.Schwering[51], U.Schwickerath[17], M.A.E.Schyns[51], F.Scuri[45], P.Seager[20], Y.Sedykh[16], A.M.Segar[34], R.Sekulin[36], R.C.Shellard[6], A.Sheridan[22], M.Siebel[51], L.Simard[39], F.Simonetto[35], A.N.Sisakian[16], G.Smadja[25], O.Smirnova[24], G.R.Smith[36], A.Sopczak[17], R.Sosnowski[50], T.Spassov[21], E.Spiriti[38], P.Sponholz[51], S.Squarcia[13], C.Stanescu[38], S.Stanic[42], K.Stevenson[34],

A.Stocchi[19], J.Strauss[49], R.Strub[10], B.Stugu[4], M.Szczekowski[50], M.Szeptycka[50], T.Tabarelli[27], F.Tegenfeldt[47], F.Terranova[27], J.Thomas[34], J.Timmermans[30], N.Tinti[5], L.G.Tkatchev[16], S.Todorova[10], A.Tomaradze[2], B.Tome[21], A.Tonazzo[9], L.Tortora[38], G.Transtromer[24], D.Treille[9], G.Tristram[8], M.Trochimczuk[50], C.Troncon[27], A.Tsirou[9], M-L.Turluer[39], I.A.Tyapkin[16], S.Tzamarias[11], O.Ullaland[9], G.Valenti[5], E.Vallazza[45], C.Vander Velde[2], G.W.Van Apeldoorn[30], P.Van Dam[30], W.K.Van Doninck[2], J.Van Eldik[30], A.Van Lysebetten[2], I.Van Vulpen[30], N.Vassilopoulos[34], G.Vegni[27], L.Ventura[35], W.Venus[36,9], F.Verbeure[2], M.Verlato[35], L.S.Vertogradov[16], V.Verzi[37], D.Vilanova[39], L.Vitale[45], A.S.Vodopyanov[16], C.Vollmer[17], G.Voulgaris[3], V.Vrba[12], H.Wahlen[51], C.Walck[43], C.Weiser[17], D.Wicke[51], J.H.Wickens[2], G.R.Wilkinson[9],

M.Winter[10], M.Witek[18], G.Wolf[9], J.Yi[1], A.Zalewska[18], P.Zalewski[50], D.Zavrtanik[42], E.Zevgolatakos[11], N.I.Zimin[16,24], G.C.Zucchelli[43], G.Zumerle[35]

[1]Department of Physics and Astronomy, Iowa State University, Ames IA 50011-3160, USA
[2]Physics Department, Univ. Instelling Antwerpen, Universiteitsplein 1, BE-2610 Wilrijk, Belgium
and IIHE, ULB-VUB, Pleinlaan 2, BE-1050 Brussels, Belgium
and Faculté des Sciences, Univ. de l'Etat Mons, Av. Maistriau 19, BE-7000 Mons, Belgium
[3]Physics Laboratory, University of Athens, Solonos Str. 104, GR-10680 Athens, Greece
[4]Department of Physics, University of Bergen, Allégaten 55, NO-5007 Bergen, Norway
[5]Dipartimento di Fisica, Università di Bologna and INFN, Via Irnerio 46, IT-40126 Bologna, Italy
[6]Centro Brasileiro de Pesquisas Físicas, rua Xavier Sigaud 150, BR-22290 Rio de Janeiro, Brazil
and Depto. de Física, Pont. Univ. Católica, C.P. 38071 BR-22453 Rio de Janeiro, Brazil
and Inst. de Física, Univ. Estadual do Rio de Janeiro, rua São Francisco Xavier 524, Rio de Janeiro, Brazil
[7]Comenius University, Faculty of Mathematics and Physics, Mlynska Dolina, SK-84215 Bratislava, Slovakia
[8]Collège de France, Lab. de Physique Corpusculaire, IN2P3-CNRS, FR-75231 Paris Cedex 05, France
[9]CERN, CH-1211 Geneva 23, Switzerland
[10]Institut de Recherches Subatomiques, IN2P3 - CNRS/ULP - BP20, FR-67037 Strasbourg Cedex, France
[11]Institute of Nuclear Physics, N.C.S.R. Demokritos, P.O. Box 60228, GR-15310 Athens, Greece
[12]FZU, Inst. of Phys. of the C.A.S. High Energy Physics Division, Na Slovance 2, CZ-180 40, Praha 8, Czech Republic
[13]Dipartimento di Fisica, Università di Genova and INFN, Via Dodecaneso 33, IT-16146 Genova, Italy
[14]Institut des Sciences Nucléaires, IN2P3-CNRS, Université de Grenoble 1, FR-38026 Grenoble Cedex, France
[15]Helsinki Institute of Physics, HIP, P.O. Box 9, FI-00014 Helsinki, Finland
[16]Joint Institute for Nuclear Research, Dubna, Head Post Office, P.O. Box 79, RU-101 000 Moscow, Russian Federation
[17]Institut für Experimentelle Kernphysik, Universität Karlsruhe, Postfach 6980, DE-76128 Karlsruhe, Germany
[18]Institute of Nuclear Physics and University of Mining and Metalurgy, Ul. Kawiory 26a, PL-30055 Krakow, Poland
[19]Université de Paris-Sud, Lab. de l'Accélérateur Linéaire, IN2P3-CNRS, Bât. 200, FR-91405 Orsay Cedex, France
[20]School of Physics and Chemistry, University of Lancaster, Lancaster LA1 4YB, UK
[21]LIP, IST, FCUL - Av. Elias Garcia, 14-1^{o}, PT-1000 Lisboa Codex, Portugal
[22]Department of Physics, University of Liverpool, P.O. Box 147, Liverpool L69 3BX, UK
[23]LPNHE, IN2P3-CNRS, Univ. Paris VI et VII, Tour 33 (RdC), 4 place Jussieu, FR-75252 Paris Cedex 05, France
[24]Department of Physics, University of Lund, Sölvegatan 14, SE-223 63 Lund, Sweden
[25]Université Claude Bernard de Lyon, IPNL, IN2P3-CNRS, FR-69622 Villeurbanne Cedex, France
[26]Univ. d'Aix - Marseille II - CPP, IN2P3-CNRS, FR-13288 Marseille Cedex 09, France
[27]Dipartimento di Fisica, Università di Milano and INFN, Via Celoria 16, IT-20133 Milan, Italy
[28]Niels Bohr Institute, Blegdamsvej 17, DK-2100 Copenhagen Ø, Denmark
[29]NC, Nuclear Centre of MFF, Charles University, Areal MFF, V Holesovickach 2, CZ-180 00, Praha 8, Czech Republic
[30]NIKHEF, Postbus 41882, NL-1009 DB Amsterdam, The Netherlands
[31]National Technical University, Physics Department, Zografou Campus, GR-15773 Athens, Greece
[32]Physics Department, University of Oslo, Blindern, NO-1000 Oslo 3, Norway
[33]Dpto. Fisica, Univ. Oviedo, Avda. Calvo Sotelo s/n, ES-33007 Oviedo, Spain
[34]Department of Physics, University of Oxford, Keble Road, Oxford OX1 3RH, UK
[35]Dipartimento di Fisica, Università di Padova and INFN, Via Marzolo 8, IT-35131 Padua, Italy
[36]Rutherford Appleton Laboratory, Chilton, Didcot OX11 OQX, UK
[37]Dipartimento di Fisica, Università di Roma II and INFN, Tor Vergata, IT-00173 Rome, Italy
[38]Dipartimento di Fisica, Università di Roma III and INFN, Via della Vasca Navale 84, IT-00146 Rome, Italy
[39]DAPNIA/Service de Physique des Particules, CEA-Saclay, FR-91191 Gif-sur-Yvette Cedex, France
[40]Instituto de Fisica de Cantabria (CSIC-UC), Avda. los Castros s/n, ES-39006 Santander, Spain
[41]Dipartimento di Fisica, Università degli Studi di Roma La Sapienza, Piazzale Aldo Moro 2, IT-00185 Rome, Italy
[42]J. Stefan Institute, Jamova 39, SI-1000 Ljubljana, Slovenia and Laboratory for Astroparticle Physics,
Nova Gorica Polytechnic, Kostanjeviska 16a, SI-5000 Nova Gorica, Slovenia,
and Department of Physics, University of Ljubljana, SI-1000 Ljubljana, Slovenia
[43]Fysikum, Stockholm University, Box 6730, SE-113 85 Stockholm, Sweden
[44]Dipartimento di Fisica Sperimentale, Università di Torino and INFN, Via P. Giuria 1, IT-10125 Turin, Italy
[45]Dipartimento di Fisica, Università di Trieste and INFN, Via A. Valerio 2, IT-34127 Trieste, Italy
and Istituto di Fisica, Università di Udine, IT-33100 Udine, Italy
[46]Univ. Federal do Rio de Janeiro, C.P. 68528 Cidade Univ., Ilha do Fundão BR-21945-970 Rio de Janeiro, Brazil
[47]Department of Radiation Sciences, University of Uppsala, P.O. Box 535, SE-751 21 Uppsala, Sweden
[48]IFIC, Valencia-CSIC, and D.F.A.M.N., U. de Valencia, Avda. Dr. Moliner 50, ES-46100 Burjassot (Valencia), Spain
[49]Institut für Hochenergiephysik, Österr. Akad. d. Wissensch., Nikolsdorfergasse 18, AT-1050 Vienna, Austria
[50]Inst. Nuclear Studies and University of Warsaw, Ul. Hoza 69, PL-00681 Warsaw, Poland
[51]Fachbereich Physik, University of Wuppertal, Postfach 100 127, DE-42097 Wuppertal, Germany
[52]On leave of absence from IHEP Serpukhov
[53]Now at University of Florida

1 Introduction

In this paper, the average lifetime of the $\mathrm{B_s^0}$ meson has been measured and limits have been derived on the oscillation frequency of the $\mathrm{B_s^0}$-$\overline{\mathrm{B_s^0}}$ system, $\Delta m_{\mathrm{B_s^0}}$, and on the decay width difference, $\Delta\Gamma_{\mathrm{B_s^0}}$, between mass eigenstates of this system.
Starting with a $\mathrm{B_s^0}$ meson produced at time t=0, the probability, $\mathcal{P}$, to observe a $\mathrm{B_s^0}$ or a $\overline{\mathrm{B_s^0}}$ decaying at the proper time t can be written, neglecting effects from CP violation:

$$\mathcal{P}(\mathrm{B_s^0} \to \mathrm{B_s^0}(\overline{\mathrm{B_s^0}})) \;=\; \frac{\Gamma_{\mathrm{B_s^0}}}{2}\mathrm{e}^{-\Gamma_{\mathrm{B_s^0}}\mathrm{t}}(\cosh(\frac{\Delta\Gamma_{\mathrm{B_s^0}}}{2}\mathrm{t}) \;\pm\; \cos(\Delta\mathrm{m}_{\mathrm{B_s^0}}\mathrm{t})) \tag{1}$$

where $\Gamma_{\mathrm{B_s^0}} = (\Gamma^H_{\mathrm{B_s^0}} + \Gamma^L_{\mathrm{B_s^0}})/2$, $\Delta\Gamma_{\mathrm{B_s^0}} = \Gamma^L_{\mathrm{B_s^0}} - \Gamma^H_{\mathrm{B_s^0}}$ and $\Delta m_{\mathrm{B_s^0}} = m^H_{\mathrm{B_s^0}} - m^L_{\mathrm{B_s^0}}$. L and H denote the light and heavy physical states, respectively; $\Delta\Gamma_{\mathrm{B_s^0}}$ and $\Delta m_{\mathrm{B_s^0}}$ are defined to be positive [1] and the plus (minus) signs refer to $\mathrm{B_s^0}$ ($\overline{\mathrm{B_s^0}}$) decays. The oscillation period gives a direct measurement of the mass difference between the two physical states. The Standard Model predicts that $\Delta\Gamma_{\mathrm{B_s^0}} \ll \Delta m_{\mathrm{B_s^0}}$, for which the previous expression simplifies to :

$$\mathcal{P}^{unmix.}_{\mathrm{B_s^0}} \;=\; \mathcal{P}(\mathrm{B_s^0} \to \mathrm{B_s^0}) \;=\; \Gamma_{\mathrm{B_s^0}}\mathrm{e}^{-\Gamma_{\mathrm{B_s^0}}\mathrm{t}}\cos^2(\frac{\Delta\mathrm{m}_{\mathrm{B_s^0}}\mathrm{t}}{2}) \tag{2}$$

and similarly:

$$\mathcal{P}^{mix.}_{\mathrm{B_s^0}} = \mathcal{P}(\mathrm{B_s^0} \to \overline{\mathrm{B_s^0}}) \;=\; \Gamma_{\mathrm{B_s^0}}\mathrm{e}^{-\Gamma_{\mathrm{B_s^0}}\mathrm{t}}\sin^2(\frac{\Delta\mathrm{m}_{\mathrm{B_s^0}}\mathrm{t}}{2}) \tag{3}$$

The oscillation frequency, proportional to $\Delta m_{\mathrm{B_s^0}}$, can be obtained from the fit of the time distributions given in relations (2) and (3), whereas expression (1), without distinguishing between the $\mathrm{B_s^0}$ and the $\overline{\mathrm{B_s^0}}$, can be used to determine the average lifetime and the difference between the lifetimes of the heavy and light mass eigenstates.

B physics allows a precise determination of some of the parameters of the V_{CKM}. All the nine elements can be expressed in term of four parameters that are, in Wolfenstein parametrization [2], λ, A, ρ and η. The values of ρ and η are the most uncertain.
Several quantities which depend on ρ and η can be measured and, if the Standard Model is correct, they must define compatible values for the two parameters, inside measurement errors and theoretical uncertainties.
These quantities are ϵ_K, the parameter introduced to measure CP violation in the K system, $|V_{ub}|/|V_{cb}|$, the ratio between the modulus of the CKM matrix elements corresponding to $b \to u$ and $b \to c$ transitions and the mass difference $\Delta m_{\mathrm{B_d^0}}$.

In the Standard Model, $\mathrm{B_q^0}$-$\overline{\mathrm{B_q^0}}$ ($q = \mathrm{d, s}$) mixing is a direct consequence of second order weak interactions. Having kept only the dominant top quark contribution, $\Delta m_{\mathrm{B_q^0}}$ can be expressed in terms of Standard Model parameters [3]:

$$\Delta m_{\mathrm{B_q^0}} = \frac{G_F^2}{6\pi^2}|V_{tb}|^2|V_{tq}|^2 m_t^2 m_{\mathrm{B_q}} f^2_{\mathrm{B_q}} B_{\mathrm{B_q}} \eta_{\mathrm{B}} F(\frac{m_t^2}{m_W^2}). \tag{4}$$

In this expression G_F is the Fermi coupling constant; $F(x_t)$, with $x_t = \frac{m_t^2}{m_W^2}$, results from the evaluation of the second order weak "box" diagram responsible for the mixing and has a smooth dependence on x_t; η_{B} is a QCD correction factor obtained at next to leading order in perturbative QCD [4]. The dominant uncertainties in Equation (4) come from the evaluation of the B meson decay constant $f_{\mathrm{B_q}}$ and of the "bag" parameter $B_{\mathrm{B_q}}$. The two elements of the V_{CKM} matrix are equal to:

$$|V_{td}| = A\lambda^3\sqrt{(1-\rho)^2+\eta^2} \quad ; \quad |V_{ts}| = A\lambda^2, \tag{5}$$

neglecting terms of order $O(\lambda^4)$.

In the Wolfenstein parametrization, $|V_{ts}|$ is independent of ρ and η. A measurement of $\Delta m_{\mathrm{B_s^0}}$ is thus a way to measure the value of the non perturbative QCD parameters. Direct information on V_{td} can be inferred by measuring $\Delta m_{\mathrm{B_d^0}}$.
Several experiments have accurately measured $\Delta m_{\mathrm{B_d^0}}$, nevertheless this precision cannot be fully exploited to extract information on ρ and η because of the large uncertainty which originates in the evaluation of the non-perturbative QCD parameters.
An efficient constraint is the ratio between the Standard Model expectations for $\Delta m_{\mathrm{B_d^0}}$ and $\Delta m_{\mathrm{B_s^0}}$, given by:

$$\frac{\Delta m_{\mathrm{B_d^0}}}{\Delta m_{\mathrm{B_s^0}}} = \frac{m_{\mathrm{B_d^0}} f^2_{\mathrm{B_d^0}} B_{\mathrm{B_d^0}} \eta_{\mathrm{B_d^0}}}{m_{\mathrm{B_s^0}} f^2_{\mathrm{B_s^0}} B_{\mathrm{B_s^0}} \eta_{\mathrm{B_s^0}}} \frac{|V_{td}|^2}{|V_{ts}|^2} \tag{6}$$

A measurement of the ratio $\Delta m_{\mathrm{B_d^0}}/\Delta m_{\mathrm{B_s^0}}$ gives the same type of constraint, in the $\rho - \eta$ plane, as a measurement of $\Delta m_{\mathrm{B_d^0}}$, and this ratio is expected to be better under control from theory than the absolute values of f_B and B_B [5].
Using existing measurements which constrain ρ and η, except those on $\Delta m_{\mathrm{B_s^0}}$, the distribution for the expected values of $\Delta m_{\mathrm{B_s^0}}$ can be obtained. It has been shown, in the Standard Model, that $\Delta m_{\mathrm{B_s^0}}$ has to lie, at 68% C.L., between 12 and 17.6 ps^{-1} and is expected to be smaller than $20ps^{-1}$ at 95% C.L. [6].

The $\mathrm{B_s^0}$ meson lifetime is expected to be equal to the $\mathrm{B_d^0}$ lifetime [7] within one percent. In the Standard Model, the ratio between the mass and decay width differences in the $\mathrm{B^0}$-$\overline{\mathrm{B^0}}$ system is of the order $(m_b/m_t)^2$, although large QCD corrections are expected.
Explicit calculations to leading order in QCD correction, in the OPE formalism [1] predict:

$$\Delta\Gamma_{\mathrm{B_s^0}}/\Gamma_{\mathrm{B_s^0}} = 0.16^{+0.11}_{-0.09}$$

where the quoted error is dominated by the uncertainty related to hadronic matrix elements.
Recent calculations [8] at next-to-leading order predict a lower value:

$$\Delta\Gamma_{\mathrm{B_s^0}}/\Gamma_{\mathrm{B_s^0}} = 0.054^{+0.016}_{-0.032}$$

An interesting approach consists in using the ratio between $\Delta\Gamma_{\mathrm{B_s^0}}$ and $\Delta m_{\mathrm{B_s^0}}$ [8]:

$$\frac{\Delta\Gamma_{\mathrm{B_s^0}}}{\Delta m_{\mathrm{B_s^0}}} = (2.63^{+0.67}_{-1.36})10^{-3} \tag{7}$$

to constrain the upper part of the $\Delta m_{\mathrm{B_s^0}}$ spectrum with an upper limit on $\Delta\Gamma_{\mathrm{B_s^0}}/\Gamma_{\mathrm{B_s^0}}$.
If, in future, the theoretical uncertainty can be reduced, this method can give an alternative approach in determining $\Delta m_{\mathrm{B_s^0}}$ via $\Delta\Gamma_{\mathrm{B_s^0}}$ and, in conjunction with the determination of $\Delta m_{\mathrm{B_d^0}}$, can provide an extra constraint on the ρ and η parameters.

The results presented in the following have been obtained from data accumulated by DELPHI between 1992 and 1995 corresponding to 3.6 million hadronic $\mathrm{Z^0}$ decays. The main features of these analyses are:

- a precise measurement of the B decay proper time;
- a determination of the charge of the b quark at the B-meson decay time (decay tag);
- a determination of the sign of the b quark at production time (production tag).

The first item is common to the three studies on $\Delta m_{\mathrm{B_s^0}}$, $\tau_{\mathrm{B_s^0}}$ and $\Delta\Gamma_{\mathrm{B_s^0}}$ while the others are specific to the oscillation analyses. For these last, the principle of the measurement is as follows. Each of the charged and neutral particles measured in an event is assigned to one of the two hemispheres defined by the plane transverse to the sphericity axis. A "production tag" is used to estimate the $\mathrm{b}/\overline{\mathrm{b}}$ sign of the initial quark at the production point. The decay time of the B hadron is evaluated and a "decay tag" is defined, correlated with the $\mathrm{b}/\overline{\mathrm{b}}$ content of the decaying hadron. The analysis is performed using events containing a lepton emitted at large transverse momentum, p_t, relative to its jet axis accompanied by an exclusively (or partially) reconstructed $\mathrm{D_s}$ in the same hemisphere and of opposite electric charge. The lepton charge defines the "decay tag". Different variables defined in the same and in the opposite hemisphere, are used to determine the "production tag".

Section 2 describes the main features of the DELPHI detector, the event selection and the event simulation. Section 3 describes the selection of the $\mathrm{D_s}\ell$ sample. Section 4 presents the $\mathrm{B_s^0}$ lifetime measurement. Section 5 presents the result on the lifetime difference. Section 6 is devoted to the study of $\mathrm{B_s^0}$-$\overline{\mathrm{B_s^0}}$ oscillations with the $\mathrm{D_s}\ell$ sample: the first part describes the "production tag" algorithm while the second part presents the fitting procedure and the result on $\Delta m_{\mathrm{B_s^0}}$.

2 The DELPHI detector

The events used in this analysis have been recorded with the DELPHI detector at LEP operating at an energy close to the $\mathrm{Z^0}$ peak. The DELPHI detector and its performance have been described in detail elsewhere [9]. In this section are summarized the most relevant characteristics for this analysis.

2.1 Global event reconstruction

2.1.1 Charged particles reconstruction

The detector elements used for tracking are the Vertex Detector (VD), the Inner Detector (ID), the Time Projection Chamber (TPC) and the Outer Detector (OD).

The VD provided the high precision needed near the primary vertex. For the data taken from 1991 to 1993, the VD consisted of three cylindrical layers of silicon detectors (radii 6.3, 9.0 and 10.9 cm) measuring points in the plane transverse to the beam direction ($r\phi$ coordinate) in the polar angle range $43^\circ < \theta < 137^\circ$. In 1994, two layers have been equipped with detector modules with double sided readout, providing a single hit precision of 7.6 μm in the $r\phi$ coordinate, similar to that obtained previously, and 9 μm in the coordinate parallel to the beam (z) [10]. For high momentum particles with associated hits in the VD, the extrapolation precision close to the interaction region is 20 μm in the $r\phi$ plane and 34 μm in the rz plane.

Charged particle tracks have been reconstructed with 95% efficiency and with a momentum resolution $\sigma_p/p < 2.0 \times 10^{-3} p$ (p in GeV/c) in the polar angle region $25^\circ < \theta < 155^\circ$.

2.1.2 Energy reconstruction

The total energy in the event is determined by using all information available from the tracking detectors and the calorimeters. For charged particles, the momentum measured

in the tracking detector is used. Photons are detected and their energy measured in the electromagnetic calorimeters, whereas the hadron calorimeter detects long lived neutral hadrons such as neutrons and K_L^0's.

The electromagnetic calorimetry system of DELPHI is composed of a barrel calorimeter, the HPC, covering the polar angle region $46^\circ < \theta < 134^\circ$, and a forward calorimeter, the FEMC, for polar angles $8^\circ < \theta < 35^\circ$ and $145^\circ < \theta < 172^\circ$. The relative precision on the measured energy E has been parametrized as $\sigma_E/E = 0.32/\sqrt{E} \oplus 0.043$ (E in GeV) in the barrel, and $\sigma_E/E = 0.12/\sqrt{E} \oplus 0.03$ (E in GeV) in the forward region.

The hadronic calorimeter, HCAL, has been installed in the return yoke of the DELPHI solenoid. In the barrel region, the energy has been reconstructed with a precision of $\sigma_E/E = 1.12/\sqrt{E} \oplus 0.21$ (E in GeV).

2.1.3 Hadronic Z^0 selection

Hadronic events from Z^0 decays have been selected by requiring a charged multiplicity greater than four and a total energy of charged particles greater than $0.12\sqrt{s}$, where $\sqrt{s}$ is the centre-of-mass energy and all particles have been assumed to be pions; charged particles have been required to have a momentum greater than 0.4 GeV/c and a polar angle between 20° and 160°. The overall trigger and selection efficiency is (95.0±0.1)% [11]. A total of 3.6 million hadronic events has been obtained from the 1992-1995 data.

2.2 Particle identification

2.2.1 Lepton identification

Lepton identification in the DELPHI detector is based on the barrel electromagnetic calorimeter and the muon chambers. Only particles with momentum larger than 2 GeV/c have been considered as possible lepton candidates.

Two layers of muon chambers covered the polar angle region $20^\circ < \theta < 160^\circ$, except for two regions of $\pm 3^\circ$ around $\theta = 42^\circ$ and $\theta = 138^\circ$. The first layer consists of three planes of chambers and is inside the return yoke of the magnet, after 90 cm of iron, while the second, with two chamber planes, is mounted outside the yoke, behind a further 20 cm of iron. The probability of a particle being a muon has been calculated from a global χ^2 of the match between the track extrapolation to the muon chambers and the hits observed there. Four identification flags are given as output of the muon identification in decreasing order of efficiency: very loose, loose, standard and tight. In this analysis the loose selection has been applied corresponding to an efficiency of $(94.8 \pm 0.1)\%$ with a hadron misidentification probability of $(1.5 \pm 0.1)\%$.

Electron identification has been performed using two independent and complementary measurements, the dE/dx measurement of the TPC (described in section 2.2.2) and the energy deposition in the HPC. Probabilities from calorimetric measurements and tracking are combined to produce an overall probability for the electron hypothesis. Three levels of identification are given: loose, standard and tight.
The loose selection has been applied for this analysis corresponding to an efficiency of 80 % with an hadron misidentifation probability of $\simeq 1.6$ %.

2.2.2 Hadron identification

Hadron identification relied on the RICH detector and on the specific ionisation measurement performed by the TPC.

The RICH detector [12] used two radiators. A gas radiator separated kaons from pions between 3 and 9 GeV/c, where kaons gave no Cherenkov light whereas pions did, and between 9 and 16 GeV/c, using the measured Cherenkov angle. It also provided kaon/proton separation from 8 to 20 GeV/c. A liquid radiator, which has been fully operational for 1994 and 1995 data, provided $p/K/\pi$ separation in the momentum range 1.5–7 GeV/c.

The specific energy loss per unit length (dE/dx) is measured in the TPC by using up to 192 sense wires. At least 30 contributing measurements have been required to compute the truncated mean. In the momentum range $3 < p < 25$ GeV/c, this is fulfilled for 55% of the tracks, and the dE/dx measurement has a precision of $\pm 7\%$.

The combination of the two measurements, dE/dx and RICH angles, provides three levels of pion, kaon and proton tag (loose, standard, tight) corresponding to different purities. A tag for "Heavy Particle" is also given in order to separate pions from heavier hadrons with high efficiency.
The Standard "Heavy Particle" flag has an efficiency of about 70 % with a pion misidentification probability of 10 % for charged particle with momentum greater than 0.7 GeV/c.

2.2.3 Λ^0 and K^0 reconstruction

The $\Lambda^0 \to p\pi^-$ and $K^0 \to \pi^+\pi^-$ decays have been reconstructed if the distance in the $r\phi$ plane between the V^0 decay point and the primary vertex is less than 90 cm. This condition meant that the decay products have track segments at least 20 cm long in the TPC. The reconstruction of the V^0 vertex and selection cuts are described in detail in reference [9].
Only K^0 candidates passing the "tight" selection criteria have been retained for this analysis.

2.2.4 π^0 reconstruction

The $\pi^0 \to \gamma\gamma$ decays are reconstructed by fitting all $\gamma\gamma$ pairs whose invariant mass is within 20 MeV of the nominal π^0 mass, using the nominal π^0 mass as a constraint. The fit probability has to be larger than 1%.

2.3 Primary vertex reconstruction and event topology

The location of the e^+e^- interaction has been reconstructed on an event-by-event basis using the beam spot position as a constraint [9]. In 1994 and 1995 data, the position of the primary vertex transverse to the beam has been determined with a precision of about 40 μm in the horizontal direction, and about 10 μm in the vertical direction. For 1992 and 1993 data, the uncertainties are larger by about 50%.

Each selected event has been divided into two hemispheres separated by the plane transverse to the sphericity axis. A clustering analysis based on the JETSET algorithm LUCLUS [13] with default parameters has been used to define the jets, using both charged and neutral particles. These jets have been used to measure the p_t^{out} of each particle in the event, defined as its momentum transverse to the axis of the rest of the jet it belonged to, after removing the particle itself.

The different detector configurations, both for hadron identification and vertex resolution, implies, in the rest of the analysis, a separate treatment of the data taken before and after 1994.

2.4 b-tagging

The b-tagging package developed by the DELPHI collaboration has been described in reference [14]. The impact parameters of the charged particle tracks, with respect to the primary vertex, have been used to build the probability that all tracks come from this vertex. Due to the long B-hadrons lifetime, the probability distribution is peaked at zero for events which contained beauty whereas it is flat for events containing light quarks. The b-tagging algorithm has been used in this analysis to select control samples with low b purity.

2.5 Event simulation

Simulated events have been generated using the JETSET 7.3 program [13] with parameters tuned as in [15] and using an updated description of B decays. B hadron semileptonic decays have been simulated using the ISGW model [16]. Generated events have been followed through the full simulation of the DELPHI detector (DELSIM) [9], and the resulting simulated raw data have been processed through the same reconstruction and analysis programs as the real data.

3 The $\mathrm{D_s^{\pm}}\ell^{\mp}$ sample selection

$\overline{\mathrm{B_s^0}}$ semileptonic decays[1] have been selected requiring the presence of a $\mathrm{D_s^+}$ meson correlated with a high p_t lepton of opposite electric charge in the same hemisphere:

$$\overline{\mathrm{B_s^0}} \to \mathrm{D_s^+}\ell^-\overline{\nu_\ell}X.$$

The $\mathrm{D_s}$ mesons have been reconstructed in six non-leptonic and two semileptonic decay channels:

$$\begin{array}{ll}
\mathrm{D_s^+} \to \phi\pi^+ & \phi \to \mathrm{K^+K^-}; \\
\mathrm{D_s^+} \to \overline{\mathrm{K}}^{\star 0}\mathrm{K^+} & \overline{\mathrm{K}}^{\star 0} \to \mathrm{K^-}\pi^+; \\
\mathrm{D_s^+} \to \mathrm{K_S^0K^+} & \mathrm{K_S^0} \to \pi^+\pi^-; \\
\mathrm{D_s^+} \to \phi\pi^+\pi^-\pi^+ & \phi \to \mathrm{K^+K^-}; \\
\mathrm{D_s^+} \to \phi\pi^+\pi^0 & \phi \to \mathrm{K^+K^-}; \\
\mathrm{D_s^+} \to \overline{\mathrm{K}}^{\star 0}\mathrm{K}^{\star +} & \overline{\mathrm{K}}^{\star 0} \to \mathrm{K^-}\pi^+, \quad \mathrm{K}^{\star +} \to \mathrm{K_S^0}\pi^+;
\end{array}$$

$$\begin{array}{ll}
\mathrm{D_s^+} \to \phi e^+\nu_e & \phi \to \mathrm{K^+K^-}; \\
\mathrm{D_s^+} \to \phi\mu^+\nu_\mu & \phi \to \mathrm{K^+K^-}.
\end{array}$$

In addition, partially reconstructed $\mathrm{D_s^+}$ have been selected requiring the presence of a ϕ meson (reconstructed in the $\mathrm{K^+K^-}$ decay channel) accompanied by an hadron h^+ in the same hemisphere.

$$\mathrm{D_s^+} \to \phi h^+ X$$

In the following the first eight decay modes will be referred as the $\mathrm{D_s}\ell$ sample and the last one as the $\phi\ell h$ sample.

[1] Charge conjugation is always implied.

3.1 Selection of the $\phi\pi^+$, $\overline{\mathrm{K}}^{*0}\mathrm{K}^+$, $\mathrm{K}^0_\mathrm{S}\mathrm{K}^+$ and $\phi\ell^+\nu$ decay modes

Each $\mathrm{D_s}$ decay mode has been reconstructed by making all possible combinations of particles in the same hemisphere. In $\mathrm{D_s^+}$ semileptonic decays, the ambiguity between the two leptons has been removed by assigning the lepton to the $\mathrm{D_s^+}$ ($\overline{\mathrm{B_s^0}}$) if the mass of the $\phi\ell$ system, $M(\phi\ell)$, is below (above) the nominal $\mathrm{D_s^+}$ mass. If the two leptons both gave a $M(\phi\ell)$ above or below the $\mathrm{D_s}$ mass, the event was rejected.
The measured position of the $\mathrm{D_s^+}$ decay vertex and momentum together with their measurement errors, have been used to form a new track (called pseudo-track) that contains the measured parameters of the $\mathrm{D_s^+}$ particle.
A candidate $\overline{\mathrm{B_s^0}}$ decay vertex has been obtained by intercepting the $\mathrm{D_s^+}$ pseudo-track with the one of a lepton. To guarantee a precise determination of the position of this secondary vertex, at least one VD hit has been required to be associated to the lepton and to at least two tracks from the $\mathrm{D_s^+}$ decay products. The χ^2 of the reconstructed $\mathrm{D_s^+}$ and $\overline{\mathrm{B_s^0}}$ vertices have been required to be smaller than 40 and 20 respectively.
In order to suppress fake leptons and B hadron cascade decays ($b \to c \to \ell^+$), additional selection criteria have been applied to the $\mathrm{D_s}\ell$ pairs, which are summarized in Table 1.
For the channel $\mathrm{D_s^+} \to \phi\ell^+\nu$ requirements on the $\phi\ell\ell$ mass and momentum have been reduced as compared to the other channels to account for the additional escaping neutrino.
Due to the smaller combinatorial background under the $\mathrm{D_s}$ signal, in the $\mathrm{D_s} \to \phi\pi^+$ and $\mathrm{D_s} \to \phi\ell^+\nu$ decay channels, the p_t cut has been lowered to 1 GeV/c.

	$\phi\pi^+$	$\phi\ell^+$	Others
$p_T(\ell)(GeV/c)$	> 1	> 1	> 1.2
$\mathrm{M(D_s}\ell)(GeV/c^2)$	$\in [3, 5.5]$	$\in [2.5, 5.5]$	$\in [3, 5.5]$
$\mathrm{P(D_s}\ell)(GeV/c)$	> 14	> 12	> 14

Table 1: *Selection criteria applied to the lepton and* $\mathrm{D_s}$ *candidates.*

A tighter selection was then applied, separately for each decay mode, using a discriminant variable built with the variables listed in Table 2.
These variables are:

- the momenta, P, and masses, M, of the decay products;
- the cosine of the helicity angle, ψ, for the $\phi\pi^+$ and $\overline{\mathrm{K}}^{*0}\mathrm{K}^+$ decay modes;
- H_{ID}, defining whether the hadron identification from section 2.2.2 favours the π, K or proton hypothesis;
- L_{ID}, defining whether the lepton identification from section 2.2.1 identifies a particle from the $\mathrm{D_s^+}$ semileptonic decay as an electron or a muon (used only for leptons coming from the $\mathrm{D_s^+}$ semileptonic decays).

For each quantity the probability densities for the signal (S) ($\mathrm{D_s}\ell$ from $\mathrm{B_s^0}$ semileptonic decays) and for the combinatorial background (B) (fake $\mathrm{D_s}\ell$ candidates in $q\overline{q}$ events) have been parametrized using the simulation; the discriminant variable $X_{\mathrm{D_s}}$ is then defined as

$$R = \prod_i R_i = \prod_i \frac{S_i(x_i)}{B_i(x_i)} \qquad X_{\mathrm{D_s}} = \frac{R}{R+1}$$

where i runs over the number of variables (which actual values are x_i). The combinatorial background is concentrated close to $X_{\mathrm{D_s}} = 0$ while the $\mathrm{D_s}$ signal accumulates close to $X_{\mathrm{D_s}} = 1$.

$\phi\pi$	$\overline{\mathrm{K^{0*}}}\mathrm{K}$	$\mathrm{K^0_S K}$	$\phi\ell^+$
$P(\mathrm{D_s})$	$P(\mathrm{D_s})$	$P(\mathrm{D_s})$	$P(\phi)$
$P(\phi)/P(\mathrm{D_s})$	$P(K^{*0})/P(\mathrm{D_s})$	$P(\mathrm{K^0_S})/P(\mathrm{D_s})$	
H_{ID} $\mathrm{K_1}$	H_{ID} $\mathrm{K_1}$	H_{ID} K	H_{ID} $\mathrm{K_1}$
H_{ID} $\mathrm{K_2}$	H_{ID} $\mathrm{K_2}$		H_{ID} $\mathrm{K_2}$
H_{ID} π	H_{ID} π		L_{ID} $\ell(\mathrm{D_s})$
$cos(\psi)$	$cos(\psi)$		
$M(\phi)$	$M(\mathrm{K^{*0}})$		

Table 2: *List of the quantities which are used, in the different decay channels, to construct a discriminant variable between* $\mathrm{B^0_s}$ *semileptonic decays and background events.*

The distributions of this variable obtained in data and in the simulation are shown in Figure 1 for the $\phi\pi^+$ decay channel.
The optimal value of the cut on the discriminant variable has been studied on simulated events separately for each channel and for each detector configuration (Table 3). For the $\phi\pi^+$ channel, because of the small combinatorial background, a loose cut is chosen while for the other channels a tighter cut has been applied.

	$\phi\pi^+$	$\overline{\mathrm{K^{0*}}}\mathrm{K}$	$\mathrm{K^0_S K}$	$\phi\ell^+$
92-93	> 0.05	> 0.75	> 0.80	> 0.75
94-95	> 0.03	> 0.85	> 0.90	> 0.90

Table 3: *Values of the cuts applied on the discriminant variable* $\mathrm{X_{D_s}}$ *to select* $\mathrm{B^0_s}$ *semileptonic decay candidates.*

In addition, for the two channels ($\overline{\mathrm{K^{*0}}}\mathrm{K}$ and $\mathrm{K^0_S K}$), which receive contributions from kinematic reflections of non strange B decays, the bachelor kaon has been required to be incompatible with the pion hypothesis.
Further background suppression has been obtained by placing a requirement on the $\mathrm{D_s}$ flight distance $L(\mathrm{D_s})$. The small effect induced on the decay time acceptance has been taken into account in the following. This requirement has been applied, depending on the resolution on the decay distance observed in the different $\mathrm{D_s}$ decay channels and on the level of the combinatorial background: $L(\mathrm{D_s}) > 0$ for $\phi\pi$ and $\overline{\mathrm{K^{*0}}}\mathrm{K^+}$, $L(\mathrm{D_s})/\sigma(L(\mathrm{D_s})) > -3$ for $\mathrm{K^0_S K^+}$ and $L(\mathrm{D_s})/\sigma(L(\mathrm{D_s})) > -1$ for $\phi\ell^+$.
Finally, for the semileptonic decay modes (with two neutrinos in the final state) an algorithm has been developed to estimate the missing energy, E_{miss}, defined as:

$$E_{miss} = E_{tot} - E_{vis}$$

where the visible energy (E_{vis}) is the sum of the energies of charged particles and photons in the same hemisphere as the $\mathrm{D_s}\ell$ candidate. Using four-momentum conservation, the

total energy (E_{tot}) in that hemisphere is:

$$E_{tot} = E_{beam} + \frac{M^2_{same} - M^2_{opp}}{4E_{beam}}$$

where M_{same} and M_{opp} are the hemisphere invariant masses of the same and opposite hemispheres respectively. A positive missing energy E_{miss} has been required.

3.2 Selection of the $\phi\pi^+\pi^+\pi^-$, $\phi\pi^+\pi^0$ and $\overline{\mathrm{K}}^{*0}\mathrm{K}^{*+}$ decay modes

These three decay modes have been searched for in the 94 and 95 data only [17].
$\mathrm{D_s}\ell$ pairs have been selected by requiring $M(\mathrm{D_s}\ell) > 3.0\ GeV/c^2$, $p_t(\ell) > 1.2\ GeV/c$ and χ^2 ($\mathrm{D_s}\ell$ vertex)< 20 (except for the $\phi\pi^+\pi^+\pi^-$ decay mode in which no χ^2 cut has been applied).
In each event only one candidate is kept. The procedure is the following: if more than one candidate passed all the selection criteria only the one with the highest lepton transverse momentum and, if the same lepton candidate is attached to several $\mathrm{D_s^+}$ candidates the highest $\mathrm{D_s^+}$ momentum, is kept.
It has been verified that this requirement keeps the signal with high efficiency and removes some of the combinatorial background.

3.2.1 $\mathrm{D_s^+} \to \overline{\mathrm{K}}^{*0}\mathrm{K}^{*+}$

$\mathrm{D_s^+}$ candidates have been selected by reconstructing $\overline{\mathrm{K}}^{*0} \to \mathrm{K}^-\pi^+$ and $\mathrm{K}^{*+} \to \mathrm{K_s^0}\pi^+$ decays. $\mathrm{K_s^0}$ candidates have been reconstructed in the mode $\mathrm{K_s^0} \to \pi^+\pi^-$ by combining all pairs of oppositely charged particles and applying the "tight" selection criteria described in [9]. The $\mathrm{K_s^0}$ has been then combined with two charged particles of the same sign, and a third with opposite charge. If more than one $\mathrm{D_s^+}$ candidate could be reconstructed by the same four particles (by swapping the two pion candidates for example) the $\mathrm{D_s^+}$ candidate minimizing the squared mass difference $(M(\mathrm{K}^-\pi^+) - M(\overline{\mathrm{K}}^{*0}))^2 + (M(\mathrm{K_s^0}\pi^+) - M(\mathrm{K}^{*+}))^2$ has been chosen, where $M(\overline{\mathrm{K}}^{*0})$ and $M(\mathrm{K}^{*+})$ are the nominal K^* masses [19]. The three charged particle tracks have been fitted to a common vertex and the χ^2 of this vertex has been required to be smaller than 30. To improve the resolution on the vertex position, all three tracks have been required to have at least one VD hit.
$\mathrm{K}^-\pi^+$ and $\mathrm{K_S^0}\pi^+$ mass combinations have been selected if their effective masses are within ± 75 and $\pm 95\ MeV/c^2$ of the nominal neutral and charged $\overline{\mathrm{K}^*}$ mass respectively.
The charged pion and kaon from $\overline{\mathrm{K}^*}$ decays must have a momentum larger than 1 and 1.5 GeV/c respectively. The charged and neutral $\overline{\mathrm{K}^*}$ mesons must have a momentum larger than 4 and 3.5 GeV/c respectively and $\mathrm{D_s^+}$ mesons have a momentum larger than 11 GeV/c.

3.2.2 $\mathrm{D_s^+} \to \phi\pi\pi\pi$

The ϕ is reconstructed in the decay channel $\phi \to \mathrm{K}^+\mathrm{K}^-$ by taking all possible pairs of oppositely charged particle tracks that have an invariant mass within 13 MeV/c^2 of the nominal ϕ meson mass [19]. Neither kaon candidate should be tagged by the combined RICH and dE/dX measurements as pions ("tight" selection). Three tracks, each compatible with the pion hypothesis as given by the combined RICH and dE/dX measurements, have been then added to the ϕ candidate to make a $\mathrm{D_s^+}$. The five tracks have been required to be compatible with a single vertex, but no requirement has been

applied on the χ^2 of the vertex fit. Three of the five tracks have been required to have at least one VD hit and two of the three pion candidates have been required to have a momentum above 1.2 GeV/c.

In addition, kaons from the ϕ decays must have a momentum larger than 1.8 GeV/c. Individual pion momenta must be larger than 700 MeV/c and the D_s candidate momentum must be larger than 9 GeV/c.

3.2.3 $D_s^+ \to \phi\pi\pi^0$

The ϕ is reconstructed using the same selection criteria as for the previous channel. A third track, which has been required not to be tagged as a kaon by the combined RICH and dE/dx, and a reconstructed π^0 (section. 2.2.4) have been added to the ϕ candidate. If more than one candidate passed the selection criteria only one has been kept by applying the same selection criteria as for the $\phi\pi\pi\pi$ channel.
The three charged tracks have been fitted to a common vertex. To improve the resolution on the vertex position, each of the three tracks has been required to be associated to at least one VD hit each.
In addition, kaons from the ϕ decay must have a momentum larger than 2.5 GeV/c. The momentum of the charged pion and of the D_s must be larger than 1 and 10 GeV/c respectively.

3.3 Summary for the $D_s\ell$ selected events

3.3.1 Non leptonic D_s modes

In the D_s^+ mass region, an excess of "right-sign" ($D_s^\pm\ell^\mp$) over "wrong-sign" ($D_s^\pm\ell^\pm$) combinations is observed in each channel (Figure 2). The estimated number of signal events and the yields for the combinatorial background in all the studied modes are summarized in Table 4. The mass distribution for non-leptonic decays has been fitted with two Gaussian distributions of equal widths to account for the D_s^+ and D^+ signals and a polynomial function for the combinatorial background. The D^+ mass has been fixed at the nominal value of 1.869 GeV/c^2 [19]. The overall mass distribution for non-leptonic decays is shown in (Figure 3a). The fit yields a signal of (206 ± 21) D_s decays in "right-sign" combinations, centred at a mass of (1.9680 ± 0.0016) GeV/c^2 with a width of (14 ± 1) MeV/c^2.

3.3.2 Semileptonic D_s modes

Selected events show an excess of "right-sign" with respect to "wrong-sign" combinations (Figure 3b). The K^+K^- invariant mass distribution for "right sign" events has been fitted with a Breit–Wigner distribution to account for the signal and a polynomial function to describe the combinatorial background. The fit gives (80 ± 16) events (see Table 4) centred at a mass of (1.020 ± 0.001) GeV/c^2 with a total width (Γ) of (5 ± 1) MeV/c^2.

3.4 Selection of the $\phi\ell h$ inclusive channel

Inclusive B_s^0 semileptonic decays are reconstructed by requiring, in the same hemisphere, a high p_t lepton and a reconstructed $\phi \to K^+K^-$ [18]. This analysis is expected to be more efficient than analyses based on completely reconstructed D_s^+, at the cost of

D_s decay modes	Estimated signal	Combinatorial background / Total
$D_s \to \phi\pi^+$	83 ± 11	0.38 ± 0.06
$D_s \to \overline{K}^{\star 0}K^+$	60 ± 11	0.45 ± 0.06
$D_s \to K^0_S K^+$	22 ± 7	0.48 ± 0.10
$D_s \to \overline{K}^{\star 0}K^{\star +}$	21 ± 5	0.31 ± 0.07
$D_s \to \phi\pi^+\pi^+\pi^-$	10 ± 4	0.39 ± 0.10
$D_s \to \phi\pi^+\pi^0$	18 ± 6	0.39 ± 0.10
$D_s \to \phi\ell^+\nu$	80 ± 16	0.38 ± 0.06

Table 4: *Numbers of* D_s *signal events and fractions of combinatorial background events measured in the different* D_s *decay channels. The level of the combinatorial background has been evaluated inside a mass interval of* $\pm 2\sigma$ *(*$\pm 1.5\Gamma$*) centred on the measured* D_s *(*ϕ*) mass.*

a higher background. The extra contamination comes mainly from combinatorial K^+K^- pairs and from non-strange B-decays.
In order to avoid a statistical overlap with the $D_s\ell$ sample considered previously, all $K^+K^-\ell$ triplets selected in the $D_s\ell$ channels containing a ϕ in the final state have been excluded from the present sample.
The analysis of the $\phi\ell h$ channel has been performed using 94-95 data only.
Leptons are required to have a momentum and a transverse momentum larger than 3.0 GeV/c and 1.0 GeV/c respectively. A pair of oppositely charged identified kaons is considered as a ϕ candidate provided their combined momentum is above 3.0 GeV/c. Considering the remaining particles of charge opposite to the lepton, the hadron h with the highest momentum projected along the ϕ direction is associated to the D_s^+ decay vertex. The $K^+K^-h^+$ vertex is fitted, and the D_s^+ pseudo-track is reconstructed and fitted with the lepton track to estimate the B decay vertex. The mass distribution of the K^+K^- pairs has been fitted with a Breit-Wigner function to account for true ϕ mesons and a polynomial function for the combinatorial background (Figure 4).
Accepting events within $\pm 1\Gamma$ of the fitted ϕ mass, where Γ corresponds to the fitted width of the signal, 441 events are retained, including a combinatorial background of $(45.2 \pm 4.5)\%$.

3.5 Sample composition

The lifetime and the oscillations of B_s^0 mesons have been studied selecting, in the $D_s\ell$ sample, right-sign events lying in a mass interval of $\pm 2\sigma$ ($\pm 1.5\Gamma$) centered on the measured D_s (ϕ) mass and, in the $\phi\ell h$ sample, events with the candidate ϕ meson in a mass interval of $\pm 1\Gamma$ centered on the measured ϕ mass.
The following components, entering into the selected sample, have to be considered:

- f_{bkg}: fraction of candidates from the combinatorial background: it has been evaluated from the fit of the mass distributions on $D_s\ell$ and $\phi\ell h$ events;
- $f_{f\ell}$: fraction of candidates coming from events having a fake lepton and a real D_s or ϕ meson (in the $\phi\ell h$ analysis this category includes also events containing true leptons and ϕ mesons coming from charm decays or light quark hadronization);

	$\phi\pi$	$\phi\ell$	Others
$f_{\mathrm{D_sD}}/f_{B_s}$	0.151 ± 0.018	0.148 ± 0.025	0.114 ± 0.020

Table 5: *Ratio between* $\mathrm{D_s}\overline{\mathrm{D}}$ *and signal yields in the three* $\mathrm{D_s}\ell$ *classes.*

- $f_{bc\ell}$: fraction of candidates in which the high p_T lepton originates from a "cascade" decay ($b \to c \to \bar{\ell}$);
- $f_{b\ell}^{\mathrm{B}}$: fraction of semileptonic decays of non-strange B mesons
- $f_{b\ell}^{\mathrm{B_s^0}}$: fraction of semileptonic decays of the $\mathrm{B_s^0}$ meson.

Only the last four components (i.e. background and signal coming from physical processes) will be detailed in the following: the estimation of the combinatorial background has been already reported in previous sections.

3.5.1 Composition of the $\mathrm{D_s}\ell$ sample

In the $\mathrm{D_s}\ell$ sample the $\mathrm{D_s}$ signal of the "right" sign correlation is dominated by $\mathrm{B_s^0}$ semileptonic decays; other minor sources of $\mathrm{D_s}\ell$ candidates are:

- $f_{f\ell}$:
  a possible contribution from this source ($\mathrm{D_s^+}$-fake ℓ) would give the same contribution in right and wrong sign candidates. Since no excess has been observed in wrong sign candidates this component has been neglected.
- $f_{bc\ell}$:
  it is the expected fraction of "cascade" decays ($\mathrm{B} \to \overline{\mathrm{D}}^{(\star)}\mathrm{D_s}^{(\star)+}\mathrm{X}$) followed by the semileptonic decay $\overline{\mathrm{D}} \to \ell^-\overline{\nu}\mathrm{X}$ yielding right-sign $\mathrm{D_s^{\pm}}\ell^{\mp}$ pairs (referred also as $f_{\mathrm{D_sD}}$). This background corresponds approximately to the same number of events as the signal [20], but the selection efficiency is lower because of the requirement of a high p_t lepton and of a high mass of the($\mathrm{D_s}\ell$) system. These selection criteria reduce the $\mathrm{D_s}\overline{\mathrm{D}}$ background fractions to the values reported in Table 5. Quoted errors on these fractions result from the uncertainties on the branching fractions of the contributing processes and from the errors on the respective experimental selection efficiencies.
- $f_{b\ell}^{\mathrm{B}}$:
  two contributions to this fraction have been considered:
  - f_{refl}: the fraction of events from $\mathrm{D^+} \to \mathrm{K^-}\pi^+\pi^+$ and $\mathrm{D^+} \to \mathrm{K_S^0}\pi^+$ decays in which a π^+ has been misidentified as a $\mathrm{K^+}$ which give candidates in the $\mathrm{D_s}$ mass region. If the $\mathrm{D^+}$ is accompanied by an oppositely charged lepton in the decay $\overline{\mathrm{B}}_{\mathrm{u,d}} \to \mathrm{D^+}\ell^-\overline{\nu}\mathrm{X}$, it looks like a $\overline{\mathrm{B_s^0}}$ semileptonic decay. The fractions $f_{refl}/f_{\mathrm{B_s}} = 0.054 \pm 0.015$ and $f_{refl}/f_{\mathrm{B_s}} = 0.069 \pm 0.025$ have been estimated for the $\overline{\mathrm{K}}^{\star 0}\mathrm{K^+}$ and $\mathrm{K_S^0K^+}$ decay channels, respectively.
  - A $\mathrm{D_s^{\pm}}\ell^{\mp}$ pair from a non-strange B meson decay, with the lepton emitted from a direct B semileptonic decay, may come from the decay $\overline{\mathrm{B}} \to \mathrm{D_sKX}\ell^-\overline{\nu}$. The production of $\mathrm{D_s}$ in B decays not originating from $W^+ \to c\overline{s}$, has been measured by CLEO [21], but no measurement of this production in semileptonic decays exists yet. This process implies the production of a $\mathrm{D^{\star\star}}$ followed by its decay into $\mathrm{D_sK}$. This decay is suppressed by phase space (the $\mathrm{D_s}$ K system has a large mass) and by the required additional $s\overline{s}$ pair. A detailed calculation shows that

	$\phi\pi$	$\phi\ell$	$\mathrm{K^0_S K^+}$	$\mathrm{K^{*0} K^+}$	Others
$f_{\mathrm{B^0_s}}$	0.869 ± 0.014	0.871 ± 0.019	0.845 ± 0.023	0.856 ± 0.018	0.898 ± 0.016
$f_{\mathrm{D_s\overline{D}}}$	0.131 ± 0.016	0.129 ± 0.022	0.096 ± 0.021	0.098 ± 0.020	0.102 ± 0.018
$f_{refl.}$	-	-	0.059 ± 0.022	0.046 ± 0.014	-

Table 6: Estimated composition of the $\mathrm{D_s}$ signal in the $\mathrm{D_s}\ell$ sample

the contribution of this process is [22]:

$$\frac{\mathrm{Br}(b \to \overline{\mathrm{B}} \to \mathrm{D_s KX}\ell^-\overline{\nu})}{\mathrm{Br}(b \to \overline{\mathrm{B^0_s}} \to \mathrm{D_s}\ell^-\overline{\nu})} < 10\%.$$

Assuming a selection efficiency similar to the one for the $\mathrm{D_s\overline{D}}$ component the contribution of this decay channel is below 2% and, for this reason, has been neglected in the following.

Taking into account the above components, the estimated number of $\mathrm{B^0_s}$ semileptonic decays in the sample of 436 candidates is 230 ± 18.
The signal composition for each $\mathrm{D_s}$ decay mode is given in Table 6.

In order to increase the effective $\mathrm{B^0_s}$ purity of the selected sample, signal and background fractions have been calculated on an event by event basis using the probability density functions of $p_T(l)$ and $X_{\mathrm{D_s}}$ (defined in Section 3.1):

$$\begin{aligned}
f^{eff}_{bkg} &= f_{bkg}\mathcal{F}_{Comb}(X_{\mathrm{D_s}})\mathcal{F}_{Comb}(p_T)/Tot \\
f^{eff}_{\mathrm{B^0_s}} &= f_{\mathrm{B^0_s}}\mathcal{F}_{\mathrm{D_s}}(X_{\mathrm{D_s}})\mathcal{F}_{\mathrm{B^0_s}}(p_T)/Tot \\
f^{eff}_{D_sD} &= f_{D_sD}\mathcal{F}_{\mathrm{D_s}}(X_{\mathrm{D_s}})\mathcal{F}_{\mathrm{D_sD}}(p_T)/Tot \\
f^{eff}_{refl} &= f_{refl}\mathcal{F}_{\mathrm{D_s}}(X_{\mathrm{D_s}})\mathcal{F}_{\mathrm{B^0_s}}(p_T)/Tot
\end{aligned}$$

where $\mathcal{F}_{\mathrm{D_s}}$, $\mathcal{F}_{Comb}$, $\mathcal{F}_{\mathrm{D_sD}}$, $\mathcal{F}_{\mathrm{B^0_s}}$ are the probability densities for the $\mathrm{D_s}$ mesons, the combinatorial background, the $\mathrm{D_sD}$ background and the $\mathrm{B^0_s}$ signal events, respectively.
In these expressions, Tot is a normalisation factor such that:

$$f^{eff}_{bkg} + f^{eff}_{\mathrm{B^0_s}} + f^{eff}_{D_sD} + f^{eff}_{refl} = 1.$$

The distributions of the values of the $X_{\mathrm{D_s}}$ and p_T variables are shown in Figure 5. The use of this procedure is equivalent to increasing the statistics by a factor 1.2.

3.5.2 Composition of the $\phi\ell h$ sample

The different contributions to $\phi\ell h$ candidates contained in the selected $\mathrm{K^+K^-}$ mass interval of $\pm 6.6 MeV/c^2$ around the ϕ nominal mass and corresponding to a real ϕ meson are shown in Table 7 and have been estimated using simulated events and measured branching fractions. Quoted uncertainties originate from the finite Monte Carlo statistics, except for one attached to the signal fraction which is dominated by $f_{\mathrm{B^0_s}} \times \mathrm{Br}(\mathrm{B^0_s} \to \mathrm{D^+_s}\ell^-\bar{\nu}_\ell \mathrm{X}) = (0.86 \pm 0.09^{+0.29}_{-0.20})\%$ [23].

The number of $\mathrm{B^0_s}$ semileptonic decays contained in this sample has been evaluated to be 41^{+15}_{-10}.

Source	(%)
$f_{f\ell}$	22.5 ± 2.4
$f_{b\ell}^{\mathrm{B}}$	49.4 ± 2.1
$f_{bc\ell}$	11.3 ± 1.2
$f_{b\ell}^{\mathrm{B_s^0}}$	$16.9^{+6.0}_{-4.3}$

Table 7: *Estimated composition of the ϕ signal in the $\phi\ell h$ sample*

3.6 Measurement of the B meson decay time

For each event, the $\mathrm{B_s^0}$ decay time is obtained from the measured decay length ($L_{\mathrm{B_s^0}}$) and the estimate of the $\mathrm{B_s^0}$ momentum ($p_{\mathrm{B_s^0}}$). The $\mathrm{B_s^0}$ momentum is estimated using the measured energies:

$$p_{\mathrm{B_s^0}}{}^2 = (E(\mathrm{D_s}\ell) + E_\nu)^2 - m_{\mathrm{B_s^0}}{}^2.$$

The neutrino energy E_ν is obtained from the measured value of E_{miss} (see Section 3.1) corrected by an amount which depends on the ($\mathrm{D_s}\ell$) energy[2] and which has been determined from simulated signal events:

$$E_\nu = E_{miss} + F(E(\mathrm{D_s}\ell)).$$

The agreement between data and simulation on E_{miss} has been verified using the side bands of the $\mathrm{D_s}\ell$ sample.
In order to have enough statistics to perform this test, cuts not correlated with the missing energy have been relaxed. In addition, to verify the resolution on the energy estimate, the studied sample has been enriched in light quark events by applying an anti–b-tagging cut (Section 2.4).
A relative shift of $\Delta(MC - Data) = 500\ MeV$ has been measured and the simulation has been corrected. Figure 6 shows the agreement between data and simulation after having applied this correction.
Finally the data-simulation agreement on $p_{\mathrm{B_s^0}}$ has been verified on the selected signal events after subtraction of the combinatorial background (estimated from events selected in side-bands of $\mathrm{D_s}$ and ϕ signals) (Figure 6).

3.7 Proper time resolution and acceptance

The predicted decay time distributions have been obtained by convoluting the theoretical distributions with resolution functions evaluated from simulated events. Due to different resolutions on the decay length, different parametrizations of the proper time resolution have been used for three different classes in the $\mathrm{D_s}\ell$ sample: $\mathrm{K_S^0K^+}$ decays, other non-leptonic decays and semileptonic $\mathrm{D_s}$ decays. Different parametrizations have been also used for the two Vertex Detector configurations installed in 91-93 and in 94-95.
The proper time resolution is obtained from the distribution of the difference between the generated (t) and the reconstructed (t_i) time. The following distributions have been considered:

[2]here $\mathrm{D_s}$ means "observed decay products of $\mathrm{D_s}$", including also the decays where the $\mathrm{D_s}$ is not fully reconstructed: specifically $\mathrm{D_s}^+ \to \phi\ell^+\nu_\ell$ and $\mathrm{D_s}^+ \to \phi h^+ X$

- $\mathcal{R}_{bl}(t-t_i)$ is the resolution function for direct semileptonic B decays.
  $\mathcal{R}_{bl}$ is parametrized, for the $D_s\ell$ sample, as the sum of three Gaussian distributions. The width of the third Gaussian is taken to be proportional to the width of the second Gaussian.

  $$\mathcal{R}_{b\ell}(t-t_i) = (1-f_2-f_3)G(t-t_i,\sigma_1) + f_2 G(t-t_i,\sigma_2) + f_3 G(t-t_i,\sigma_3)$$
  $$\text{with } \sigma_1 = \sqrt{\sigma_{L1}^2 + \sigma_{P1}^2 t^2}$$
  $$\sigma_2 = \sqrt{\sigma_{L2}^2 + \sigma_{P2}^2 t^2}$$
  $$\sigma_3 = s_3\sigma_2$$

  In the $\phi\ell h$ analysis a fourth Gaussian distribution has been added.
  The decay length resolutions σ_{L_i}, the momentum resolutions σ_{P_i} and relative fractions f_i are listed in Table 8. A typical parametrization of the resolution, for the $D_s\ell$ sample, is shown in Figure 7 for the $\phi\pi^+$ decay mode obtained with the 94-95 Vertex-Detector configuration.

- $\mathcal{R}_{bcl}$ is the resolution function applied to "cascade" events.
  Since the charm decay products have been only partially reconstructed in these events, the momentum of the $\overline{B_s^0}$ candidate is underestimated giving a long positive tail in the proper time resolution function.
  The function, $\mathcal{R}_{bcl}(t-t_i)$, is well described by a Gaussian distribution convoluted with an exponential distribution. The variation of the shape of this distribution with the generated proper time has been neglected.

$D_s\ell$ sample							
D_s decay mode	$\sigma_{L1}(ps)$	σ_{P1}	$\sigma_{L2}(ps)$	σ_{P2}	s_3	f_2	f_3
$K_S^0K^+$ (92-93)	0.16	0.08	1.04	0.16	-	0.50	0
$K_S^0K^+$ (94-95)	0.16	0.08	0.98	0.16	-	0.28	0
other non-leptonic (92-93)	0.11	0.07	0.39	0.16	5	0.26	0.07
other non-leptonic (94-95)	0.11	0.07	0.37	0.16	3	0.16	0.02
$\phi\ell^+\nu$ (92-93)	0.14	0.075	0.31	0.15	6	0.29	0.09
$\phi\ell^+\nu$ (94-95)	0.14	0.075	0.31	0.15	6	0.21	0.07

$\phi\ell h$ sample										
$\sigma_{L1}(ps)$	σ_{P1}	$\sigma_{L2}(ps)$	σ_{P2}	$\sigma_{L3}(ps)$	σ_{P3}	$\sigma_{L4}(ps)$	σ_{P4}	f_1	f_2	f_3
0.13	0.08	0.28	0.09	0.32	0.19	1.06	0.42	0.31	0.41	0.10

Table 8: *Fitted values of the parameters of the resolution function $\mathcal{R}_{bl}(t-t_i)$ obtained, on simulated events, for the $D_s\ell$ and $\phi\ell h$ samples.*

Distortions on the recostructed proper time can be due to a non-uniform reconstruction efficiency (acceptance) as a function of the true proper time.
Non-uniform efficiencies have been observed, on simulated events, in the D_s decay modes $\phi\pi$, $K^{*0}K$ and $\phi\ell\nu$ because of the selection criteria on $L/\sigma(L)$.
This effect has been taken into account by inserting, for those channels, an acceptance function parametrized on simulated events.

4 Measurement of the B_s^0 lifetime

The B_s^0 meson lifetime has been studied using the signal sample (Section 3.5) and a background sample containing events selected in the sidebands of D_s (ϕ) candidates. Sidebands events are "right" sign events lying in the D_s mass interval $[1.91-1.93]U[2.01-2.15]$ GeV/c^2 for the D_s hadronic decays and "right" sign events lying in the ϕ mass interval $[0.990, 1.005]U[1.035, 1.060]$ GeV/c^2 for the D_s semileptonic decays.
In the $D_s\ell$ analysis "wrong" sign candidates have been also included in the background sample. This background sample is assumed to have the same proper time distribution as the combinatorial background in the signal sample. This assumption has been verified using the simulation. The probability density function used for events in the signal region is given by:

$$P(t_i) = f_{b\ell}^{B_s^0} P_{b\ell}^{B_s^0}(t_i) + f_{b\ell}^{B} P_{b\ell}^{B}(t_i) + f_{bc\ell} P_{bc\ell}(t_i) + f_{f\ell} P_{f\ell}(t_i) + f_{bkg} P_{bkg}(t_i).$$

where t_i and t are the measured and true proper times respectively.
The different probability densities are expressed as convolutions of the physical probability densities with the appropriate resolution ($\mathcal{R}$) and acceptance ($\mathcal{A}$) functions:

- for the signal:

$$P_{b\ell}^{B_s^0}(t_i) = exp(-t/\tau_{B_s^0}) \mathcal{A}(t) \otimes \mathcal{R}_{b\ell}(t - t_i)$$

- for the background coming from non strange B mesons:

$$P_{b\ell}^{B}(t_i) = \sum_{q \neq s} f_{b\ell}^{B_q} exp(-t/\tau_{B_q}) \mathcal{A}(t) \otimes \mathcal{R}_{b\ell}(t - t_i)$$

  where q runs over the various B-hadrons species contributing to this background,
- for the "cascade" background:

$$P_{bc\ell}(t_i) = \sum_{q} f_{bc\ell}^{B_q} exp(-t/\tau_{B_q}) \mathcal{A}(t) \otimes \mathcal{R}_{bc\ell}(t - t_i)$$

- for "fake lepton" candidates the function $P_{f\ell}(t_i)$ has been parametrized using simulated events;
- for the combinatorial background two different parametrizations have been used:
  - $D_s\ell$ sample.

$$\begin{aligned} P_{bkg}^{j}(t_i) = \; & f^- exp(-t/\tau^-) \otimes G(t - t_i, \sigma_j) + f^+ exp(-t/\tau^+) \otimes G(t - t_i, \sigma_j) + \\ & (1 - f^- - f^+) G(t - t_i, \sigma_j) \end{aligned}$$

    Three distributions have been used for each of the three classes of decay time resolution σ_j ($j = 1, 3$) (see Section 3.7). A negative exponential for poorly measured events (with lifetime τ^-), an exponential distribution for the flying background (with lifetime τ^+) and a central Gaussian for the non-flying one. The seven parameters (f^-, f^+, τ^+, τ^- and σ_j ($j = 1, 3$)) have been fitted independently for the 92-93 and 94-95 data samples. The parameter σ_j ($j = 1, 3$) are taken to be different for the three classes of decay time resolution.

– $\phi\ell h$ sample.
The combinatorial background shape has been described with a sum of four smeared exponentials ($exp(t_i, \tau, \sigma) \otimes G(t_i, \sigma)$).

B_s^0 lifetime fit has been perfomed simultaneously on the signal and background samples. All parameters describing the shape of the background time distributions in the $D_s\ell$ and $\phi\ell h$ samples are left as free parameters. Results of the fit are shown in Figure 8 ($D_s\ell$ sample) and in Figure 9 ($\phi\ell h$ sample). Table 9 summarizes the different lifetimes measurements with their statistical errors.

Decay mode	Data set	$\tau_{B_s^0}(ps)$
$D_s\ell; D_s \to \phi\pi$	(92-95)	$1.44^{+0.26}_{-0.21}$
$D_s\ell; D_s \to \overline{K}^{\star 0}K^+$	(92-95)	$1.31^{+0.30}_{-0.25}$
$D_s\ell; D_s \to K_S^0K^+$	(92-95)	$1.43^{+0.61}_{-0.44}$
$D_s\ell; D_s \to \overline{K}^{\star 0}K^{\star +}$	(94-95)	$1.00^{+0.50}_{-0.31}$
$D_s\ell; D_s \to \phi\pi^+\pi^0$	(94-95)	$1.46^{+0.61}_{-0.42}$
$D_s\ell; D_s \to \phi\pi^+\pi^+\pi^-$	(94-95)	$1.96^{+1.16}_{-0.64}$
$D_s\ell; D_s \to \phi\ell^+\nu$	(92-95)	$1.49^{+0.34}_{-0.27}$
$\phi\ell h$	(94-95)	1.41 ± 0.68

Table 9: B_s^0 *lifetime determinations using the* $D_s\ell$ *and* $\phi\ell h$ *events samples.*

4.1 Systematic errors on the B_s^0 lifetime

Systematic uncertainties attached to the B_s^0 lifetime determination are summarized in Table 10.

The main contributions to the systematic uncertainties come from:

- Systematics from the evaluation of the B_s^0 purity.

  – $D_s\ell$ sample:
  The different fractions for signal and background events have been calculated on an event by event basis. The expressions defining the effective purities are given in Section 3.5.1. The value of $f_{bkg.}$ has been varied according to the statistical uncertainties of the fitted combinatorial background fractions present in the different, D_s or K^+K^-, mass distributions. The value of $f_{bc\ell}$ has been varied according to the errors given in Table 7 and in Table 6, which takes into account both the statistical error from the simulation and the errors on measured branching ratios.
  The evaluation of the systematics due to the procedure used to evaluate the B_s^0 purity on a event by event basis has been evaluated in two steps. The distributions of the variable X_{D_s} (Figure 5) for signal and background events have been re-weighted with as linear function in order to maximize the Data-

Systematics	$\tau_{B_s^0}$ variation in ps
$f_{bkg.}$	$^{+0.0090}_{-0.0130}$
$f_{bc\ell}$	$^{-0.0100}_{+0.0110}$
$f_{b\ell}^{B}$	$^{-0.0020}_{+0.0020}$
X_{D_s} discrim. var.	$+0.008$
p_T discrim. var.	± 0.004
$\tau_{B^+}(1.65 \pm 0.04\ ps)$	$^{-0.0010}_{+0.0010}$
$\tau_{B_d^0}(1.56 \pm 0.04\ ps)$	$^{-0.0012}_{+0.0013}$
t resolution	± 0.008
t acceptance	± 0.010
Simulated evts. statistics	± 0.020
Total Syst.	± 0.03

Table 10: *Different contributions to the systematic uncertainty attached to the* B_s^0 *lifetime measurement.*

simulation agreement:

$$\frac{S(X_{D_s})}{B(X_{D_s})}_{\text{new}} = \frac{S(X_{D_s})}{B(X_{D_s})}_{\text{old}} (a + bX_{D_s})$$

The linear behaviour of the correction has been chosen because of the limited statistics in the data: it has been verified that a quadratic correction does not change the result significantly.
The fit has been redone with this new probability distribution and the variation of the fitted lifetime value has been taken as the systematic error.
Because of the agreement between data and simulation (Figure 5-e and 5-f) for the p_T distribution, the systematic error associated to this variable has been evaluated varying its distributions by the uncertainties of the parametrization obtained from simulated events.

– $\phi\ell h$ sample:
In this analysis the fractions of signal and background events have not been calculated on an event by event basis. The systematic uncertainty due to the variation of the $f_{bc\ell}$, $f_{b\ell}^B$ and f_{bkg} fractions have been obtained by varying these parameters by the errors reported in Table 7. The systematic uncertainty attached to the $f_{f\ell}$ fraction, affecting only the $\phi\ell$ sample, has a negligible effect on the global result.

- Validation of the fitting procedure using simulated events.
The fitting method has been verified on pure B_s^0 simulated events: the measured value on this sample has been $\tau_{B_s^0}(D_s^{\pm}\ell^{\mp})^{\text{MC}} = (1.605 \pm 0.020)$ps in agreement with the generated value ($\tau_{B_s^0} = 1.6\ ps$). The statistical error of this verification has been included in the systematic uncertainties.
A similar check has been performed on the $\phi\ell h$ sample giving $\tau_{B_s^0}(\phi\ell\text{h})^{\text{MC}} = (1.65 \pm 0.04)$ps. Since the statistical weight of the $\phi\ell h$ channel is small compared to the full sample, the error on the fitting procedure is dominated by the statistics of

$D_s\ell$ simulated events.

- Systematic from the proper time resolution.
  Uncertainties on the determination of the resolution on the proper time receive two contributions: one from errors on the decay distance evaluation and the other from errors on the measurement of the B_s^0 momentum. The agreement between real and simulated events on the evaluation of the errors on the decay distance has been verified by comparing the widths of the negative part of the flight distance distributions, for events which are depleted in B-hadrons. The difference between the two widths has been found to be of the order of 10%. The agreement between data and simulated events concerning the measurement of the B_s^0 momentum has been verified by comparing corresponding distributions (see Section 3.5.1). Finally the systematic error coming from uncertainties on the time resolution has been evaluated by varying the parameters σ_{L_i} and σ_{P_i} of the resolution functions (see Table 8) by $\pm 10\%$. Uncertainties on the acceptance determination have been also considered: the parameters entering in the definition of the acceptance function have been varied according to the errors given by the fit on simulated events.

The final result is:

$$\tau_{B_s^0} = 1.42^{+0.14}_{-0.13}(stat.) \pm 0.03(syst.)\ ps. \tag{8}$$

5 Lifetime difference between B_s^0 mass eigenstates

As strange B mesons are selected using their semileptonic decays, the measured decay time distribution is relative to $\overline{B_s^0}$ (or B_s^0) mesons which are well defined superpositions of the two mass eigenstates:

$$|(\overline{B})^0\rangle = \frac{1}{\sqrt{2}}(|B_H^0\rangle \pm |B_L^0\rangle).$$

The time probability density is then given by:

$$\mathcal{P}(t) = C_{norm}(e^{-\Gamma_H t} + e^{-\Gamma_L t}) \tag{9}$$

where

$$\begin{array}{ll} \Gamma_{L(H)} & = \Gamma \pm \Delta\Gamma/2 \\ C_{norm} & = \Gamma_H\Gamma_L/(\Gamma_H + \Gamma_L) \\ \tau & = 1/\Gamma \end{array}$$

Two independent variables are then considered:

$$\tau_{B_s^0} \quad \text{and} \quad \Delta\Gamma_{B_s^0}/\Gamma_{B_s^0}$$

The method used to extract information on $\Delta\Gamma_{B_s^0}/\Gamma_{B_s^0}$ consists in calculating the log-likelihood for the time distributions measured on the $D_s\ell$ and $\phi\ell h$ samples and constraining the B_s^0 lifetime to be equal to the B_d^0 lifetime $(1.56 \pm 0.04)\ ps$ (the theory predicts $\tau_{B_s^0}/\tau_{B_d} = 1 \pm \mathcal{O}(0.01)$ [7]):

$$\begin{array}{rl} log\mathcal{L}_{tot}(\tau_{B_s^0}, \Delta\Gamma_{B_s^0}/\Gamma_{B_s^0}) = & log\mathcal{L}_{D_s\ell}(\tau_{B_s^0}, \Delta\Gamma_{B_s^0}/\Gamma_{B_s^0}) + log\mathcal{L}_{\phi\ell h}(\tau_{B_s^0}, \Delta\Gamma_{B_s^0}/\Gamma_{B_s^0}) + \\ & log\mathcal{L}_{(\tau_{B_s^0} = \tau_{B_d^0})}(\tau_{B_s^0}) \end{array} \tag{10}$$

This log-likelihood is minimized in the ($\tau_{B_s^0}$,$\Delta\Gamma_{B_s^0}/\Gamma_{B_s^0}$) plane and the likelihood difference with respect to the minimum $\Delta\mathcal{L}$ is computed:

$$\Delta\mathcal{L} = -log\mathcal{L}_{tot}(\tau_{B_s^0}, \Delta\Gamma_{B_s^0}/\Gamma_{B_s^0}) + log\mathcal{L}_{tot}((\tau_{B_s^0})^{min}, (\Delta\Gamma_{B_s^0}/\Gamma_{B_s^0})^{min})$$

Figure 10-a and Figure 10-b show the $\Delta\mathcal{L}$ function with and without the constraint on the B_s^0 lifetime.
The probability density for the variables $\tau_{B_s^0}$ and $\Delta\Gamma_{B_s^0}/\Gamma_{B_s^0}$ is computed using:

$$\mathcal{P}(\tau_{B_s^0}, \Delta\Gamma_{B_s^0}/\Gamma_{B_s^0}) = F_{norm}e^{-\Delta\mathcal{L}}$$

where F_{norm} is a normalization factor defined by:

$$\int \mathcal{P}(\tau_{B_s^0}, \Delta\Gamma_{B_s^0}/\Gamma_{B_s^0}) d\tau_{B_s^0} d\Delta\Gamma_{B_s^0}/\Gamma_{B_s^0} \;=\; 1.$$

The $\Delta\Gamma_{B_s^0}/\Gamma_{B_s^0}$ probability distribution is then obtained by integrating over $\tau_{B_s^0}$. The upper limit on $\Delta\Gamma_{B_s^0}/\Gamma_{B_s^0}$ at 95 % confidence level is:

$$\Delta\Gamma_{B_s^0}/\Gamma_{B_s^0} < 0.45 \text{ at the } 95\% \text{ C.L.}$$

This limit takes into account statistical uncertainties and the systematic coming from the uncertainty on the B_d^0 lifetime.
The systematic uncertainty originating from other sources has been evaluated by convoluting the probability function $\mathcal{P}(\tau_{B_s^0}, \Delta\Gamma_{B_s^0}/\Gamma_{B_s^0})$ with the probability function of the corresponding parameters:

$$\mathcal{P}(\Delta\Gamma_{B_s^0}/\Gamma_{B_s^0}) = \int \mathcal{P}(\tau_{B_s^0}, \Delta\Gamma_{B_s^0}/\Gamma_{B_s^0}, x^1_{sys}, ..., x^n_{sys}) d\tau_{B_s^0} dx^1_{sys} ... dx^n_{sys}$$

where x^i_{sys} are the n parameters considered in the systematic uncertainty.
Since the method implies heavy numerical integrations over a n-dimensional grid only two systematics have been considered here: the purity in B_s^0 meson of the selected sample and the acceptance. This approximation is justified since systematic uncertainties are expected to be small (as they are in the lifetime measurement) and dominated by these two parameters.
The $\Delta\Gamma_{B_s^0}/\Gamma_{B_s^0}$ probability distribution is shown in Figure 10-b, the most probable value for $\Delta\Gamma_{B_s^0}/\Gamma_{B_s^0}$ is 0 and the upper limit at 95 % confidence level is:

$$\Delta\Gamma_{B_s^0}/\Gamma_{B_s^0} < 0.46 \text{ at the } 95\% \text{ C.L.}$$

The world average of the B_s^0 lifetime could not be used to constrain, in an efficient way, $\tau_{B_s^0}$; the measured B_s^0 lifetime is, indeed, a function of $\Delta\Gamma_{B_s^0}/\Gamma_{B_s^0}$ and $\tau_{B_s^0}$[3] (all the lifetime analyses assumed $\Delta\Gamma_{B_s^0}/\Gamma_{B_s^0} = 0$):

$$\tau_{B_s^0} = \frac{1 + (\frac{1}{2}\Delta\Gamma_{B_s^0}/\Gamma_{B_s^0})^2}{\Gamma(1 - (\frac{1}{2}\Delta\Gamma_{B_s^0}/\Gamma_{B_s^0})^2)}$$

6 Study of B_s^0-$\overline{B_s^0}$ oscillations

The study of B_s^0-$\overline{B_s^0}$ oscillations requires the tagging of the sign of the b quark in the B_s^0 meson at the decay and production times.
The algorithm used for the $b(\overline{b})$ tagging at production time has been tuned in order to have the best performances on the $D_s\ell$ sample, where all the charged particles from the B_s^0 decays have been reconstructed.

[3]This formula, obtained by averaging the proper time on the probability function in Equation (9), has been checked with fast simulation and found to be quite accurate.

6.1 $b(\overline{b})$ tagging at production time

The signature of the initial production of a $b(\overline{b})$ quark in the jet containing the B_s^0 or $\overline{B_s^0}$ candidate is determined using a combination of different variables which are sensitive to the initial quark state. For each individual variable X_i, the probability density functions $f_b(X_i)$ ($f_{\overline{b}}(X_i)$) for b ($\overline{b}$) quarks are obtained from the simulation and the ratio $R_i = f_{\overline{b}}(X_i)/f_b(X_i)$ is computed. The combined tagging variable is defined as:

$$x_{tag} = \frac{1-R}{1+R}, \text{ where } R = \prod R_i. \tag{11}$$

The variable x_{tag} varies between -1 and 1. High values of x_{tag} correspond to a high probability that a given hemisphere contains a b quark in the initial state. If some of the variables X_i are not defined in a given event, the corresponding ratios R_i are set to 1, corresponding to equal probabilities for the initial state to be b or $\overline{b}$. The definition of x_{tag} provides an optimal separation between b and $\overline{b}$ initial states if the individual discriminant variables X_i are independent; in case of correlations the separation power decreases but no bias is introduced.
An event is split into two hemispheres by the plane passing through the beam interaction point and perpendicular to the direction of the B_s^0 candidate; then nine discriminant variables have been selected for this analysis. Five variables are defined in the hemisphere opposite to the B_s^0 meson, in which reconstructed charged particles have been used:

- the mean jet charge which is defined as :

$$Q_{hem} = \frac{\sum_{i=1}^{n} q_i(|\vec{p_i} \cdot \vec{e_s}|)^\kappa}{\sum_{i=1}^{n}(|\vec{p_i} \cdot \vec{e_s}|)^\kappa}. \tag{12}$$

  In this expression n is total number of charged particles in the hemisphere, q_i and $\vec{p_i}$ are, respectively, the charge and the momentum of particle i $\vec{e_s}$ is the unit vector along the thrust axis and κ=0.6;
- the weighted sum of the charges of particles with tracks identified as kaon candidates:

$$Q_K = \sum q_i(\vec{p_i} \cdot \vec{e_s})^\kappa;$$

- the sum of the charges of tracks having significant impact parameters with respect to the event primary vertex;
- the sum of the charges of the particles whose tracks are compatible with the event primary vertex;
- the momentum transverse to the jet axis multiplied by the charge of the identified lepton candidate with the highest momentum.

  These variables have been combined to form the discriminant variable x^o_{tag}.

Another set of three variables are evaluated in the hemisphere which contains the B_s^0 meson candidate and only tracks not included in the B_s^0 candidate decay products have been used in their determination [4]. They are:

- the mean jet charge, computed using (12) with $\vec{e_s}$ directed along the reconstructed momentum of the B_s^0 candidate;

[4] In the $D_s\ell$ analysis all the B_s^0 decay products are identified and removed, for more inclusive analyses this is only partially possible

- the rapidity with respect to the direction of the thrust axis multiplied by the charge of the identified kaon candidate with the highest momentum having a trajectory compatible with the primary vertex (this algorithm aims at reconstructing the fragmentation kaon produced with the $\overline{\mathrm{B}^0_\mathrm{s}}$, this kaon has a sign opposite to the b quark contained in the meson);
- the momentum of any reconstructed Λ^0 candidate multiplied by the charge of the proton from its decay (same principle as in the previous item when a baryon instead of meson is produced).

These variables have been combined to form the discriminant variable x^s_{tag}. In addition the distribution of the polar angle of the direction of the thrust axis, common to both hemispheres, is also used to benefit from the forward-backward asymmetry of the b quark production relative to the electron beam axis.

6.2 Measurement of the tagging purity in events with an exclusively reconstructed D^*

The purity of the tagging at production time, ϵ_{tag}, has been measured in the real data, accumulated in 1994-1995, using the analysis of the $\mathrm{B}^0_\mathrm{d} - \overline{\mathrm{B}^0_\mathrm{d}}$ mixing in events with an exclusively reconstructed $\mathrm{D}^{*\pm}$. The $\mathrm{D}^{*\pm}$ candidates have been selected by reconstructing the decay chain $\mathrm{D}^{*+} \to \mathrm{D}^0\pi^+$ followed by $\mathrm{D}^0 \to \mathrm{K}^-\pi^+$ or $\mathrm{D}^0 \to \mathrm{K}^-\pi^+\pi^0$. The selection criteria rely mainly on the small mass difference between D^{*+} and D^0 mesons [24]. The measurement of the $\mathrm{B}^0_\mathrm{d} - \overline{\mathrm{B}^0_\mathrm{d}}$ mixing is performed by correlating *a)* the sign of the $\mathrm{D}^{*\pm}$ charge, which tags the B flavour at decay time (since D^{*-} in these events are mainly produced from B^0_d and D^{*+} from $\overline{\mathrm{B}^0_\mathrm{d}}$), with *b)* the global tagging variable, x^o_{tag}, evaluated in the hemisphere opposite to the $\mathrm{D}^{*\pm}$ and obtained by combining the five first quantities defined in the previous section. If the B^0_d meson, decaying into a $\mathrm{D}^{*\pm}$, has oscillated, the $\mathrm{D}^{*\pm}$ charge and the value of the variable x^o_{tag} are expected to be of unlike sign. The mass difference, $\Delta m_{\mathrm{B}^0_\mathrm{d}}$, between the two physical states of the $\mathrm{B}^0_\mathrm{d} - \overline{\mathrm{B}^0_\mathrm{d}}$ system is obtained from the study of the D^0 decay distance distribution for unlike and like sign events. Details of the analysis can be found in [24]. The amplitude of the time dependent oscillation is sensitive to the probability of correctly tagging events as unmixed and mixed B^0_d candidates. A fit has been performed, fixing the mass difference $\Delta m_{\mathrm{B}^0_\mathrm{d}}$ to the world average [23], and leaving ϵ_{tag} as a free parameter. The fit has been repeated for different minimum values of the global tagging variable x^o_{tag}. Results are reported in Table 11, together with the predictions from the simulation. The fraction of events f_{events} remaining after the cut on the tagging variable is also reported.

The tagging efficiency, estimated using the $\mathrm{D}^{*\pm}$ sample, is consistent within its uncertainty with the expectation from the simulation.

The selected sample of exclusively reconstructed $\mathrm{D}^{*\pm}$ still contains a significant fraction of events originating from charm and light quarks. In order to study the distribution of the tagging variable x^o_{tag}, the b-tag probability for all tracks in the event has been required to be smaller than 10^{-3} [14]. The fraction of non-b events in the remaining sample is estimated to be 5%. The distribution of the product between the $\mathrm{D}^{*\pm}$ charge and the value of the tagging variable x^o_{tag} is shown in Figure 11–a, together with the expectation from the simulation.

Another check has been performed by selecting events with an exclusively reconstructed $\mathrm{D}^{*\pm}$ accompanied by a lepton of opposite charge. This sample is highly enriched in B^0_d,

	Data		Simulation	
	ϵ_{tag}	f_{events}	ϵ_{tag}	f_{events}
$\lvert x^o_{tag}\rvert > 0.0$	0.68 ± 0.02	1.0	0.69	1.0
$\lvert x^o_{tag}\rvert > 0.1$	0.69 ± 0.02	0.88	0.71	0.89
$\lvert x^o_{tag}\rvert > 0.2$	0.71 ± 0.02	0.77	0.74	0.78

Table 11: *Values of ϵ_{tag} obtained from the analysis of exclusively reconstructed $D^{*\pm}$ for different cuts on the value of the tagging variable x^o_{tag}. Also reported is the fraction of events remaining after the cut. Expectations from the simulation are also given.*

but has a limited statistics. However, it allows the study of the tagging variable x^s_{tag} defined, in the same hemisphere as the $D^{*\pm}$-lepton candidate, by combining the other three variables mentioned in the previous section. The variable which quantifies the presence of an identified kaon of highest momentum compatible with the primary vertex has been removed from the definition of x^s_{tag}. The distribution of the product between the $D^{*\pm}$ charge and the value of the tagging variable, x^s_{tag}, is shown in Figure 11–b together with the expectation from the simulation.
The selected $D_s\ell$ sample do not have enough statistics to perform a quantitative check. The x_{tag} distributions expected from the simulation and measured data, using the $D_s\ell$ sample, are found to be compatible within statistics (Figure 12).

6.3 Tagging procedure

An event is classified as a mixed or an unmixed candidate according to the relativ signs of the D_s electric charge, Q_D, and of the x_{tag} variable. Mixed candidates have $x_{tag} \times Q_D < 0$, and unmixed ones $x_{tag} \times Q_D > 0$.
The probability, ϵ_b, of tagging the b or the $\overline{b}$ quark correctly from the measurement of x_{tag} has been evaluated using a dedicated simulated event sample and has been found to be, in the $D_s\ell$ sample, $74.5 \pm 0.5\%$ in 94-95 data and $71.5 \pm 1.2\%$ in 92-93 data.
In the $\phi\ell h$ sample the tracks from the B decay have not been all reconstructed. The tagging purity is lower with respect to the one estimated in the $D_s\ell$ sample due to some possible misidentification between primary and secondary tracks present in the same hemisphere as the ϕ meson. The value found in simulated events is ($\epsilon_b = 0.69 \pm 0.01$).
To improve the tagging purity further, the shape of the x_{tag} distribution can be included in the analysis.
Four purities enter in the analysis:

- $\epsilon_{b\ell}$: tagging purity for the direct $b \to \ell$ decays;
- $\epsilon_{bc\ell}$: tagging purity for $b \to c \to \ell$ "cascade" decays;
- $\epsilon^{mix(unmix)}_{bkg}$ probability of classifying background candidates as mixed or as unmixed (computed on sidebands events);
- $\epsilon^{mix(unmix)}_{f\ell}$ probability of classifying fake lepton candidates as mixed or as unmixed.

using x_{tag} as a discriminant variable each of these purities is replaced by the function $\epsilon X(x_{tag})$, where X is the x_{tag} probability density function.
The global probability density function has been divided by the sum $\epsilon X^r_{b\ell}(x_{tag}) + (1 - \epsilon)X^w_{b\ell}(x_{tag})$ ($r \equiv$ right tag and $w \equiv$ wrong tag) in order to keep, for the signal part, the relation $\epsilon^w = 1 - \epsilon^r$.

The functions entering in the final likelihood are then re-defined as:

$$X^r_{b\ell} = \frac{\epsilon_{b\ell} X^r_{b\ell}(x_{tag})}{\epsilon_{b\ell} X^r_{b\ell}(x_{tag}) + (1-\epsilon_{b\ell}) X^w_{b\ell}(x_{tag})} \qquad X^w_{b\ell} = 1 - X^r_{b\ell}$$

$$X^r_{bc\ell} = \frac{\epsilon_{bc\ell} X^r_{bc\ell}}{\epsilon_{b\ell} X^r_{b\ell}(x_{tag}) + (1-\epsilon_{b\ell}) X^w_{b\ell}(x_{tag})} \qquad X^w_{bc\ell} = \frac{(1-\epsilon_{bc\ell}) X^w_{bc\ell}}{\epsilon_{b\ell} X^r_{b\ell}(x_{tag}) + (1-\epsilon_{b\ell}) X^w_{b\ell}(x_{tag})}$$

$$X^{mix}_{bkg} = \frac{\epsilon^{mix}_{bkg} X^{mix}_{bkg}}{\epsilon_{b\ell} X^r_{b\ell}(x_{tag}) + (1-\epsilon_{b\ell}) X^w_{b\ell}(x_{tag})} \qquad X^{unmix}_{bkg} = \frac{\epsilon^{unmix}_{bkg} X^{unmix}_{bkg}}{\epsilon_{b\ell} X^r_{b\ell}(x_{tag}) + (1-\epsilon_{b\ell}) X^w_{b\ell}(x_{tag})}$$

$$X^{mix}_{f\ell} = \frac{\epsilon^{mix}_{f\ell} X^{mix}_{f\ell}}{\epsilon_{b\ell} X^r_{b\ell}(x_{tag}) + (1-\epsilon_{b\ell}) X^w_{b\ell}(x_{tag})} \qquad X^{unmix}_{f\ell} = \frac{\epsilon^{unmix}_{f\ell} X^{unmix}_{f\ell}}{\epsilon_{b\ell} X^r_{b\ell}(x_{tag}) + (1-\epsilon_{b\ell}) X^w_{b\ell}(x_{tag})}$$

The effective tagging purities obtained, in the $\mathrm{D_s}\ell$ sample, with this method correspond to $78 \pm 0.5\%$ for 94-95 data and to $74 \pm 1.2\%$ for 92-93 data.

6.4 Fitting procedure

From the expected proper time distributions and the tagging probabilities, the probability functions for mixed and unmixed events candidates have been computed [5]:

$$P^{mix}(t_i) = f^{\mathrm{B^0_s}}_{b\ell} P^{mix}_{\mathrm{B^0_s}}(t_i) + f^{\mathrm{B}}_{b\ell} P^{mix}_{\mathrm{B}}(t_i) + f_{bc\ell} P^{mix}_{bc\ell}(t_i) + f_{f\ell} P^{mix}_{f\ell}(t_i) + f_{bkg} P^{mix}_{bkg}(t_i). \quad (13)$$

where t_i is the reconstructed proper time. The analytical probability densities are as follows, with t being the true proper time:

- $\mathrm{B^0_s}$ mixing probability.

$$P^{mix}_{\mathrm{B^0_s}}(t_i) \;\; = \{ \;\; X^r_{b\ell} \mathcal{P}^{mix}_{\mathrm{B^0_s}}(t) + X^w_{b\ell} \mathcal{P}^{unmix}_{\mathrm{B^0_s}}(t) \;\; \} \mathcal{A}(t) \otimes \mathcal{R}_{b\ell}(t - t_i) \quad (14)$$

- "cascade" background mixing probability.

$$\begin{aligned} P^{mix}_{bc\ell}(t_i) = \{ \quad & f^{\mathrm{B_d}}_{bc\ell} (\; X^r_{bc\ell} \mathcal{P}^{unmix}_{\mathrm{B_d}}(t) + (\; X^w_{bc\ell} \mathcal{P}^{mix}_{\mathrm{B_d}}(t) \;) + \\ & (f^{\mathrm{B^0_s}}_{bc\ell}/2) (\; X^r_{bc\ell} \mathcal{P}^{unmix}_{\mathrm{B^0_s}}(t) + X^w_{bc\ell} \mathcal{P}^{mix}_{\mathrm{B^0_s}}(t) \;) + \\ & (f^{\mathrm{B^0_s}}_{bc\ell}/2) (\; X^w_{bc\ell} \mathcal{P}^{unmix}_{\mathrm{B^0_s}}(t) + X^r_{bc\ell} \mathcal{P}^{mix}_{\mathrm{B^0_s}}(t) \;) + \\ & f^{\mathrm{B^+}}_{bc\ell} X^r_{bc\ell} / \tau_{\mathrm{B^+}} \exp(-t/\tau_{\mathrm{B^+}}) \\ & f^{\Lambda_b}_{bc\ell} X^r_{bc\ell} / \tau_{\Lambda_b} \exp(-t/\tau_{\Lambda_b}) \qquad \} \mathcal{A}(t) \otimes \mathcal{R}_{bc\ell}(t - t_i) \end{aligned} \quad (15)$$

Note that the two terms contributing to the $\mathrm{B^0_s}$ are due to the fact that, in the decay $\mathrm{B^0_s} \to \mathrm{D^+_s D^-_s X}$, the lepton can originate from either $\mathrm{D_s}$ mesons. The $\mathrm{B^0_s}$ contribution can then be simplified in the expression and becomes, mixing independent:

$$f_{\mathrm{B^0_s}} / \tau_{\mathrm{B^0_s}} \exp(-\mathrm{t}/\tau_{\mathrm{B^0_s}})$$

- non-strange B-hadrons mixing probability.

$$\begin{aligned} P^{B\ mix}_{b\ell}(t_i) = \{ \quad & f^{\mathrm{B_d}}_{b\ell} (\; X^r_{b\ell} \mathcal{P}^{mix}_{\mathrm{B_d}}(t) + X^w_{b\ell} \mathcal{P}^{unmix}_{\mathrm{B_d}}(t) \;) + \\ & f^{\mathrm{B^+}}_{b\ell} X^w_{b\ell} / \tau_{\mathrm{B^+}} \exp(-t/\tau_{\mathrm{B^+}}) \\ & f^{\Lambda_b}_{b\ell} X^w_{b\ell} / \tau_{\Lambda_b} \exp(-t/\tau_{\Lambda_b}) \qquad \} \mathcal{A}(t) \otimes \mathcal{R}_{b\ell}(t - t_i) \end{aligned} \quad (16)$$

[5] In the following, only the probability function for mixed events is written explicitly; the corresponding probability for unmixed events can be obtained by changing $r \to w$.

- mixing probability for candidates from light quark events or fake leptons:

$$\mathrm{P}^{mix}_{f\ell}(t_i) = X^{mix}_{f\ell}\mathcal{P}_{f\ell}(t_i) \tag{17}$$

- combinatorial background mixing probability:

$$\mathrm{P}^{mix}_{bkg}(t_i) = X^{mix}_{bkg}\mathcal{P}_{bkg}(t_i) \tag{18}$$

  The proper time distribution for this background has been determined in the lifetime fit.

The oscillation analysis has been performed in the framework of the amplitude method [25] which consists in measuring, for each value of the frequency $\Delta m_{\mathrm{B^0_s}}$, an amplitude A and its error $\sigma(A)$. The parameter A is introduced in the time evolution of pure B^0_s or $\overline{\mathrm{B}^0_s}$ states so that the value $A = 1$ corresponds to a genuine signal for oscillation:

$$\mathcal{P}(\mathrm{B}^0_s \to (\mathrm{B}^0_s,\ \overline{\mathrm{B}^0_s})) \ = \ \frac{1}{2\tau_s}e^{-\frac{t}{\tau_s}} \times (1 \pm A\ cos(\Delta m_{\mathrm{B^0_s}} t))$$

The 95% C.L. excluded region for $\Delta m_{\mathrm{B^0_s}}$ is obtained by evaluating the probability that, in at most 5% of the cases, a real signal having an amplitude equal to unity would give an observed amplitude smaller than the one measured. This corresponds to the condition:

$$A(\Delta m_{\mathrm{B^0_s}}) + 1.645\ \sigma(A(\Delta m_{\mathrm{B^0_s}})) \ < \ 1.$$

In the amplitude approach it is possible to define the exclusion probability, that is the probability that a certain $\Delta m_{\mathrm{B^0_s}}$ value lies in an excluded region if the generated $\Delta m_{\mathrm{B^0_s}}$ was very large ($\Delta m_{\mathrm{B^0_s}} \to \infty$). The sensitivity is the value of $\Delta m_{\mathrm{B^0_s}}$ corresponding to 50 % of exclusion probability.

Using the amplitude approach (Figure 13), and considering only statistical uncertainties, a limit has been obtained:

$$\Delta m_{\mathrm{B^0_s}} > 7.5\ \mathrm{ps}^{-1} \text{ at } 95\% \text{ C.L.} \tag{19}$$

with a corresponding sensitivity at $\Delta m_{\mathrm{B^0_s}} = 8.3\ \mathrm{ps}^{-1}$. At $\Delta m_{\mathrm{B^0_s}} = 10\ ps^{-1}$, the error on the amplitude is 0.85.
Several checks have been done to verify the reliability of the amplitude fit: the proper time distributions for mixed and unmixed events have been verified to be well reproduced by the fit (Figure 14-a,-b) and the ratio between mixed events and the total number of events in bins of the proper time has been compared with the expected distribution for $\Delta m_{\mathrm{B^0_s}} = 5\ ps^{-1}$ and $\Delta m_{\mathrm{B^0_s}} = 10\ ps^{-1}$. These values have been choosen to illustrate the behaviour of the expected oscillation curve for $A = 0$ ($\Delta m_{\mathrm{B^0_s}} = 5\ ps^{-1}$) and $A = 1$ ($\Delta m_{\mathrm{B^0_s}} = 10\ ps^{-1}$) (Figure 14-c). It could be seen that, qualitatively, there is a good agreement, thought not conclusive, between the oscillation curve and the distribution of data points for $\Delta m_{\mathrm{B^0_s}} = 10\ ps^{-1}$ an oscillation is favoured whereas, for $\Delta m_{\mathrm{B^0_s}} = 5\ ps^{-1}$, data prefer no oscillation.

6.5 Study of systematic uncertainties

Systematic uncertainties have been evaluated by varying the parameters which have been kept constant in the fit, according to their measured or expected errors.

- Systematics from the tagging purity.
  - $D_s\ell$ sample.
    The studies done in Section 6.2 show that, using the tagging variables in the opposite hemisphere and requiring $|x^o_{tag}| > 0.$, the difference between the values of the tagging purity measured in real and simulated events is $\epsilon_{tag}(DATA) - \epsilon_{tag}(MC)$ = -0.01 ± 0.02. It has been verified that the real and the simulated distributions for the tagging purities agree in both hemispheres.
    The systematics coming from the control of the tagging purity has been evaluated by varying the probability distributions of the discriminant variable for b and $\overline{b}$ quarks in a way to induce an absolute variation on the effective value of the tagging purity of ±3.0%.

  - $\phi\ell h$ sample. The agreement between data and simulation has not been checked for this sample; a conservative absolute variation of 5% in the tagging purity has been assumed.
- Systematics from the B^0_s purity.
  The same procedure already applied for the lifetime measurement has been used.
- Systematics from the resolution on the B decay proper time.
  The same procedure already applied for the lifetime measurement has been used. In addition, the systematic error due to the variation of the proper time distribution of the combinatorial background, has been considered: the parameters used to define the background shape, in the lifetime fit, have been varied according to their fitted errors.

The inclusion of systematic uncertainties lowers the sensitivity to 8.2 ps^{-1} without affecting the 95% C.L limit.
The exclusion probability of $\Delta m_{B^0_s} = 7.5\ ps^{-1}$ is 54% while the probability of obtaining a limit on $\Delta m_{B^0_s}$ higher than the actual one is 38% (Figure 15-c).
Figure 15-a and Figure 15-b represent, respectively, the error on the amplitude and the exclusion probability as a function of $\Delta m_{B^0_s}$.

7 Conclusion

A sample of 436 $D^{\pm}_s\ell^{\mp}$ candidate events has been selected from about 3.6 million hadronic Z^0 decays accumulated by DELPHI between 1992 and 1995, using seven different D_s decay modes. The number of events coming from B^0_s semileptonic decays has been estimated to be 230 ± 18 in this sample. In addition, a sample of 441 $\phi\ell h$, containing 41 ± 12 B^0_s semileptonic decays, has been also used. Events contained in the $D_s\ell$ sample, with a reconstructed ϕ and have been removed from this last sample.
Using these samples, three analyses have been performed. The B^0_s lifetime has been measured and a limit on the fractional width difference between the two physical B^0_s states has been set:

$$\tau(B^0_s) = (1.42^{+0.14}_{-0.13}(\text{stat.}) \pm 0.03(\text{syst.}))\ \text{ps}$$

$$\Delta\Gamma_{B^0_s}/\Gamma_{B^0_s} < 0.46 \text{ at the } 95\% \text{ C.L.}$$

This last result has been obtained under the hypothesis that $\tau_{B^0_s} = \tau_{B_d}$.
The study of $B^0_s - \overline{B^0_s}$ oscillations sets a limit at 95% C.L. on the mass difference between

the physical B_s^0 states:

$$\Delta m_{B_s^0} > 7.5 \text{ ps}^{-1} \text{ at } 95\% \text{ C.L.} \quad (20)$$

with a corresponding sensitivity equal to 8.2 ps^{-1}.
Previous DELPHI results obtained with $D_s\ell$ and $\phi\ell$ samples ([26],[20]) are superseeded by the analyses presented in this paper.

Acknowledgements

We are greatly indebted to our technical collaborators, to the members of the CERN-SL Division for the excellent performance of the LEP collider, and to the funding agencies for their support in building and operating the DELPHI detector.
We acknowledge in particular the support of
Austrian Federal Ministry of Science and Traffics, GZ 616.364/2-III/2a/98,
FNRS–FWO, Belgium,
FINEP, CNPq, CAPES, FUJB and FAPERJ, Brazil,
Czech Ministry of Industry and Trade, GA CR 202/96/0450 and GA AVCR A1010521,
Danish Natural Research Council,
Commission of the European Communities (DG XII),
Direction des Sciences de la Matière, CEA, France,
Bundesministerium für Bildung, Wissenschaft, Forschung und Technologie, Germany,
General Secretariat for Research and Technology, Greece,
National Science Foundation (NWO) and Foundation for Research on Matter (FOM), The Netherlands,
Norwegian Research Council,
State Committee for Scientific Research, Poland, 2P03B06015, 2P03B03311 and SPUB/P03/178/98,
JNICT–Junta Nacional de Investigação Científica e Tecnológica, Portugal,
Vedecka grantova agentura MS SR, Slovakia, Nr. 95/5195/134,
Ministry of Science and Technology of the Republic of Slovenia,
CICYT, Spain, AEN96–1661 and AEN96-1681,
The Swedish Natural Science Research Council,
Particle Physics and Astronomy Research Council, UK,
Department of Energy, USA, DE–FG02–94ER40817.

References

[1] M. Beneke, G. Buchalla, I. Dunietz *Phys. ReV.* **D54** (1996) 4419-4431
[2] L. Wolfenstein, *Phys. ReV. Lett.* **51** (1983) 1945.
[3] G. Altarelli and P.J. Franzini, *Z. Phys.* **C37** (1988) 271.
P.J. Franzini, *Phys Rep.* **173** (1989) 1.
[4] A. J. Buras, Acta. Phys. Polon. **B26** (1995) 755-788.
[5] A.X. El-Khadra, A. Kronefeld, P.B. Mackenzie, S.M. Ryan and J.N. Simone, *Phys. Rev.* 014506-1 (1998).
C. Bernard et al. (MILC Collaboration), *Phys. Rev. Lett.* **81**, 4812 (1998).
D. Becirevic, Ph. Boucaud, J.P. Leroy, V. Lubicz, G. Martinelli, F. Mescia and F. Rapuano, (hep-lat/9811003).
[6] P. Paganini, F. Parodi, P. Roudeau and A. Stocchi, *Physica Scripta* **Vol. 58**, 556 (1998).
F. Parodi, P. Roudeau and A. Stocchi, LAL 98-49, hep-ph/9802289.
F. Parodi, P. Roudeau and A. Stocchi, contributed paper to the ICHEP98 Conference (Vancouver 23^{th}-29^{th} July 1998), paper 586.
F. Parodi, P. Roudeau and A. Stocchi, LAL 99-03, hep-ph/9903063.
[7] "The QCD perspective on lifetimes of heavy-flavour hadrons", I.I. Bigi, UND-HEP-95-BIG02.
[8] M. Beneke, G. Buchalla, C. Greub, A. Lenz, U. Nierste *CERN-TH/***98-261**
[9] DELPHI Coll., P. Abreu et al., Nucl. Instr. and Meth. **A378** (1996) 57.
[10] V. Chabaud et al., *Nucl. Instr. Meth.* **A368** (1996) 314.
[11] DELPHI Collaboration, P. Abreu et al., *Nucl. Phys.* **B418** (1994) 403.
[12] E.G. Anassontzis et al., *Nucl. Instr. Meth.* **A323** (1992) 351.
[13] T. Sjöstrand, *Comp. Phys. Comm.* **82** (1994) 74.
[14] DELPHI Collaboration,P. Abreu et al., *Zeit. Phys.* **C70** (1996) 531.
[15] DELPHI Coll., P. Abreu et al, *Z. Phys.* **C73** (1996) 11.
[16] N. Isgur, D. Scora, B. Grinstein and M. Wise, *Phys. Rev.* **D39** (1989) 799.
[17] Search for $\mathrm{B_s^0}$-$\overline{\mathrm{B_s^0}}$ Oscillation with the DELPHI Detector, A. W. Borgland, PhD. thesis, University of Bergen, June 1999.
[18] Decay Parameters of the $\mathrm{B_s^0}$ Meson in the Inclusive $\phi\ell^+$ Channel, Ole Myren Røhne, PhD. Thesis, Department of Physics, University of Oslo, August 1998.
[19] Particle Data Group, Caso et al., *Eur. Phys. J.* **C3** (1998) 1.
[20] DELPHI Coll., P. Abreu et al., *Zeit. Phys.* **C71** (1996) 11.
[21] CLEO Coll., "$\mathrm{D_s}$-Lepton Charge Correlations in B Meson Decays: A Study of the $\mathrm{D_s}$ Meson Production Mechanism", EPS0169 contribution to the ICHEP95, (Brussels, July 1995).
[22] E. Golowich, A. Le Yaouanc, L. Oliver, O. Pène, J.C. Raynal, *Zeit. Phys.* **C48** (1990) 89;
A. Stocchi, Ph. D. Thesis, LAL 93-10 (May 1993).
[23] The LEP Oscillations Working Group " LEP Combined Results on B^0 Oscillations: Results for Summer 1998 Conferences" LEPBOSC NOTE 98/3
[24] DELPHI Collaboration, W. Adam et al., *Zeit. Phys.* **C76** (1997) 579.
[25] H.G. Moser and A. Roussarie, *Nucl. Instr. and Meth.* **A384** (1997) 491.
[26] DELPHI Collaboration, W. Adam et al., *Phys. Lett.* **B414** (1997) 382.

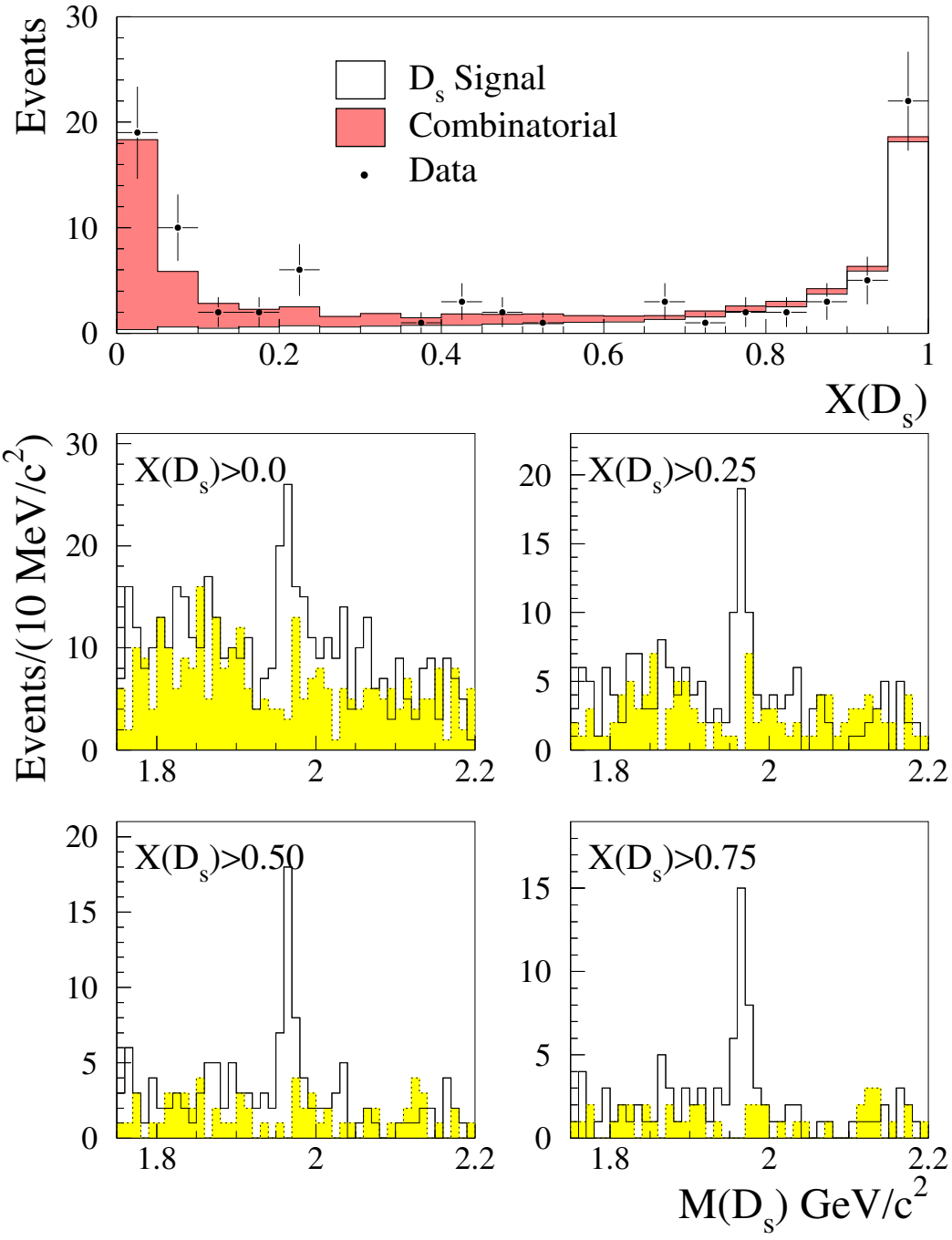

Figure 1: *The plot on the top shows the distribution of the X_{D_s} discriminant variable. The points with error bars represent the data, the full line histogram shows the contribution from the simulated signal and the shaded histogram shows the contribution coming from simulated background events. The four figures on the bottom show the effect, on the $\phi\pi$ signal in the 94-95 data, of a cut on the discriminant variable (empty histograms represent "right-sign" events while shaded histogram show "wrong-sign" events).*

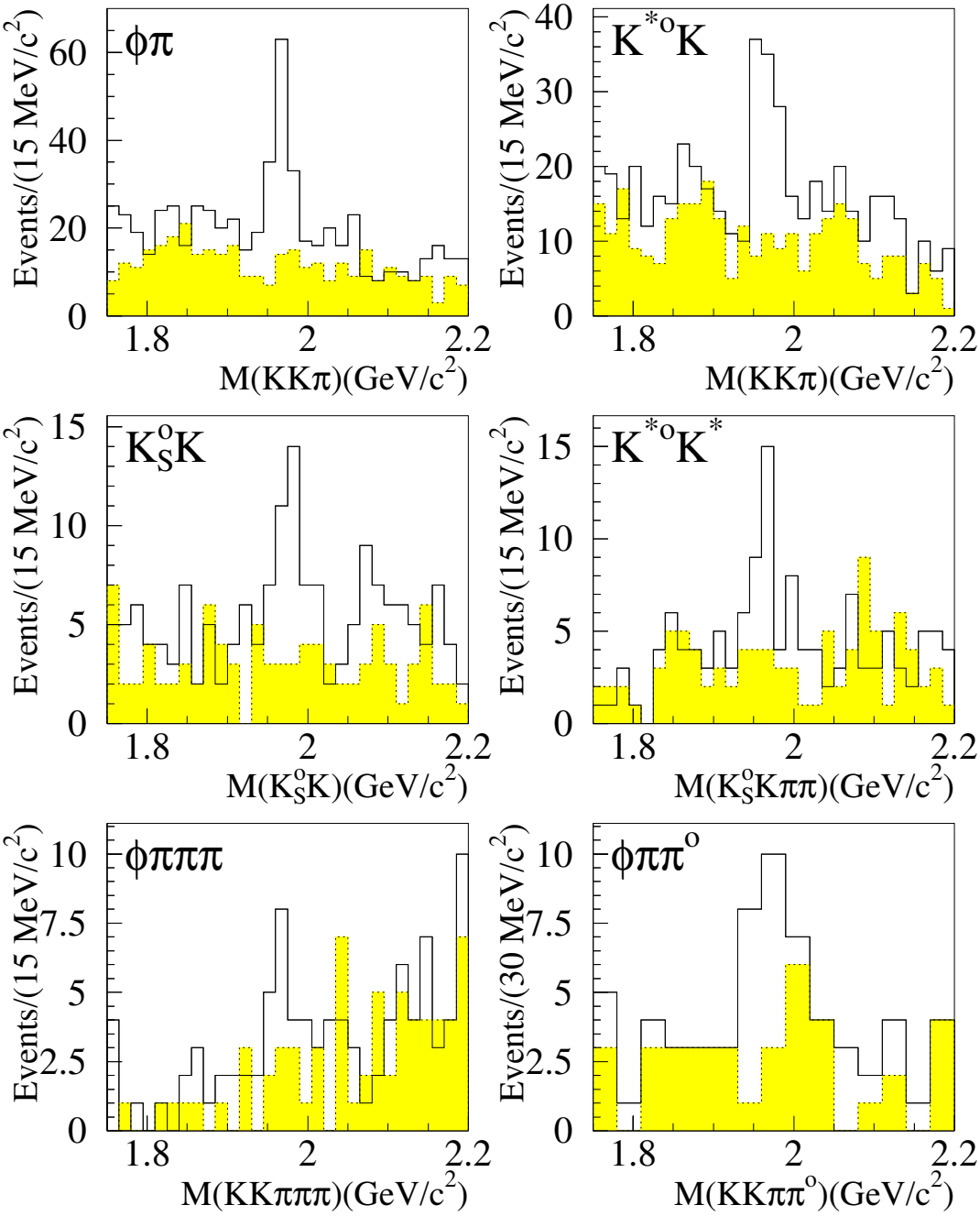

Figure 2: *Invariant mass distributions for* D_s *candidates in six non-leptonic decay modes* ($\phi\pi^+$, $\overline{K}^{*0}K^+$, K^0K^+, $\overline{K}^{*0}K^{*+}$, $\phi\pi^+\pi^-\pi^+$ *and* $\phi\pi^+\pi^0$). *The last three decay modes have been reconstructed using only the 94-95 statistics. The corresponding distribution for wrong-sign combinations are given by the shaded histograms*

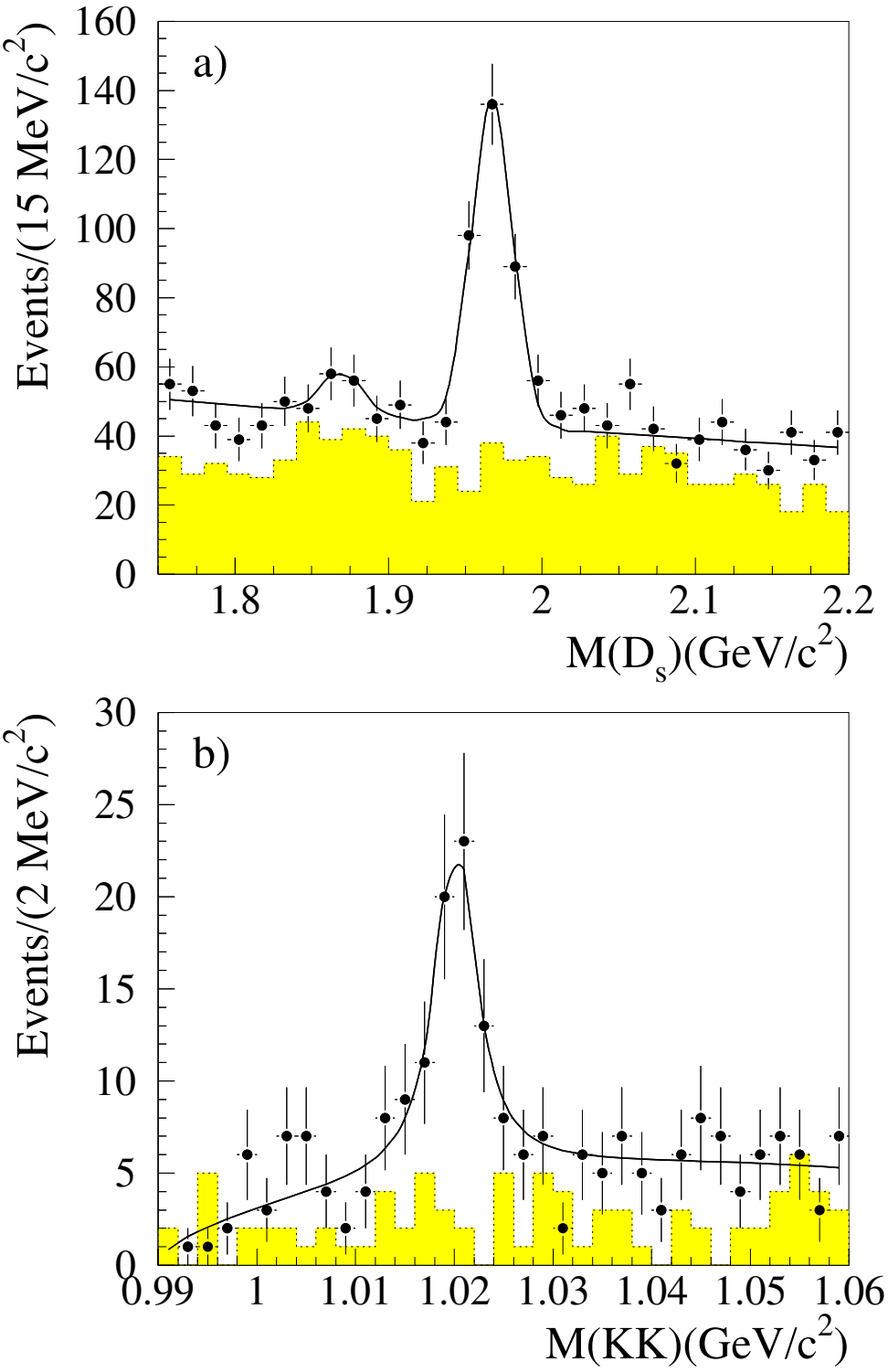

Figure 3: *a) Invariant mass distributions for* $\mathrm{D_s}$ *candidates in non-leptonic decay modes* ($\phi\pi^+$, $\overline{\mathrm{K}}^{\star 0}\mathrm{K}^+$, $\mathrm{K}^0\mathrm{K}^+$, $\overline{\mathrm{K}}^{\star 0}\mathrm{K}^{\star +}$, $\phi\pi^+\pi^-\pi^+$ *and* $\phi\pi^+\pi^0$*). b)* $\mathrm{K}^+\mathrm{K}^-$ *invariant mass distribution for* $\mathrm{D_s}$ *candidates selected in the two semileptonic decay modes. The corresponding distribution for wrong-sign combinations are given by the shaded histograms. The curves show the result of fits described in the text.*

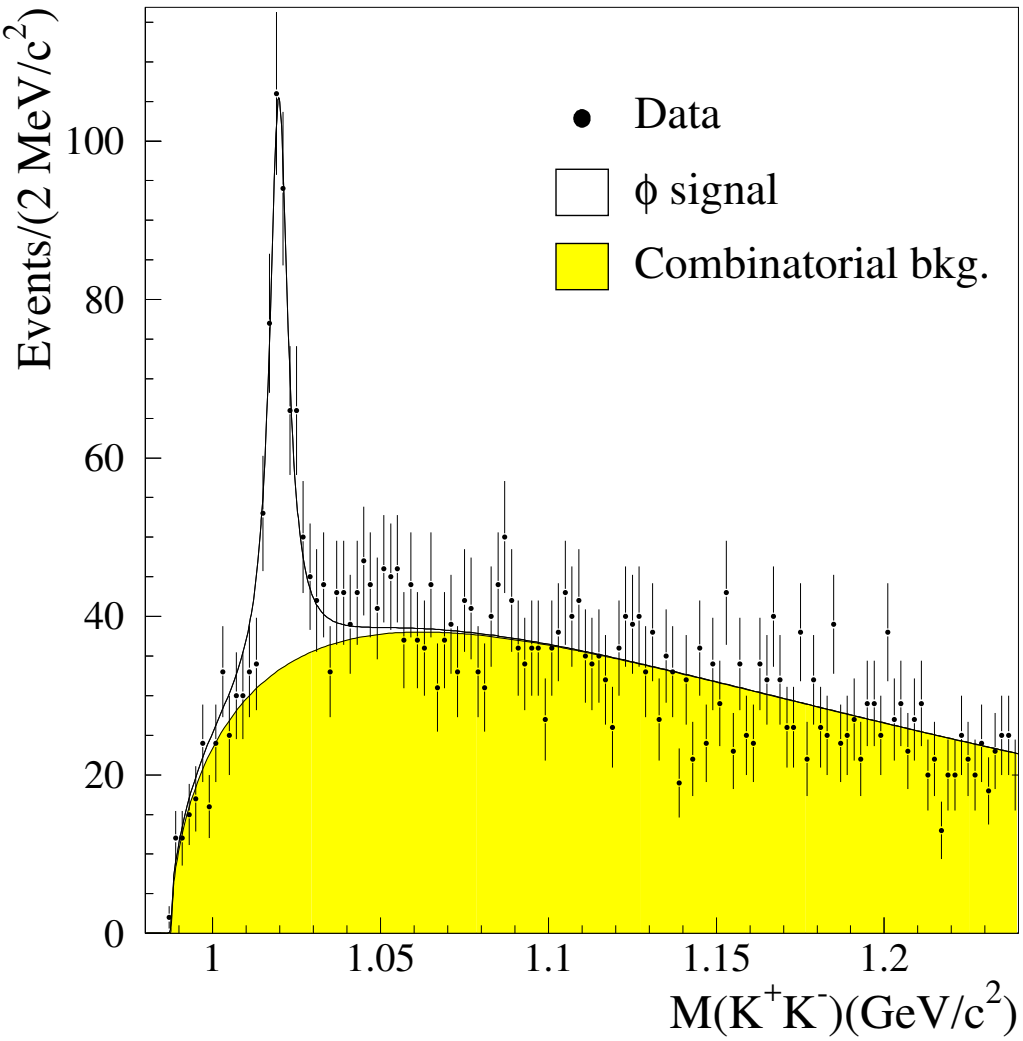

Figure 4: *K^+K^- invariant mass distribution of the $\phi\ell h$ candidates. The curves show the result of the fit described in the text.*

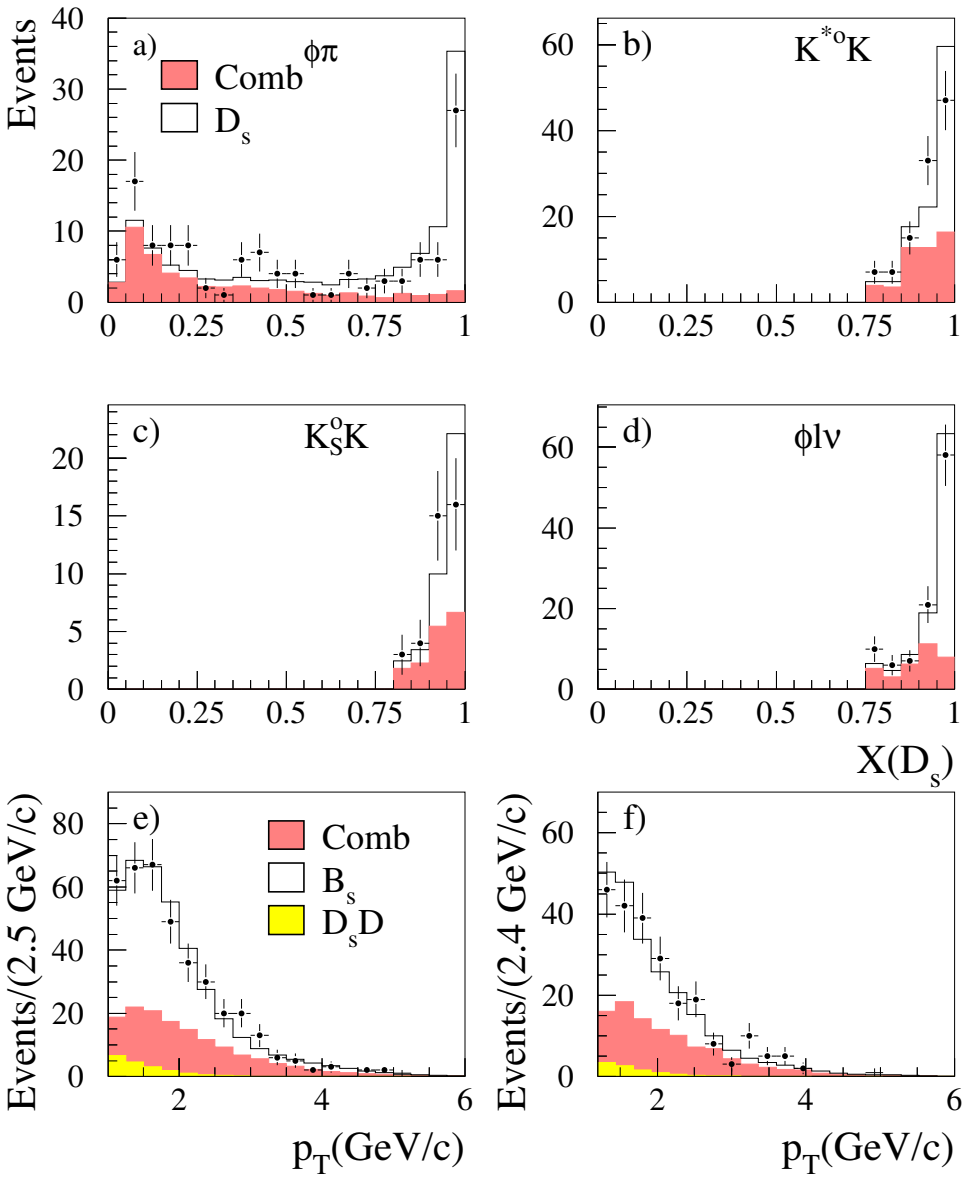

Figure 5: *The plots illustrate the agreement between data and simulation for the variables used in the estimate of the* $\mathrm{B_s^0}$ *purity on an event by event basis.*
a),b),c) and d) show the $X_{\mathrm{D_s}}$ *distributions for the channels* $\phi\pi$, $\overline{\mathrm{K^{0*}}}\mathrm{K}$, $\mathrm{K_S^0K}$ *and* $\phi\ell^+$ *respectively. Full histograms and shaded histograms represent the signal and the background respectively.*
e) and f) show the p_T *distributions for the samples selected with* $p_T > 1$ *GeV/c* ($\phi\pi^+$ *and* $\phi\ell^+\nu$) *and* $p_T > 1.2$ *GeV/c (all the others) respectively.*
For the p_T *distribution the* $\mathrm{D_s}\overline{D}$ *and the combinatorial background are considered separately.*

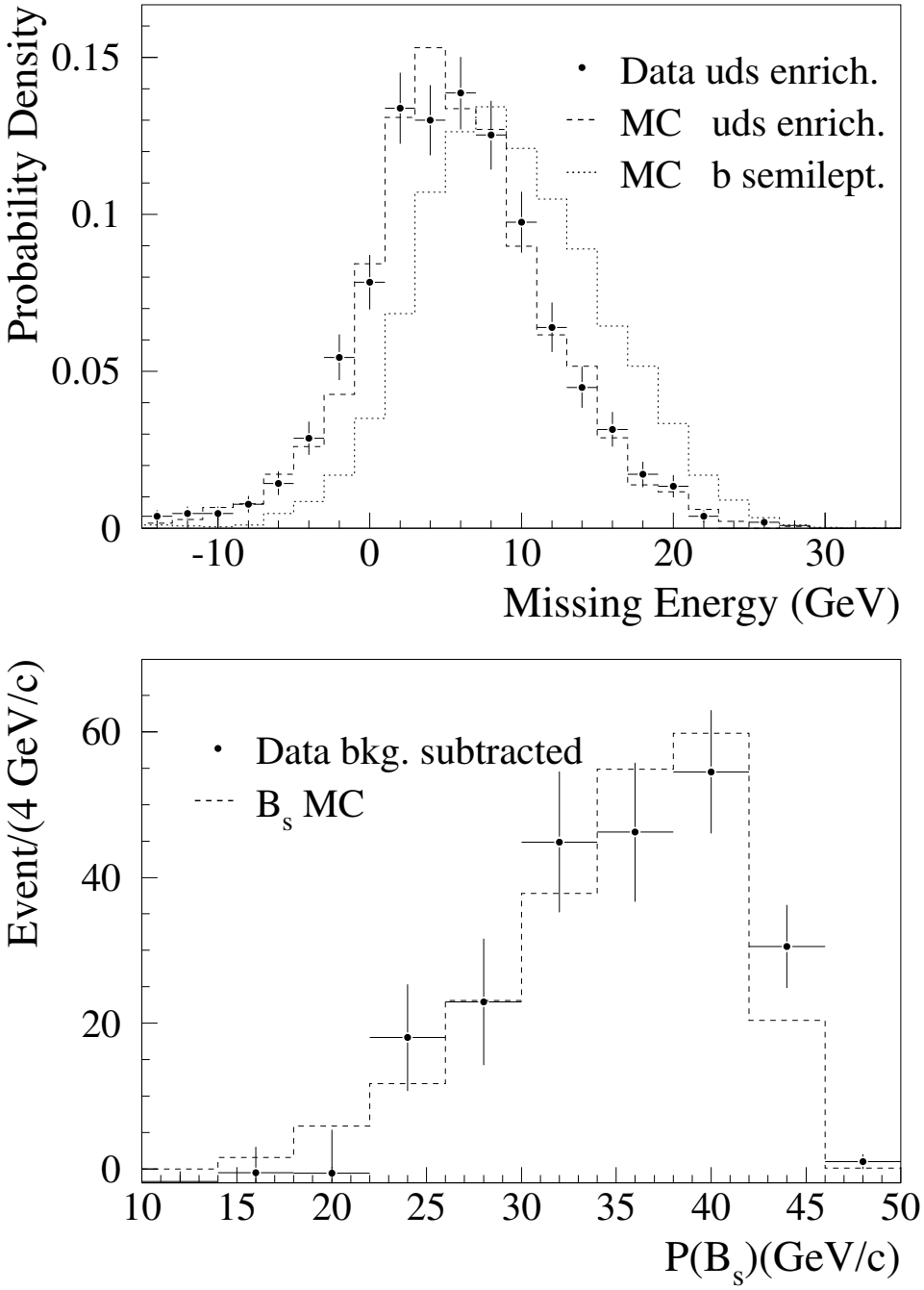

Figure 6: *The plot on the top shows the comparison between data and the simulation for the missing energy distribution after correction (see Section 3.5.1). The data (dots with error bars) and the simulation (dashed histogram) are enriched in light quark events. The dotted histogram shows the missing energy distribution in simulated b semileptonic decays. The plot on the bottom shows the comparison between the energy distribution for simulated events and the one estimated from datain the signal region by subtracting the energy distribution of events in the* D_s *side bands from that of the events in the signal region.*

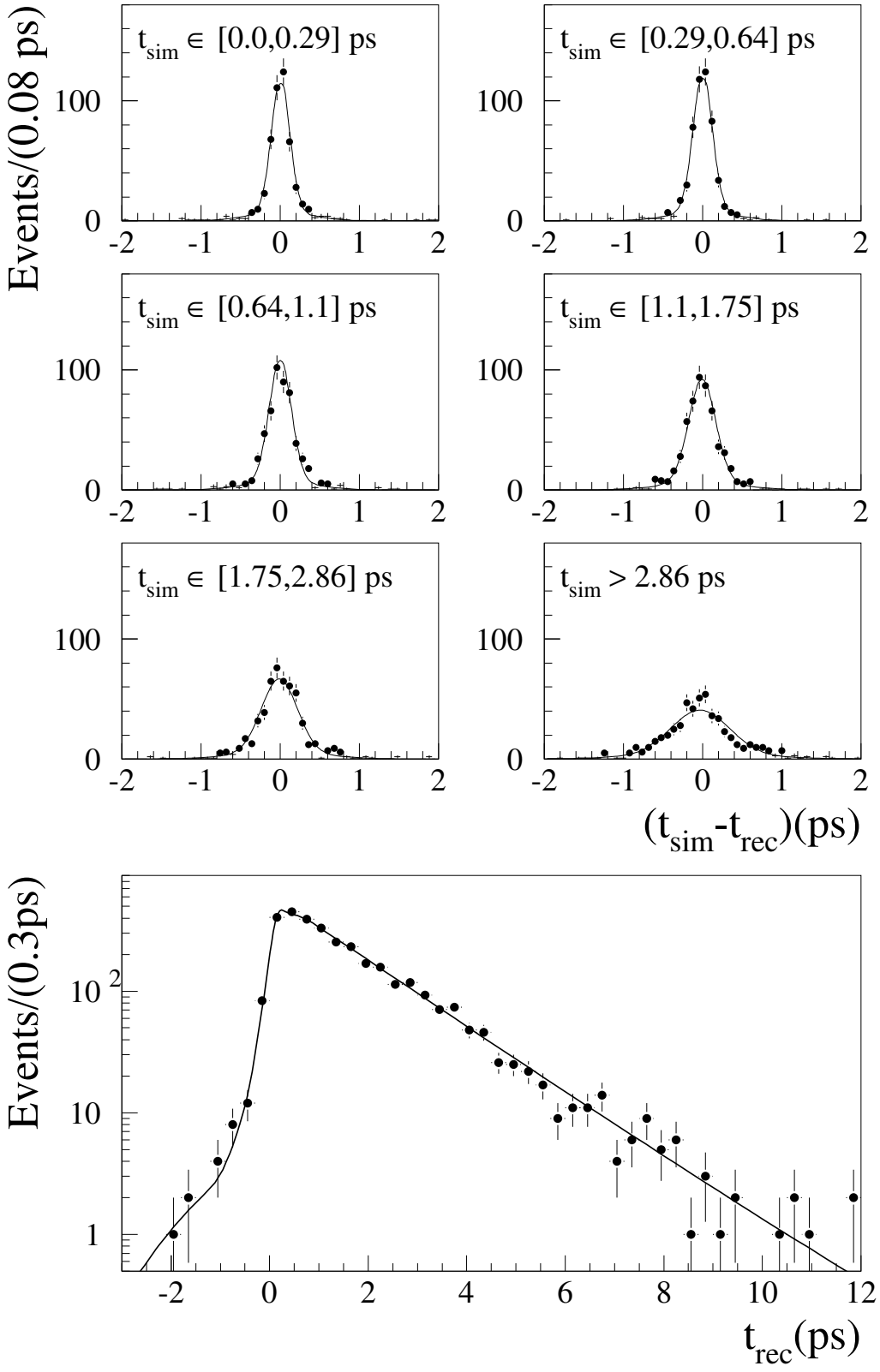

Figure 7: *The six plots on the top show the proper time resolution, defined as the difference between the generated time (t_{sim}) and the reconstructed time (t_{rec}), in bins of generated time. The plot on the bottom shows the distribution of the reconstructed time with the fit superimposed.*

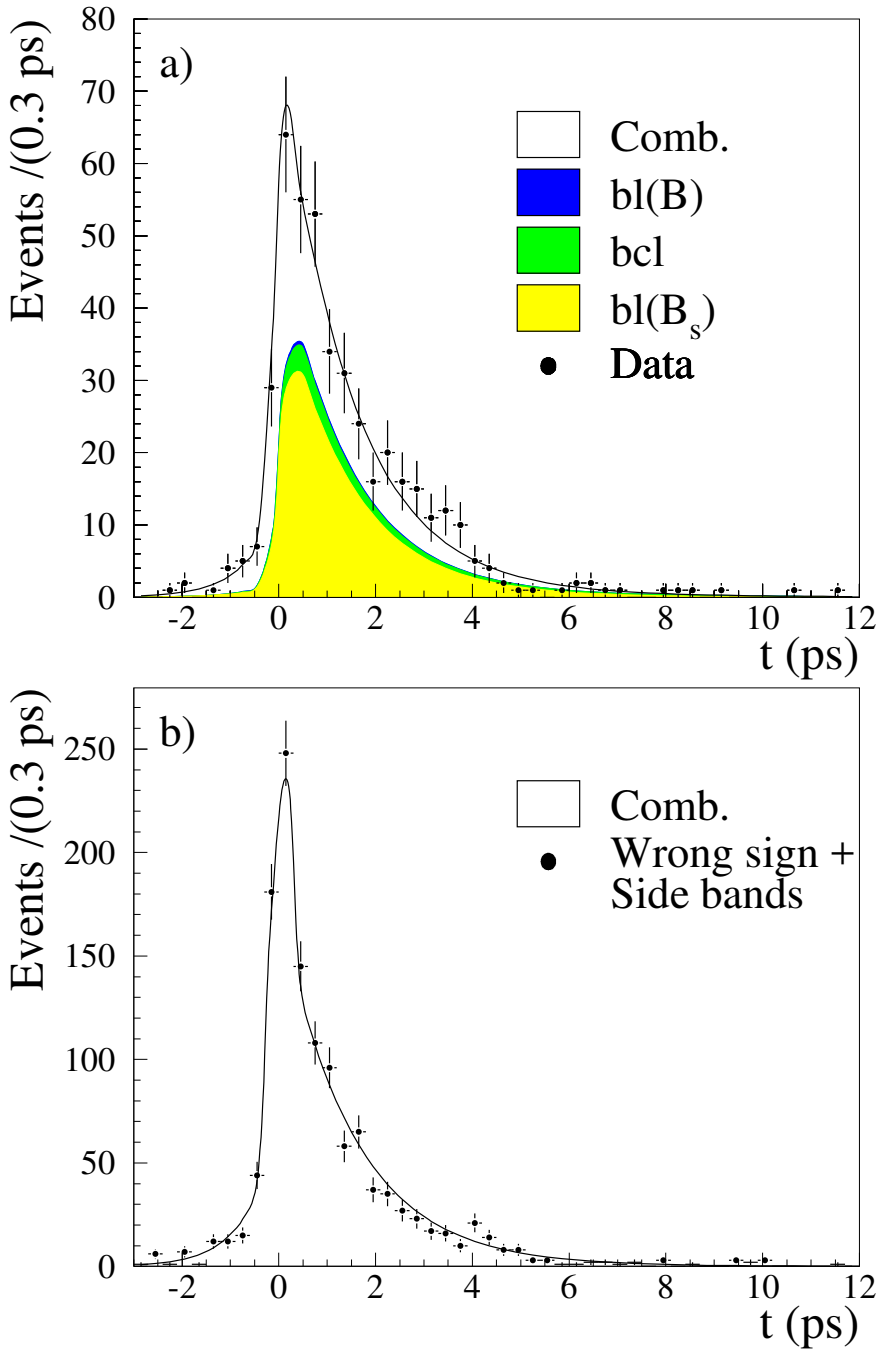

Figure 8: $D_s\ell$ *sample. a) Likelihood fit for events in the signal mass region. The points show the data and the curves correspond to the different contributions to the selected events. b) The same as a) but for "wrong-sign" events and for events situated in the side band region*

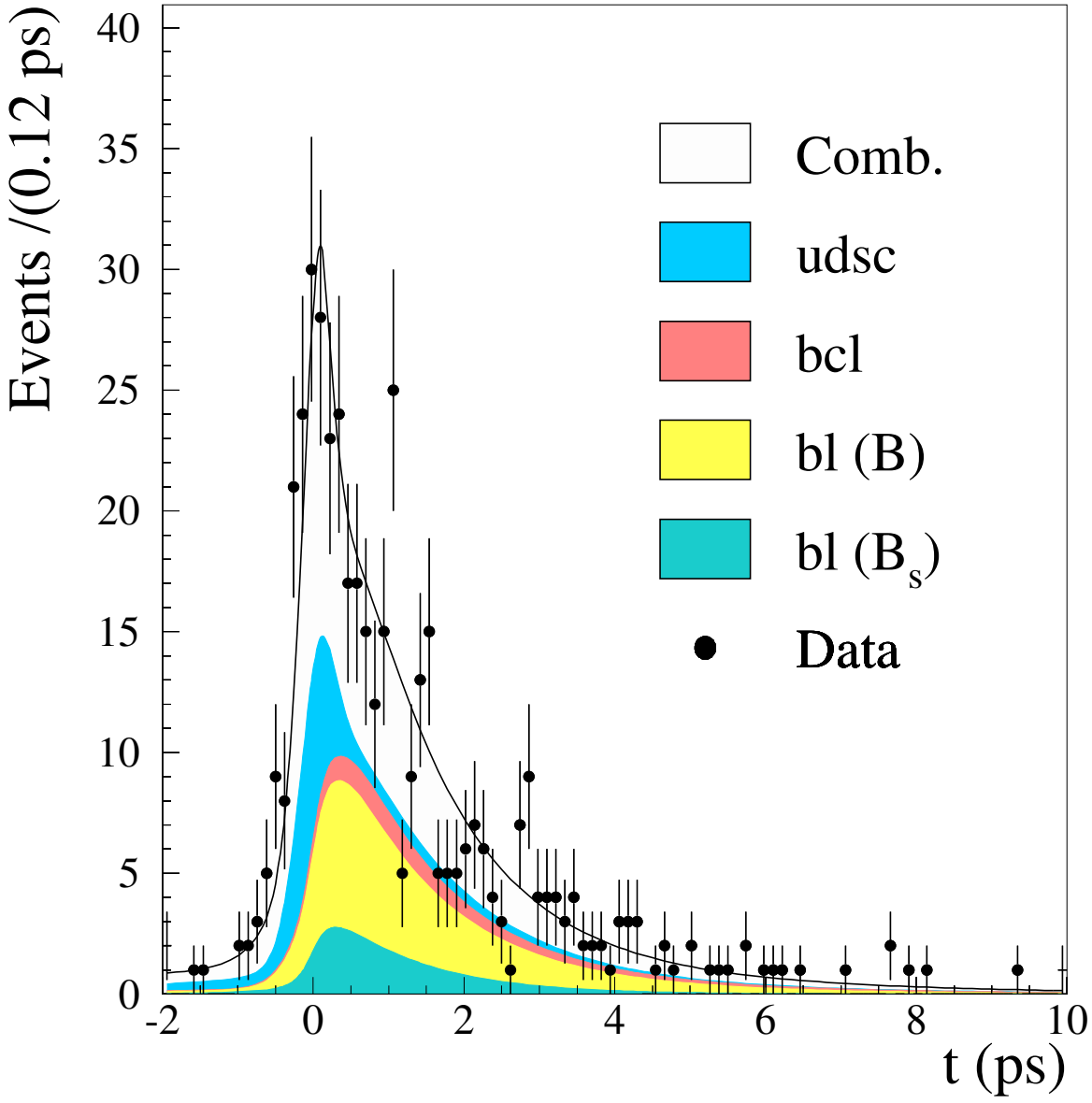

Figure 9: *$\phi\ell h$ sample.*
Likelihood fit for events in the signal mass region. The points show the data and the curves correspond to the different contributions to the selected events.

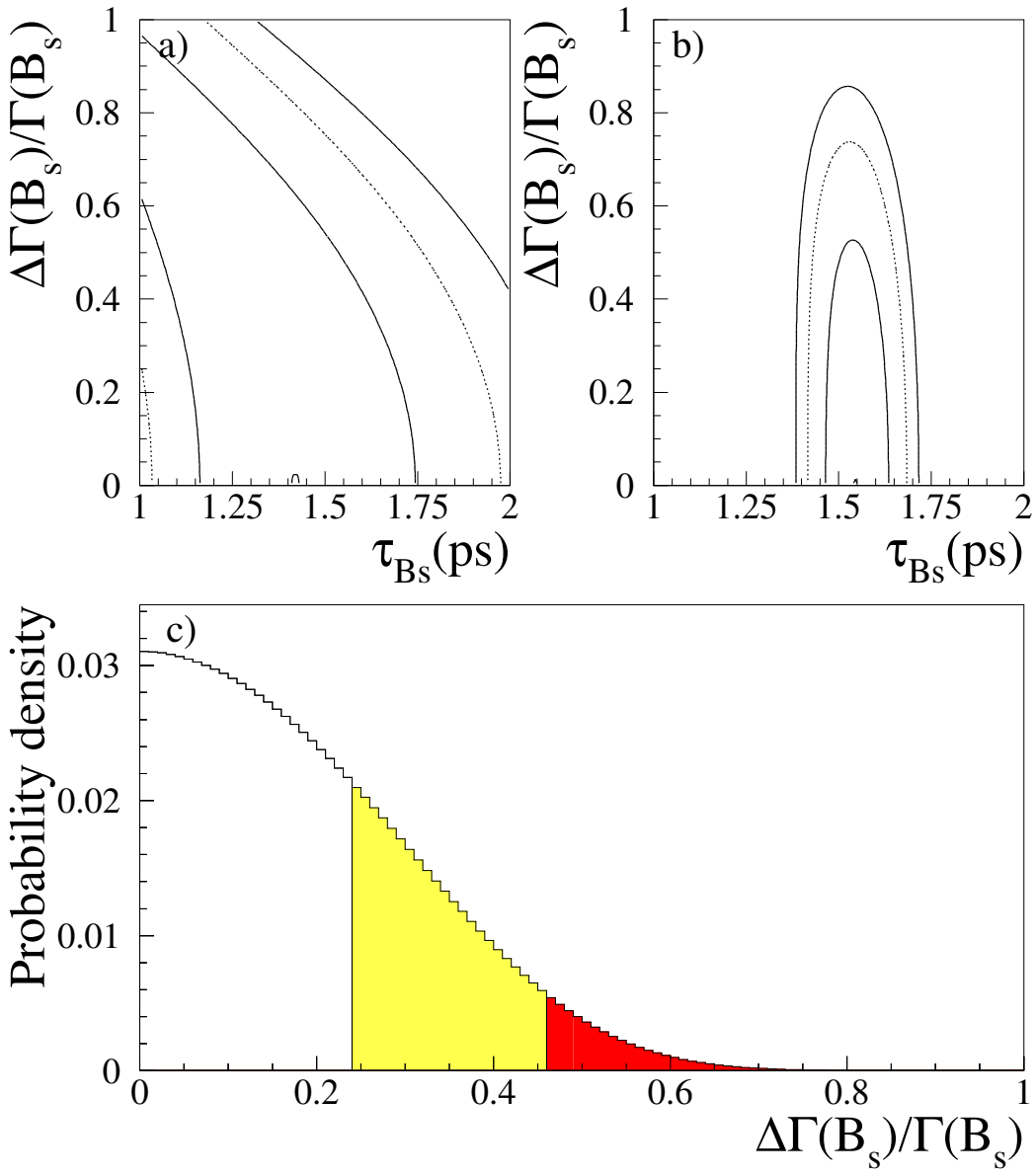

Figure 10: *a) contours corresponding to 68, 95 and 99 % C.L. of the negative log-likelihood in the plane* $\tau_{B_s^0}$-$\Delta\Gamma_{B_s^0}/\Gamma_{B_s^0}$ *evaluated on the* $D_s\ell$ *sample. b) Same as a) but with the constraint* $\tau_{B_s^0} \equiv \tau_{B_d^0}$. *c) Probability density distribution for* $\Delta\Gamma_{B_s^0}/\Gamma_{B_s^0}$*; the two shaded regions show the limits at 68 % C.L. and 95 % C.L. respectively.*

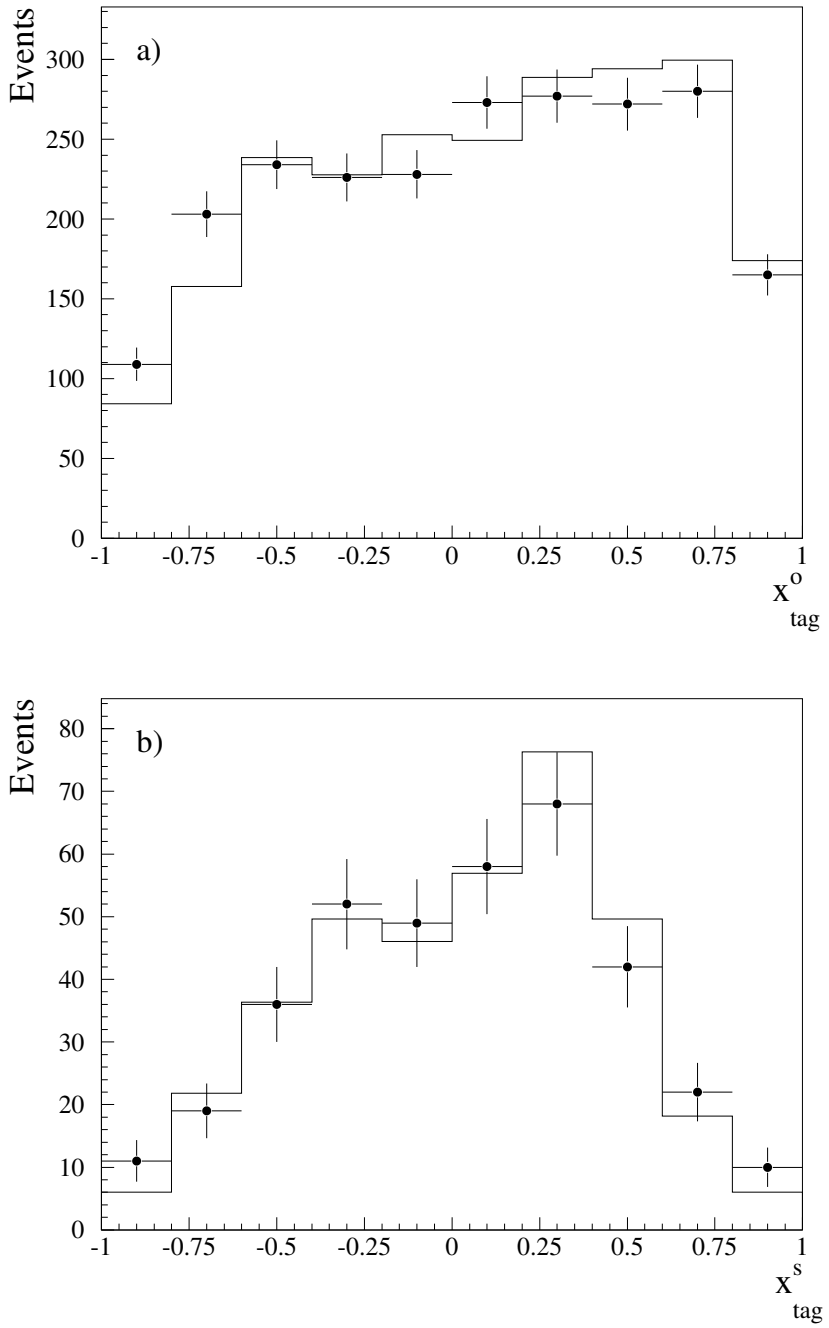

Figure 11: *a) Distribution of the global tagging variable x^o_{tag} in the hemisphere opposite to the $D^{*\pm}$ candidate.*
b) Distribution of the global tagging variable x^s_{tag} in the same hemisphere as the $D^{*\pm}$-lepton candidate.
The full dots with the error bars represent the data. The histogram is obtained in the simulation.

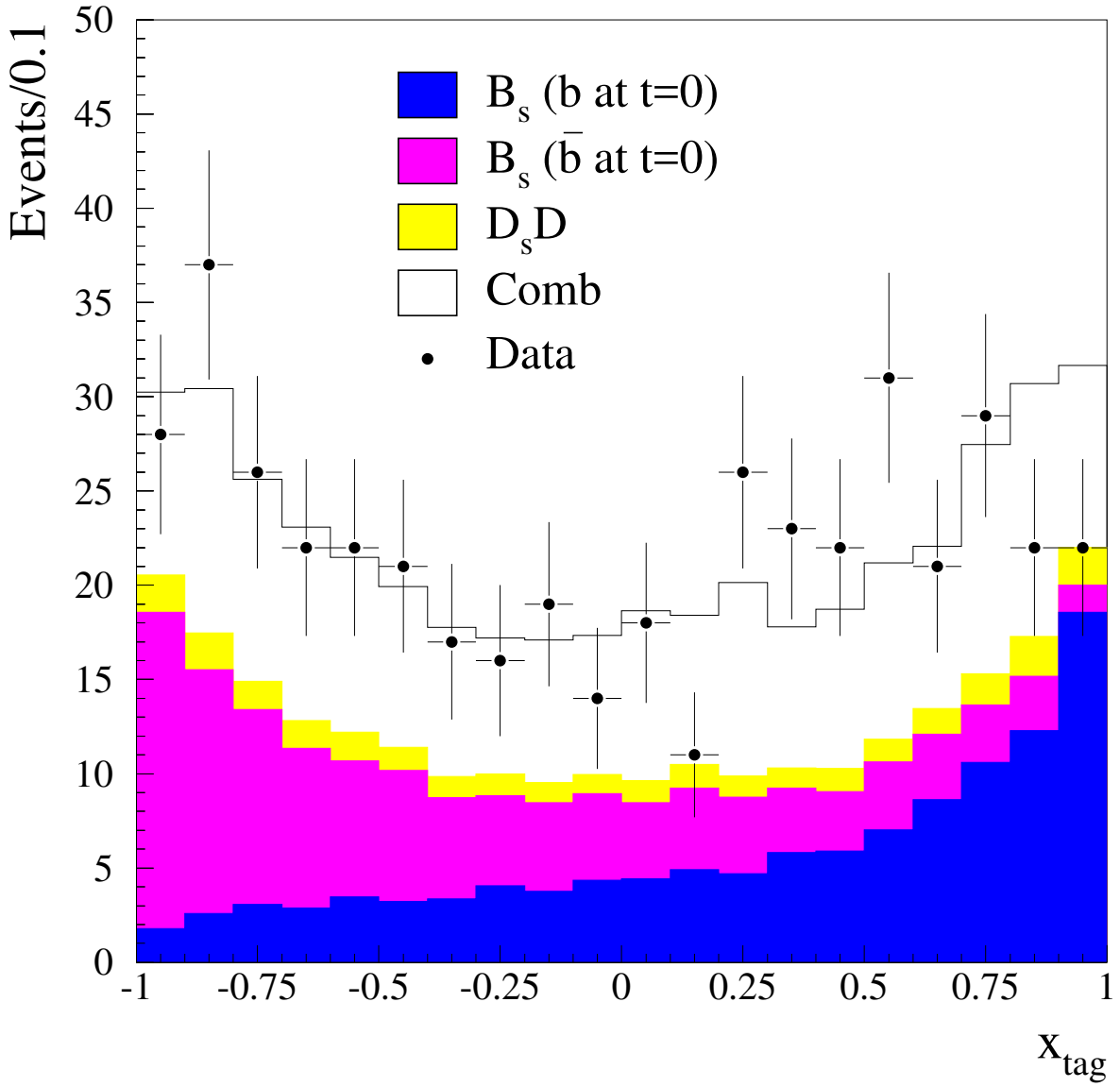

Figure 12: *The plot shows the distribution of the x_{tag} discriminant variable in the $D_s\ell$ sample. The points with the error bars represent the data, the full line histogram shows the contribution from combinatorial background, the lighter histogram the contribution from D_sD events and the darker histograms the contribution from the B_s^0 signal in which B_s^0 mesons produced from b or $\bar{b}$ quarks have been distinguished.*

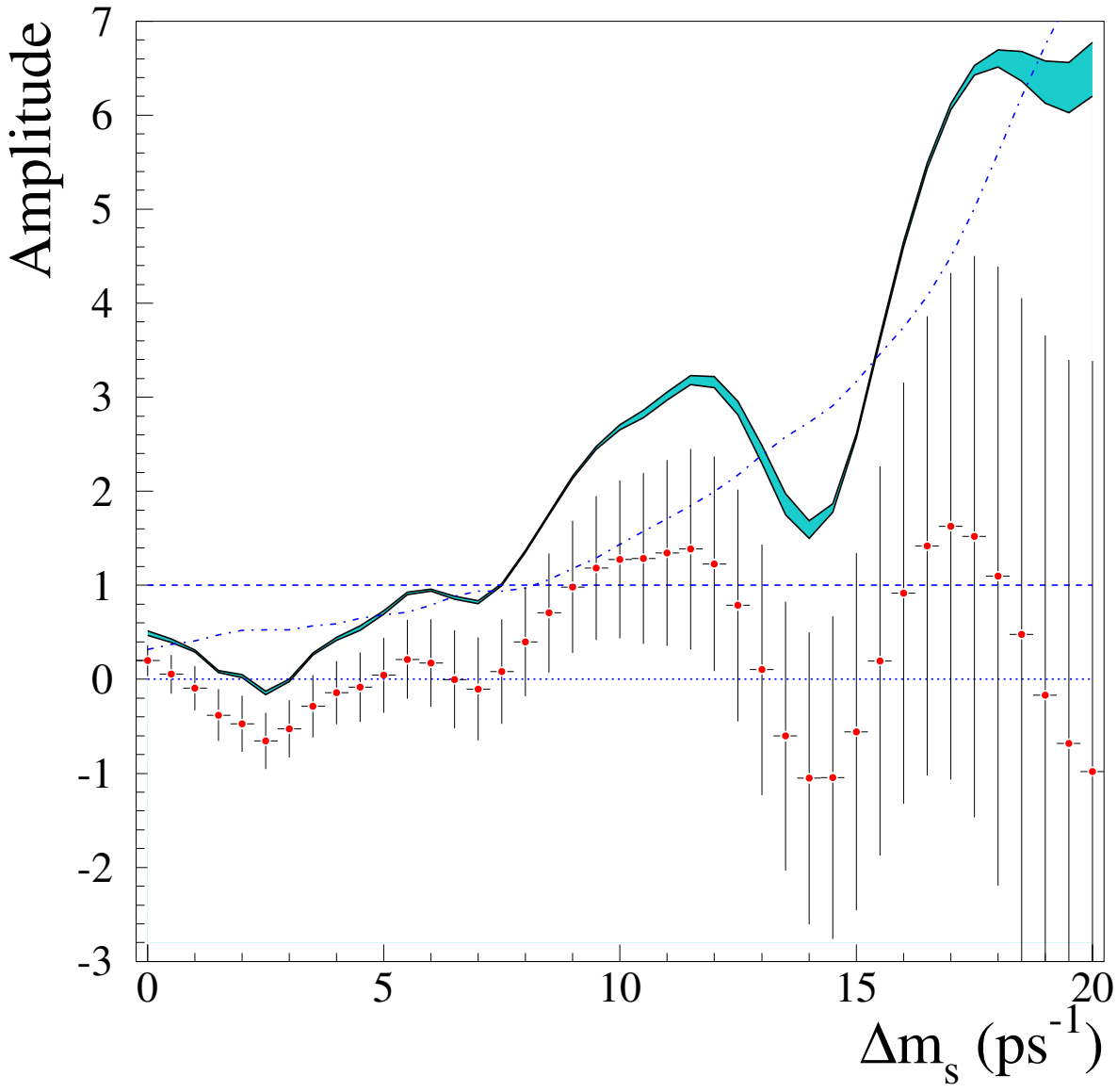

Figure 13: *Variation of the oscillation amplitude A as a function of Δm_s. The lower continuous line corresponds to $A + 1.645\ \sigma_A$ where σ_A includes statistical uncertainties only, while the shaded area includes the contribution from systematics. The dashed-dotted line corresponds to the sensitivity curve. The lines at A=0 and A=1 are also given.*

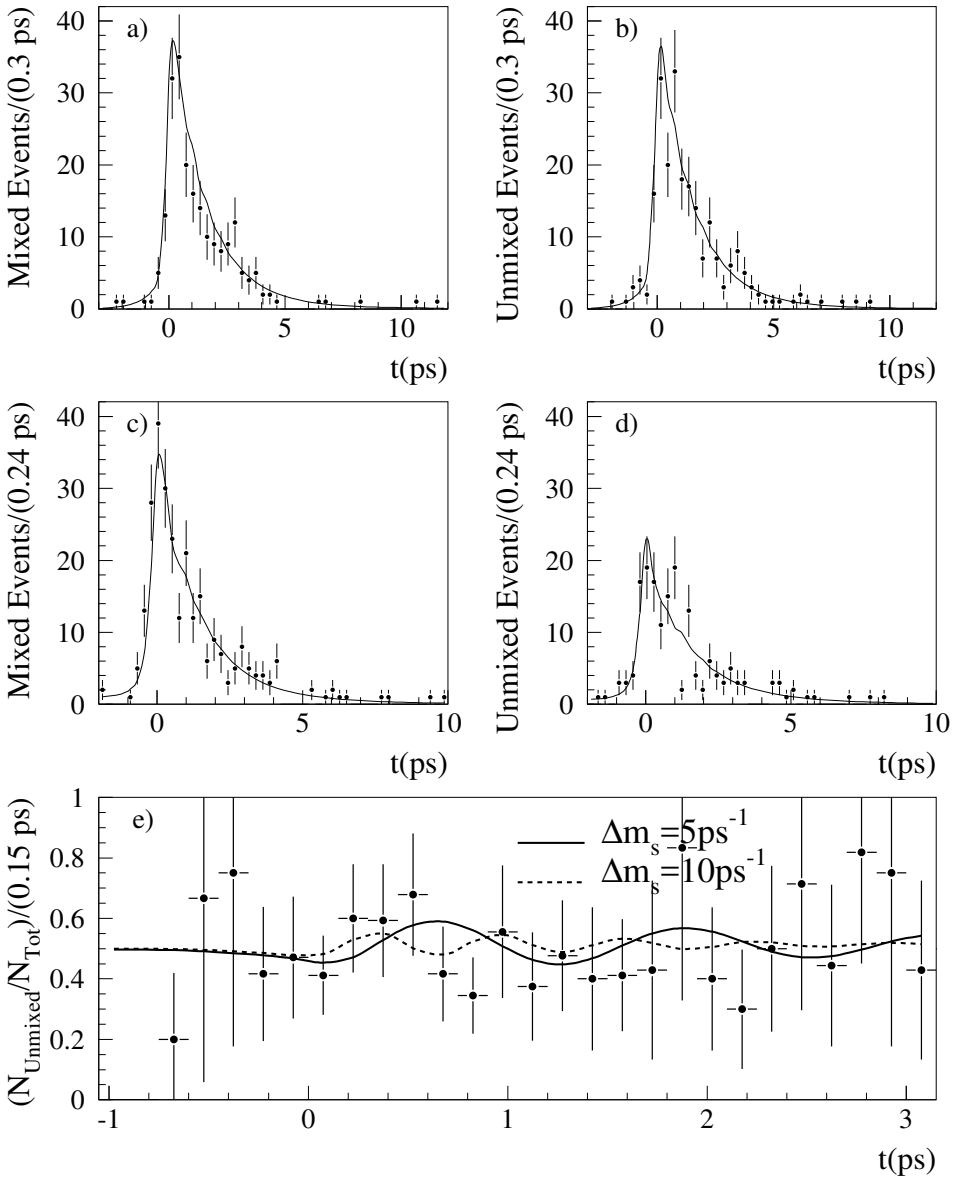

Figure 14: *Proper time distribution of mixed and unmixed events in* $\mathrm{D_s}\ell$ *sample (a-b) and in the* $\phi\ell$ *sample (c-d); the full dots with error bars represent the data, the curves are the corresponding fitted distribution (for* $\Delta m_{\mathrm{B_s^0}} = 10\ ps^{-1}$*).*
c) Ratio between the mixed events and the total number of events in bins of proper time in the $\mathrm{D_s}\ell$ *sample. The full (dashed) line represents the prediction for an oscillation* ($A = 1$) *with* $\Delta m_{\mathrm{B_s^0}} = 5\ ps^{-1} (10\ ps^{-1})$.

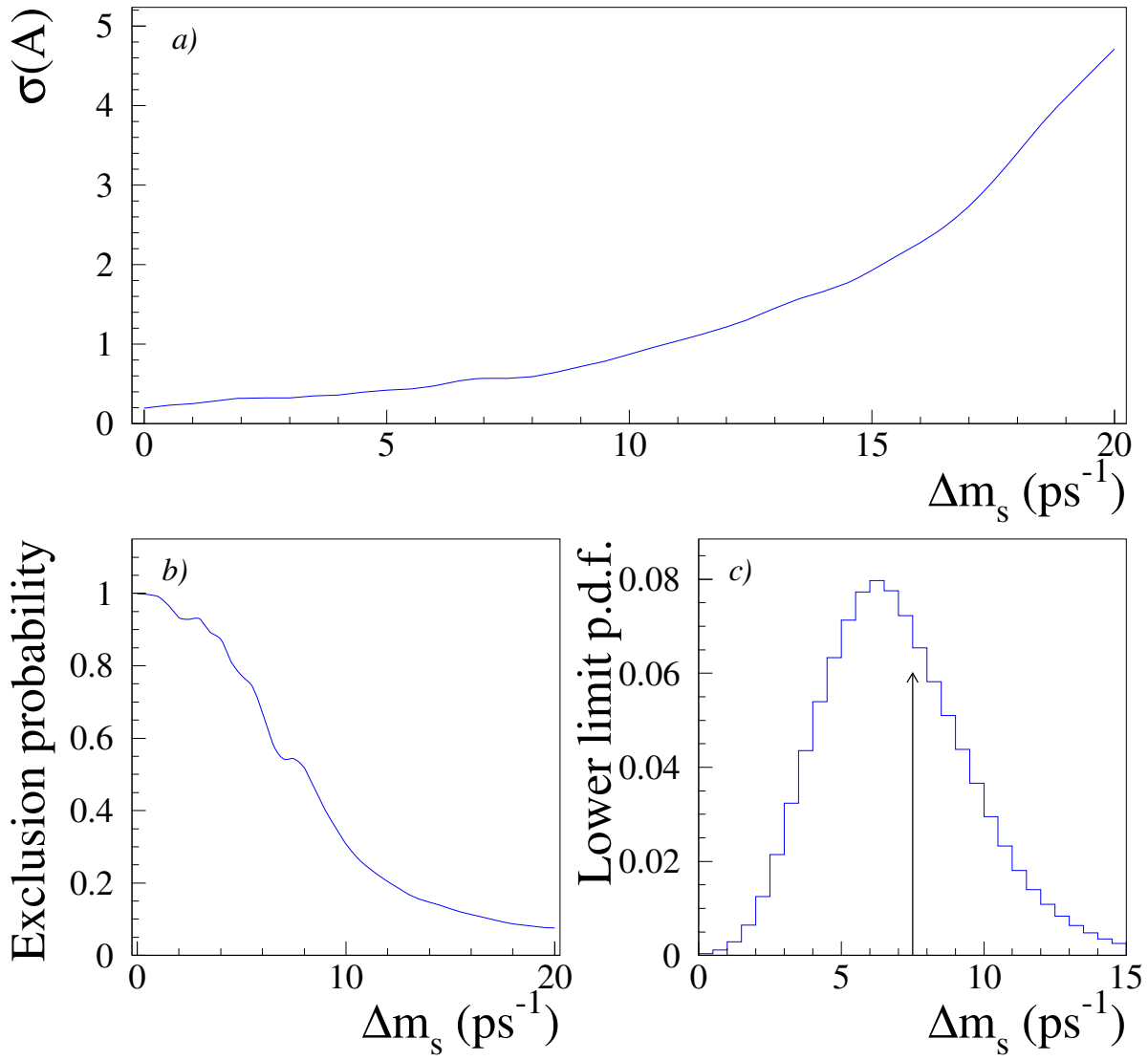

Figure 15: *a) Variation of the error on the amplitude as a function of Δm_s. b) Exclusion probability vs. Δm_s. c) Lower limit probability density function vs. Δm_s.*